博士論文

Study on analytical methods based on DNA/RNA-small ligand interactions

(DNA/RNA-小分子リガンド相互作用に基づく分析法の開発**)**

Yushuang ZHANG

2014年

Contents

Abstract

(1) <u>Development of abasic site-containing DNA duplex-based aptamers for theophylline's detection</u> [1]

Aptamers, short nucleic acids with significant binding ability, have emerged as promising candidates for molecular recognition events to various ligands. Our group has reported a fluorescent signaling aptamer that targets a common drug, theophylline.[2] In this DNA duplex aptamer, an abasic site (AP site) was utilized as an active cavity for binding events (cf. Fig. 1), and a fluorescent adenine analogue, 2-aminopurine, was incorporated into the duplex so as to flank the AP site. However, the need of the modification with 2-aminopurine makes the assay expensive, and the poor photostability of 2-aminopurine is also problematic.

In this work, a modification-free AP site-containing DNA duplex aptamer (AP-aptamer) is developed for the detection of theophylline. The assay is based on the competitive binding of theophylline with riboflavin at the AP site. As shown in Fig. 1, in the absence of theophylline, riboflavin binds to the receptor nucleobase opposite the AP site, and this is accompanied by fluorescence quenching. Upon addition of theophylline, the competitive binding of theophylline with riboflavin occurs, which results in the effective fluorescence restoration due to the release of riboflavin from the AP site.
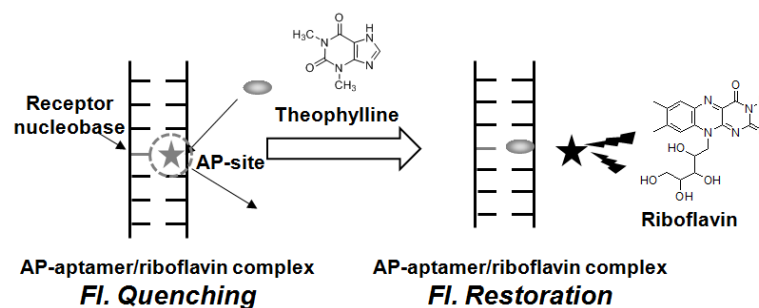
Fig.1. Competitive binding of theophylline with a fluorescent ligand at an AP site in a DNA duplex aptamer.

Riboflavin/23-mer AP aptamer (5'-TCT GCG TCC AGX GCA ACG CAC AC-3'/5'-GTG TGC GTT GCC CTG GAC GCA GA-3'; X: the AP site (Spacer C3, a propylene residue)) system is found to be effective for the detection of theophylline with a high selectivity over caffeine, theobromine and other substrates. In serum samples, a linear response to theophylline can be obtained in the concentration range from 10 μM to 33 μM (50 μM to 163 μM in original serum samples), which covers the monitoring of serum theophylline concentration in the therapeutic range (60 μM to 100 μM). This system is thus expected to be applicable to practical use.

(2) Development of a highly selective ligand binding with cytosine opposite an abasic site in DNA duplexes[3]

Detection of single-nucleotide polymorphisms (SNPs) in human genome has become increasingly important in the fields of genetics, molecular diagnostics and cancer research. Our group has reported that a naphthyridine derivative (AMND, Fig. 2)[4] was capable of selectively binding to cytosine (C) opposite an AP-site in DNA duplexes, and the binding-induced fluorescence quenching was applicable to the analysis of the C- related single base mutation. However, AMND showed an insufficient selectivity for C/T discrimination: the difference in the binding affinity of AMND for C over T is only two- or three-fold.[3,4]

CF$_3$-AMND: R = CF$_3$
AMND: R = H
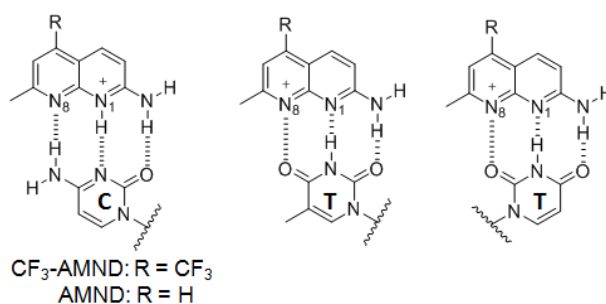
Fig.2. Binding modes of AMND/CF$_3$-AMND with C and T (2 possible patterns).

In this work, AMND is modified for highly selective detection of C by introducing of CF$_3$ group to the naphthyridine ring. The binding constant of the resulting CF$_3$-AMND (Fig. 2) for C ($K_{11}/10^5$ M^{-1} ($n = 3$): 7.1 $\pm$0.2) is found to be more than 50-fold larger than those for the other three nucleobases ($K_{11}/10^5$ M^{-1} ($n = 3$): T, 0.14 $\pm$0.016; G, 0.16 $\pm$0.029; A, <0.10). The high selectivity might be caused from more favorable protonation at the N1 position than the N8 position due to the electron-withdrawing effect of the CF$_3$ group, which then enables the effective pseudo-base pairing with C through hydrogen bonding (Fig. 2). Furthermore, CF$_3$-AMND is applicable to the analysis of single-base mutation in 107-mer DNAs (K-ras gene; codon 12, sense strand) amplified by asymmetric PCR, with highly selectivity for C. This will facilitate the accurate analysis of C-related single-base mutation in practical use.

(3) Development of peptide nucleic acid-thiazole orange conjugates for discrimination of terminal mismatches in DNA/RNA

In general, detection of mismatches of DNA/RNAs relies on the method based on the thermal stability of duplex hybridization. A mismatch near or at the terminus of a duplex is less destabilized than an internal mismatch, so as to be difficult for terminal mismatch detection. Recently, our group has developed a peptide nucleic acid conjugated with thiazole orange (PNA-TO) for siRNA imaging in living cells.[5] This ligand was capable of binding to 3'-overhanging nucleotides with a good selectivity for perfect match sequences over other

mismatched ones. For the binding of this ligand, PNA unit recognizes the terminal two nucleobases via complementary hydrogen-bonding, and TO unit works as a fluorescent probe by intercalation into the duplex (cf. Fig.3).

(A)

(B)
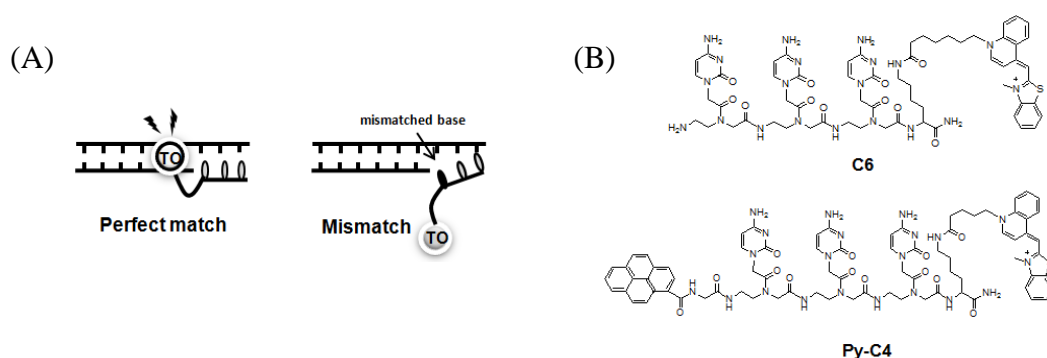
Fig.3. (A) Illustration of PNA-TO binding to terminal nucleobases;
(B) Structures of representative PNA-TO ligands (**C6** and **Py-C4**).

In this work, PNA-TO conjugates are developed for the detection of a single nucleobase mismatch at the terminal positions of DNA/RNAs (Fig. 3). All of the synthesized PNA-TO conjugates show a good selectivity at 3' end, but the selectivity is moderate for terminal mismatches at 5' end. To improve the binding selectivity at 5' end, pyrene as a π-stacking cap has been introduced into the N-terminal of PNA-TO. The resulting Pyrene-PNA-TO shows a specific binding ability for perfect match over terminal mismatches, including the most disturbing position, the very 1st terminal mismatch. In addition, Pyrene-PNA-TO is applicable to microRNA detection to recognize let-7d out of let-7 family with LOD as low as 0.9 nmol in 50 μL sample. It's thus expected that our method is promising for terminal mismatch detection and the ligand design would have flexibility for any kind of terminal sequences.

References

[1] Y. Sato, Y. Zhang, et al., *Chem. Eur. J.*, **2012**, 18, 12719.
[2] M. Li et al., *J. Am. Chem. Soc.*, **2009**, 131, 2448.
[3] Y. Sato, Y. Zhang, et al., *Org. Biomol. Chem.*, **2012**, 10, 4003.
[4] K. Yoshimoto et al., *J. Am. Chem. Soc.*, **2003**, 125, 8982. ;
     Y. Sato et al., *Nucleic Acids Res.*, **2009**, 37, 1411.
[5] T. Sato et al., *Chem. Commun.*, **2015**, 51, 1421.

Chapter 1: General introduction

1-1. Introduction

As we known, nucleic acids—DNA/RNAs are genetic material and play a crucial role in coding, decoding, regulation, and expression of genes. Thus, DNA/RNAs become a long-standing target for the diagnosis and treatment for multitude of human diseases.

Small ligands, which are capable of interacting with DNA/RNA sequences, become powerful tools in many kinds of fields. For example, Neomycin B which can bind to HIV-1 TAR RNA is typical of such ligands for drug development.[1]

As another one of those useful fields, oligo-DNA/RNAs can be the targets to be recognized by stain ligands in developing analytical methods, or as aptamers for specific small ligand-recognitions.

In this thesis, I will show three applications all based on utilizing DNA/RNA-small ligand interactions. In chapter 2, a modification-free AP-aptamer for the detection of theophylline has been developed. In chapter 3, a specific binding ligand for cytosine opposite an AP-site in DNA duplexes has been developed, which is applicable in C- related single base mutation. And in chapter 4, a series of PNA-TO conjugates for the terminal mismatch detection of DNA/RNAs has been achieved.

1-2. Typical binding modes of small ligands toward DNA/RNAs

According to the binding happened positions, the binding modes of small ligands toward DNA/RNAs can be divided into intercalation, groove binding, internal- or bulge- or hairpin-loop binding, backbone binding, and capping (**Figure 1-1**).[2,3] Ethidium bromide[4] (intercalation) and Hoechst 33258[5] (minor groove binding) are typical of such ligands.
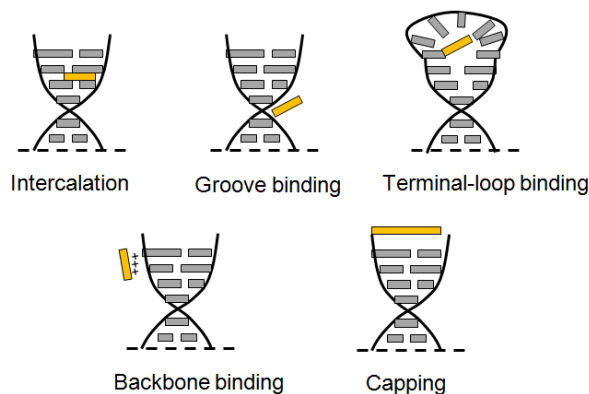
Figure 1-1. Binding modes of small ligands interacting with nucleic acid duplexes.

In our group, abasic site (AP site) as the binding site has been paid attention to for

detecting the nucleobase genotype, mainly because of its chemical stability (ref. section 2-1-5). Designed small ligands are able to bind at an AP site and recognize the specific nucleobase opposite the AP site with high affinity and specificity. This is generally achieved by a combination of molecular shape complementarity, hydrogen-bonding and stacking interactions. Such binding events typically involve the ligand-induced structural changes of the aptamers, resulting in the formation of unique secondary and tertiary structures responsible to the ligand binding. (ref. Chapter 2)

1-3. Differences of structure between DNA and RNA duplexes

DNA and RNA are both nucleic acids, which are similar but not exactly the same.

Biologically, almost all of life use DNA as its genetic code. Only when there is a mistake happened during the duplication period, DNA-cleavage enzymes will generate, thus this makes the information stored by DNA consistent. However, RNA's main duty is assist DNA's duplication. So RNA strands are continually made, broken down, and reused. It requires the energy of cleaving RNA not be too high. For the three-dimensional structure, the double stranded DNA has relatively small grooves as opposed to the larger grooves on RNA molecules. This provides ample docking space of RNA for damaging enzymes.

Structurally, DNA contains deoxyribose, while RNA contains ribose. The deoxyribose sugar in DNA is less reactive than the ribose sugar for there is no hydroxyl group attached to the pentose ring in the 2' position. However, RNA has hydroxyl groups, which make RNA less stable for its more prone to hydrolysis.[6]

Importantly, DNA and RNA's secondary structure (the base-pairing interactions) and tertiary structure (three-dimensional structure) are different. As we all know, the complementary base to adenine (A) is thymine (T) in DNA, but uracil (U) in RNA, which is an unmethylated form of thymine. In addition, the double helix structure of DNA is general slim B-form; while it's compact A-form for RNA (**Figure 1-2** and **Table 1-1**). This formation difference results the difference for small ligands' binding. For example, compared to B-formed DNA, the overlap of a small ligand with the adjacent nucleobases are more feasible in A-formed RNA structure, which can make stacking interactions stronger for the ligand.[7]
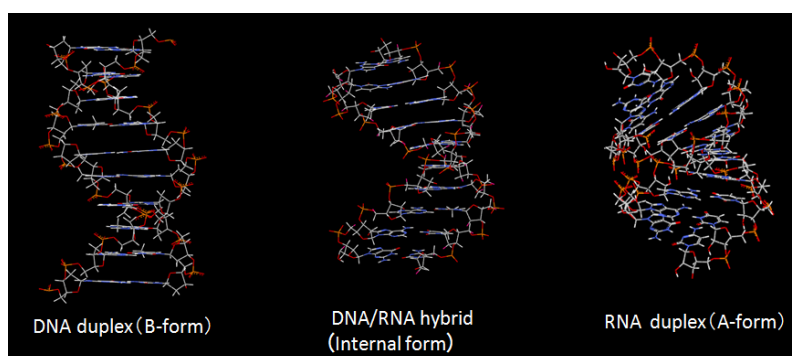
Figure 1-2. Tertiary structures of DNA duplex, DNA/RNA hybrid, and RNA duplex.

Geometry attribute:	B-form	A-form
Helix sense	right-handed	right-handed
Rotation/bp	35.9 °	33.6 °
Mean bp/turn	10.5	11
Rise/bp along axis	3.4 Å	2.4 Å
Rise/turn of helix	33.2 Å	24.6 Å
Mean propeller twist	+16 °	+18 °
Nucleotide phosphate to phosphate distance	7.0 Å	5.9 Å
Sugar pucker	C2'-endo	C3'-endo
Diameter	20 Å	23 Å

Table 1-1. Comparison of B-form and A-form nucleic acid structures.[8]

Since those differences between DNA and RNA duplexes, although some small ligands designed for DNA or RNA could have the universal to the other kind of nucleic acid, it's not always workable. In another word, the ability for designed ligands to bind with DNA is not always maintained to RNA, and vise versa.

In chapter 2, considered the similarity, DNA aptamer was utilized because it is more stable and economic than corresponding RNA aptamers (ref. section 2-1-2-4). In chapter 4, our final application showed a microRNA assay, although DNAs were utilized for the preliminary experiments for the same reason. In that application, we successfully achieved our goal by using RNAs based on the preliminary experiments by DNAs. Still, I have to point out that we should always keep in mind that DNA and RNA are different, and the ligands which can bind to a DNA strand, could be not able to simply transfer to the corresponding RNA.

References

1. Sucheck, S. J., Wong, C.-H., *Curr. Opin. Chem. Biol.,* **2000**, 4, 678-686.

2. Ananya Paul, and Santanu Bhattacharya, *Current Science*, **2012**, 102(2), 212-231.

3. Jason R. Thomas and Paul J. Hergenrother, *Chemical Reviews*, **2008**, 108(4), 1171-1224.

4. Ren J, Jenkins TC, Chaires JB., *Biochemistry*, **2000,** 39, 8439.

5. Haq I, Ladbury JE, Chowdhry BZ, Jenkins TC, Chaires JB., *J. Mol. Biol*, **1997**, 271, 244.

6. http://en.wikipedia.org/wiki/RNA

7. S. Arnott, R. Chandrasekaran, D.W.L. Hukins, P.J.C. Smith, and L. Watts, *J. Mol. Biol*, **1974**, 88, 523-533.

8. http://en.wikipedia.org/wiki/A-DNA

Chapter 2: Development of abasic site-containing DNA duplex-based aptamers for theophylline's detection[9]

2-1. Introduction

2-1-1. Theophylline

2-1-1-1. Introduction

Theophylline, also known as dimethylxanthine, is one of the most commonly used drug as bronchodilators and respiratory stimulators for the treatment of the symptoms of acute and chronic asthmatic conditions.[10-12] The therapeutic range for theophylline in serum is very narrow, and a steady-state concentration is within the range of 60-100 µM.[12] If overdose of theophylline would lead to lethal or permanent neurological damage.[12,13] For this reason, accurate and careful monitoring of theophylline concentration in serum becomes indispensable to effective treatments.
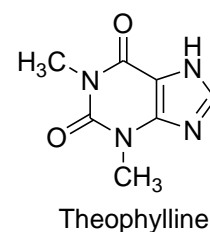
Theophylline is naturally found in tea and cocoa beans. As a member of the xanthine (3,7-dihydro-purine-2,6-dione) family, it bears structural and pharmacological similarity to caffeine and theobromine. Therefore, in order to get a specific signal for theophylline, discrimination from the latter molecules becomes necessary during the monitoring process.
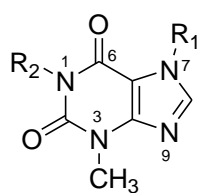
Theophylline: R_1 = H, R_2 = CH_3
Caffeine: R_1 = CH_3, R_2 = CH_3
Theobromine: R_1 = CH_3, R_2 = H

Figure 2-1. Structures of methylxanthine compounds: theophylline, caffeine, and theobromine.

2-1-1-2. Existence methods for theophylline detection

Currently, there are mainly two routine methods in the clinical laboratories, which are based on gas/liquid chromatographic and immunoassay techniques.[10,11] However, these techniques show relatively low selectivity for theophylline over structurally similar caffeine and theobromine. In order to solve these problems, the chromatographic techniques combined with the gradient elution[14] and column switching[15] have been developed. However, these chromatographic techniques still require time-consuming pretreatments such as solvent extraction and protein precipitation.[16,17] On the other hand, the immunoassay with the increased selectivity using the theophylline-oxidizing enzyme was reported,[18-21] but restricted availability and low stability of the theophylline-oxidizing enzyme limit the practical use of such enzyme.[22]

In 1994, Jenison et al. developed a RNA aptamer[23] with high binding affinity to theophylline and high discriminative ability against caffeine, which can be considered as a new emerging detection method for theophylline. Since then, more and more new aptamers were broached out based on electrochemical,[24-26] fluorescent,[27-29] and colorimetric[30] techniques.

However, one of the main problems with aptamer applicability is the stability and proneness to nuclease attack particularly with reference to RNA rather than DNA aptamers.[31] In another word, RNA is known to be susceptible to degradation by the endogenous ribonucleases typically found in serum. Therefore, it is desirable to establish a detection method based on DNAs with high chemical and/or enzymatic stability.

2-1-2. Aptamer

2-1-2-1. Background

Aptamers are artificial short nucleic acid species with high affinity and selectivity that can bind to a wide range of nonnucleic acid targets, such as metal cations, drugs, peptides, organic and inorganic molecules, proteins, or even whole cells.[32-44] The name "aptamer" is derived from the Latin aptus, meaning "to fit". [45]

Aptamers were first reported in 1990 by two groups (Ellington and Szostak; Tuerk and Gold)[46,47]. They generated aptamers by an in vitro selection process called SELEX (systematic evolution of ligands by exponential enrichment). Since then, the SELEX method has been widely used to develop aptamers targeting various molecules. In simple terms, SELEX is a method that permits the identification of unique DNA/RNA molecules, which bind to the target molecule with high affinity and specificity, from very large populations of random sequence oligomers (DNA or RNA libraries).[48]

As mentioned above, aptamers have a very high affinity for targets, with dissociation constants generally from the micromolar to picomolar range, which are comparable to those of antibodies, sometimes even better.[23,48] Aptamers also have a good selectivity for the targets over other disturbing molecules. For example, the anti-theophylline aptamer showed a 10,000-fold discrimination ability against caffeine[23], and an anti-l-arginine RNA aptamer showed a 12,000-fold affinity reduction toward d-arginine[49].

Since the discovery of aptamers, many researchers have used aptamer selection as a means for application and discovery. More recently, aptamers have been served as research tools in molecular recognition of analysis, diagnosis and therapy.

2-1-2-2. SELEX process

SELEX (systematic evolution of ligands by exponential enrichment) has proven to be an excellent tool for searching oligonucleotide molecules out of a random pool, with high affinity for a particular target under specific conditions. It involves the following processes, separately: synthesis and selection of ligand sequences that bind to a target; partitioning of aptamers from non-aptamers via affinity methods; and amplification of bound aptamers.

In the SELEX process (**Figure 2-2**), synthesis of single-stranded library oligonucleotides begins first. Each oligonucleotide comprises a random sequence region in the center part and defined region from the 5' and 3' ends. Each member of the library is a

linear oligomer with a unique sequence. A large number of random sequences in the library are necessary to provide a complexity, and so as to a high possibility to select out useful aptamers for certain targets. Typically, the initial circle contains about 10^{15} individual sequences[48], which is a fine number for selection.

First, the random single-stranded DNA pool is amplified by the polymerase chain reaction (PCR) to form a double-strand DNA (dsDNA) pool. And the dsDNA pool is further transcribed (for RNA selection) or separated into single strand (for single-stranded DNA selection, using the T7 RNA polymerase) to become a suitable form for further selection.

Second, the library is incubated with the target and the first cycle of absorption is initiated. The target can be immobilized (e.g. on magnetic beads, affinity column, microtitre plates[50,51]) or free in solution. After incubation, the partition of the DNA/RNA aptamer-target complex from non-aptamers is necessary by washing steps. In this way, the non-aptamers (non-specific or low affinity for the target) will be removed.

Then, the bound species are regenerated by enzymatic amplification processes (Reverse Transcription-PCR for RNA libraries, or PCR for DNA libraries) for the next selection cycle.[52] The whole cycle is repeated until obtaining a specific population of RNA/DNA, and finally is isolated and characterized. To complete entire selection process, 12 cycles are usually required, after that the selected molecules can be cloned into an appropriate vector and sequenced.[52]
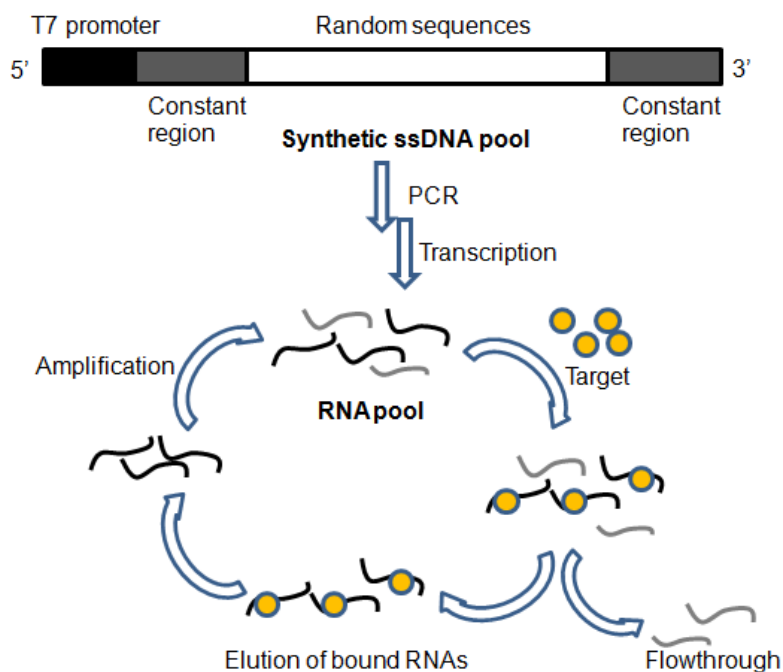
Figure 2-2. Scheme of the in vitro selection of an RNA aptamer (SELEX process).[48]

2-1-2-3. Advantages of aptamers (comparison with antibody)

Besides the high binding affinity and specificity to target, aptamers also have other merits including but not limited to the following points.

1) Little or no immunogenicity

To compare with antibodies, the main advantage of aptamers is overcoming of the animal's use for their production. Typically, antibody production comes from biological systems by inducing an immune response to the target analyte. However, the immune response can be failed when the structure of target protein is similar to endogenous proteins, and when the antigen consists of toxic compounds. In addition, the in vivo parameters restrict the identification of antibodies to targets.

On the contrary, aptamers are selected by in vitro process against any kind of target, including proteins and toxic compounds.[48]

2) Various target region at different binding conditions

The generation process of antibodies is taken out in vivo, which leads to the restriction of biological environment. Such as, the animal immune system can only select the specific sites of the target protein to which the antibodies bind. And the recognition of antibodies to their targets only happens under physiological conditions, which limits the extension use of antibodies.[48]

However, aptamers are able to be generated to bind a certain region of the target (not refrained from the immuno effect), and with specific binding ability in different binding conditions (temperature, pH, buffer, etc.).[31,48]

3) Stability and ability of regeneration

Antibodies could hardly avoid the batch-to-batch variation, while aptamers are produced and purified to a very high degree to eliminate the variation by chemical synthesis. And chemical modifications in the aptamer can be introduced enhancing the stability, affinity and specificity of the molecules.

Because of aptamers' simple structure, sensor layers based on aptamers can be regenerated more easily than antibody-based layers. Aptamers are more resistant to denaturation and have a much longer shelf life.[48]

4) Enrichment and amplification

The selections process of aptamers contains amplification step, which is advantageous for enrichment.

Antibodies	Aptamers
Antibodies often suffer variations from batch to batch	Smaller size and chemically synthesized without batch variation
Labelling can cause loss in affinity	Can be labelled without affecting their affinity
Production requires the use of animals	In vitro production
Manipulation only under physiological conditions	Selection conditions can be manipulated, temperature, pH, buffer, etc.
Limited to molecules that produce an immunoresponse	Able to bind with drugs or toxic substances
Sensitive to temperature and humidity changes	Storage and transport can be done at room temperature

Table 1-1. List of aptamers' advantages.[31]

2-1-2-4. Limitations of RNA aptamers (comparison of RNA and DNA aptamers)

The primary limitation of RNA aptamers is their nuclease sensitivity which is very critical for the use in ex-vivo and in vivo applications.[53]

Besides of the low chemical and enzymatic stability, the synthesis costs of RNA aptamers are much higher than DNAs. For example, one tube of the 11-mer DNA single strand containing dSpacer, which was used in our preliminary experiment, costs 9,975 yen. While the same sequence of RNA single strand at a similar Optical Density (O.D.) unit, costs 111,888 yen, which is over 10 times of the DNA's cost.

Generally speaking, DNA aptamers have all the characters of RNA aptamers. They can form the secondary and tertiary structures suitable for the effective binding of targets. Meanwhile, DNA aptamers are more stable in vivo conditions and cheaper to achieve. Therefore, DNA aptamers are more preferable than RNA aptamers.

2-1-2-5. Fluorescent sensing aptamers

As mentioned in the section 2-1-1-2, aptamers can be applied by using electrochemical, fluorescent, and colorimetric techniques. Here we only summarized the aptamer types based on fluorescent technique. This is because fluorescence signals can be measured conveniently with high sensitivity and so have been widely used.

2-1-2-5-1. Introduction

Aptamers, which bind nonnucleic acid analytes, act as three-dimensional bioreceptors. They can form various secondary or tertiary structures with an internal- or stem-loop as the active sites. The binding is generally achieved by a combination of molecular shape complementary, hydrogen bonding and stacking interactions.

As same as other nucleic acids, aptamers are inherently non-fluorescent, and therefore extra modifications with fluorophores must be performed to convert aptamers into fluorescence-signaling molecules. As schematically shown in **Figure 2-3**, an aptamer plays as a sensing element here. When target binds to it, the adoption will generate a transduction fluorescence signal and this signal can be detected by spectrofluorometers. In this process, the fluorophore's property should obviously have some changes when the aptamer binds to the target analyte. In addition, a rational design of aptamer should also consider the following aspects, which are photo stability, pH-dependence, the nature and length of aptamer, position of the fluorophore attachment (internal or end modification), etc.[54]
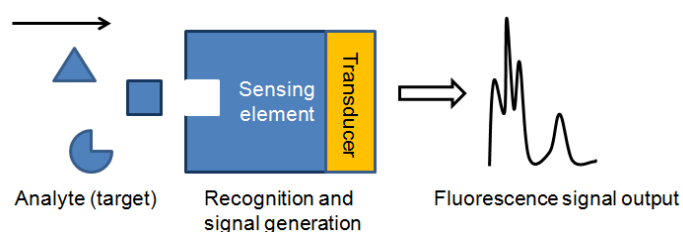
Figure 2-3. Schematic layout of a fluorescent recognition process.[54]

2-1-2-5-2. Typical design strategies of aptamer

The strategies for designing aptamer can be divided into two groups based on the attached fluorophores and quenchers on aptamer. One group makes aptamer labeled with one single fluorophore, and the other affords aptamer labeled with a pair of fluorophore and quencher, or two fluorophores.

For the first group, the binding to target makes aptamer undergoes a conformational change, and this change gives a fluorescence signal (**Figure 2-4**).[55] Also, the location of fluorophore is important for an effective fluorescence signaling, which has been shown in the report of Jhaveri's group in 2000.[35]
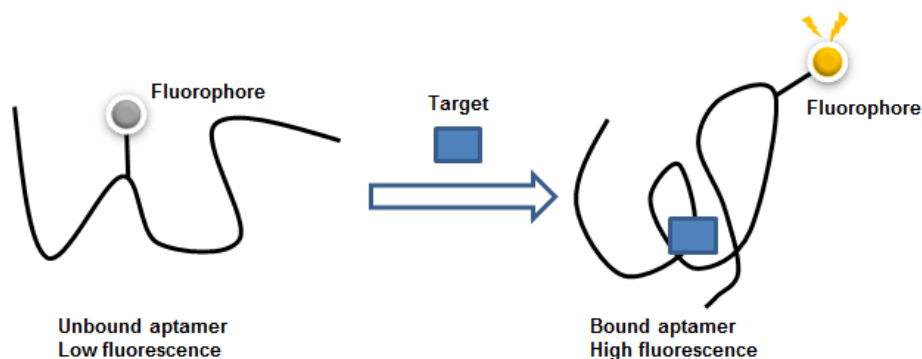
Figure 2-4. Design strategy for aptamer with one single fluorophore.[55]

For the second group, there are several mechanisms for the fluorescence detection. (**Figure 2-6**) Probes containing two dyes that cause the transduction processes from binding to signaling may rely on: 1) fluorescence quenching (static or dynamic mechanisms); 2) fluorescence resonance energy transfer (FRET); and 3) monomer-excimer emission switching with pyrene fluorophores.[55] The third type is out of our concern so is not described in this introduction here.

Some proper nouns:

Molecular Beacon (MB): MB has a hairpin structure with fluorophore and quencher probes at 5' and 3' terminal, respectively, but close to each other. At this time, the fluorescence quenching occurs between the fluorophore and the quencher. However, when the target analyte binds to MB, the hairpin conformation of MB will be opened. And as a result, the fluorophore and the quencher will be separated from each other with emitting of a fluorescence signaling. (**Figure 2-6a**)

Fluorescence resonance energy transfer (FRET): In a typical FRET system, a biopolymer is labeled with two different fluorophores (a donor and an acceptor) at different positions. The excitation energy of donor molecule will be transferred to the receptor in a nonradiative way because of the interactions between the excited states of these fluorophores. After that, the acceptor molecule emits a fluorescence signal.

The distance between the donor and acceptor fluorophores should be close (typically 10-80 Å), and the spectra of donor's emission and acceptor's absorption should have an overlap.[54](**Figure 2-5**)
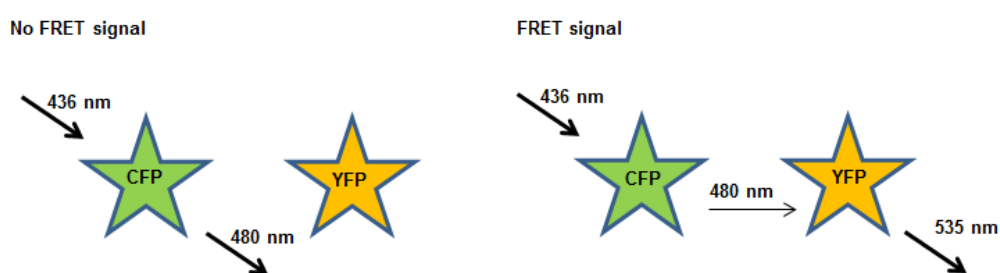

Figure 2-5. Example of FRET between CFP and YFP (two dyes; Wavelength vs. Absorption).[56]

In **Figure 2-6a**, it shows an MB structure with a fluorophore and a quencher at the 5' and 3' ends, respectively. And the stem-loop region will be responsible for the binding with target molecule. In the absence of target, there is only fluorescence quenching signal. Upon addition of target, the hairpin structure will be destroyed and caused a change in the distance between the fluorophore and the quencher, resulting in a fluorescent enhancement signal. Hamaguchi et al. reported this type molecular-beacon approach for thrombin.[57]

In **Figure 2-6b**, a simpler aptamer is shown, which is attached by a fluorophore and a quencher at two ends without a stem-loop structure. High fluorescence intensity can be observed in the absence of target. And in the presence of target, a compact structure is formed and the fluorophore will be brought close to the quencher, resulting in a fluorescence quenching signal. In the work of Stojanovic's group, 50% quenching was observed with 1 mmol L^{-1} cocaine.[58]

In **Figure 2-6c**, a longer strand and two shorter strands are used. The two shorter strands are modified with a fluorophore at the 5' end, and a quencher at the 3' end, respectively. They are complementary to longer strand at different region, and thus these three strands will form a duplex. When the target analyte is in presence, the duplex turns to a target-induced complex structure with releasing of quencher-labeled strand and meanwhile give out a fluorescence signal.[59]

And the mechanisms in Figure 2-6d/ 2-6e/ 2-6c are generated based on these strategies above. Generally speaking, the fluorescence signaling is ascribed to the conformational change of aptamer when binding to the target. And the diversity of aptamer's structure, including secondary or tertiary structure, provides us more possibilities and chances to develop the technique in this region.
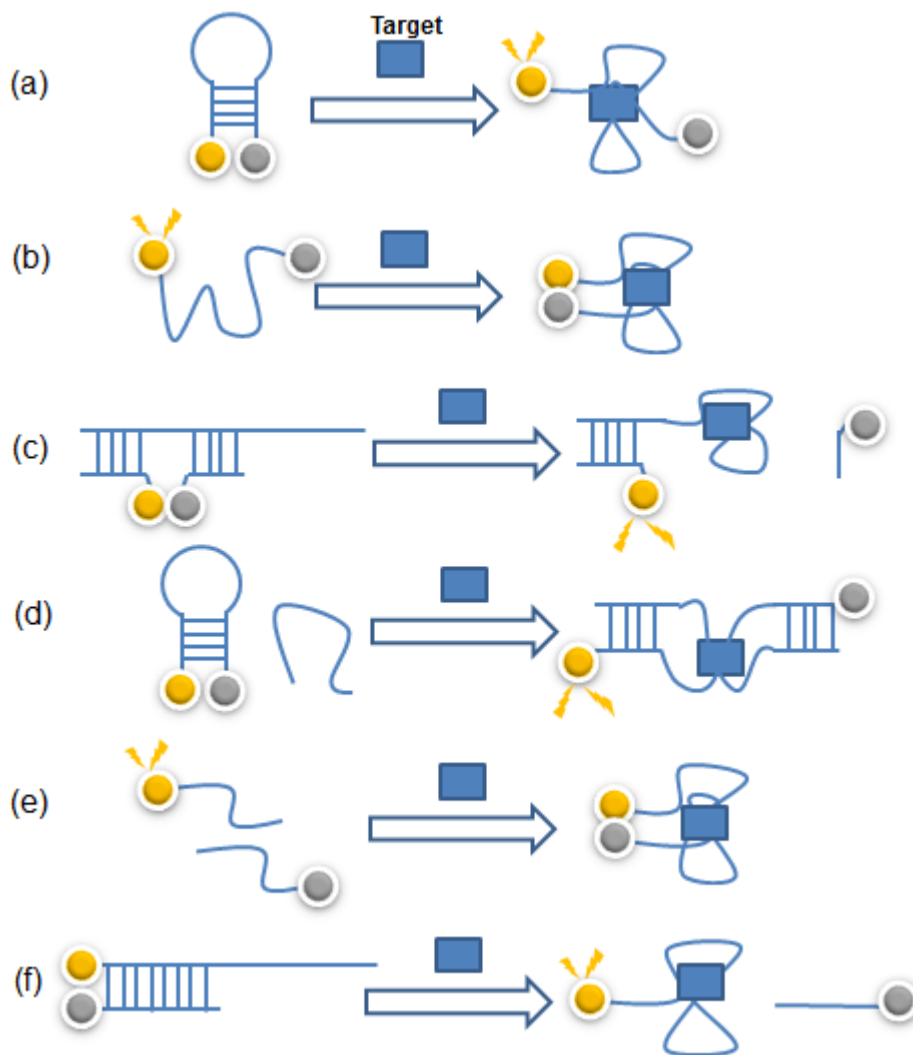
Figure 2-6. Design strategy for aptamer with one fluorophore and one quencher.[54]

2-1-3. RNA aptamer for theophylline detection

The first reported RNA aptamer for theophylline was exploited by Jenison et al.[23] As shown in **Figure 2-7**, this 33-mer aptamer provided an internal-loop which acted as a suitable pocket for theophylline's binding event. The binding could be ascribed to molecular shape complementarity, stacking interaction and the forming of hydrogen bonding with the receptor nucleobase (cytosine). This RNA aptamer showed high binding affinity (dissociation constant K_d of 0.3-0.4 μM) and specific binding to theophylline (the binding affinity is 10,000-fold greater than the RNA molecule's affinity for caffeine). Therefore, this RNA aptamer could be a promising candidate for theophylline detection.
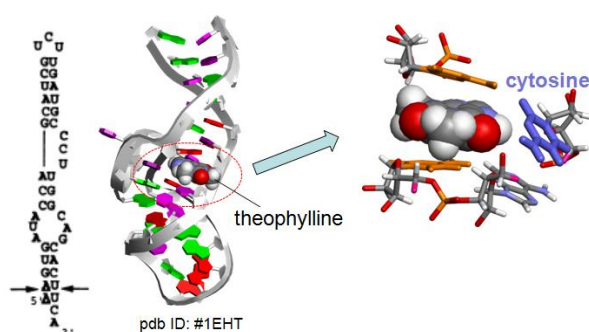
Figure 2-7. 33-mer RNA structure and its binding pattern with theophylline.[23]

An application of this RNA aptamer into an electrochemical biosensor was demonstrated (**Figure 2-8**).[23] The RNA aptamer was immobilized on a gold electrode and the other terminal was labeled with a ferrocene (Fc) as a redox probe. In presence of theophylline, the aptamer folded into the hairpin structure. This conformational change resulted in increased efficiency of eT (decrease in the average eT distance) between the Fc probe and the electrode surface. This enabled calibration of the signal versus theophylline concentration.
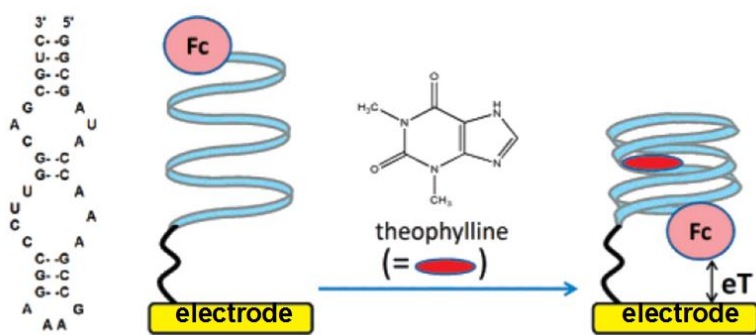
Figure 2-8. Electrochemical biosensor for theophylline based on the RNA aptamer.[24]

However, as we emphasized before, RNA aptamers have some disadvantages. One is unstable especially in the biological fluid such as serum and plasma. Another is high cost for RNA synthesis compared to DNA. And these disadvantages impede their routine clinical application.

2-1-4. 2-aminopurine modified DNA aptamer for theophylline detection

To overcome RNA aptamer's deficiency, a 2-aminoputine modified DNA aptamer (5'-TCTGC GTCCT PXT TAACG CACAC-3'/3'-AGACG CAGGA TCA ATTGC GTGTG-5', P = 2-aminopurine, X = abasic site; Spacer C3, C = receptor nucleobase) has been developed by our lab recently.[60]

An abasic site (AP site) located at the middle of DNA strand was utilized as the active binding site. 2-aminopurine (an analogue of adenine) was put into the adjacent place of AP site, and worked as a fluorescent probe. The base facing AP site was denoted receptor nucleobase, which was expected to form hydrogen bonding with target molecule. (**Figure 2-9A**)

In absence of theophylline, the high fluorescence of 2-aminopurine was observed due to the weak stacking interaction with neighboring nucleobase. Upon the binding of theophylline molecule, the stacking interaction was improved between 2-aminopurine and neighbors, which resulted the fluorescence quenching of 2-aminopurine. And this fluorescence change can be used to detect the target molecule—theophylline.
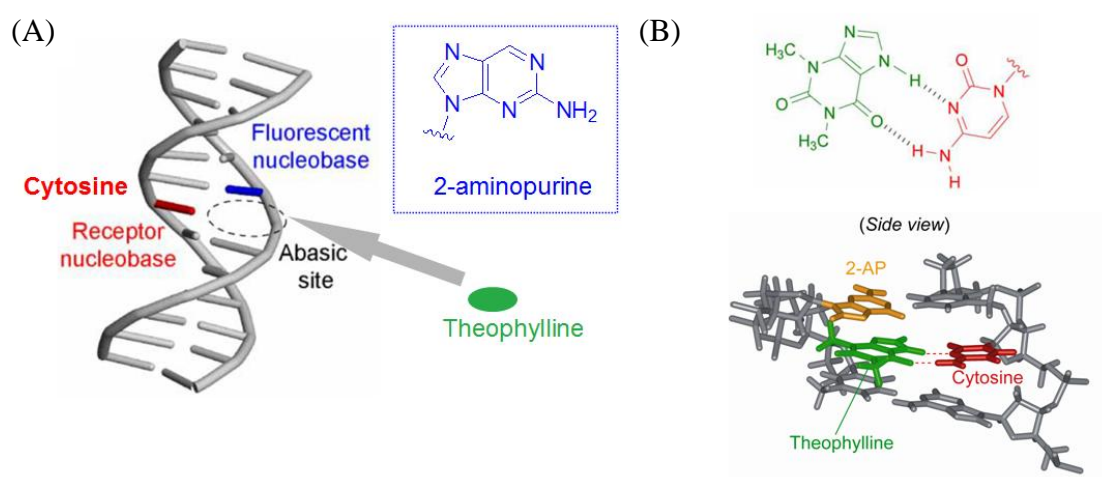
Figure 2-9. 2-Aminopurine modified abasic site (AP site)-containing DNA aptamer for theophylline.
(A) Working scheme; (B) Possible binding mode of cytosine with theophylline.[60]

This aptamer was capable to monitor theophylline's concentration with a dissociation constant of 10 μM (at 5°C, pH 7.0, I = 0.11 M) by getting a quenching signal when putting theophylline into the buffer solution (**Figure 2-10**). When apply it to detect theophylline in serum, a linear response to theophylline concentration was obtained with a good selectivity (**Figure 2-11**). That means we can also apply this DNA aptamer to serum samples.
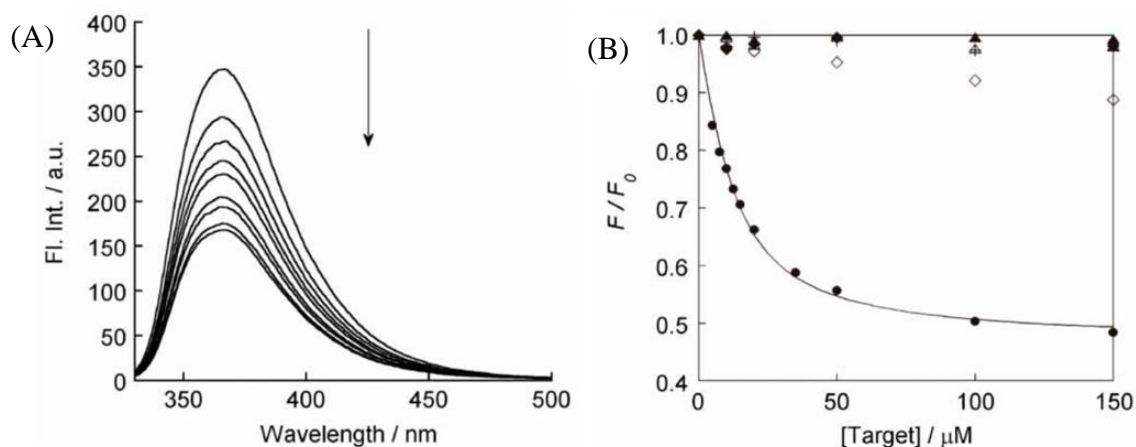
Figure 2-10. Fluorescence response and selectivity to theophylline by using 2-aminopurine modified DNA aptamer.[60] (A) Fluorescence response to theophylline (0-150 μM); (B) Binding selectivity for theophylline against caffeine, theobromine, uric acid, creatinine, and glucose.

F and F_0 denote the fluorescence intensities in the presence and absence of ligands, respectively.

[DNA duplex] = 5 μM, [NaCl] = 100 mM, [EDTA] = 1.0 mM, [Sodium cacodylate buffer] = 10 mM, pH 7.0, 5°C, Excitation: 320 nm, Analysis: 367 nm.
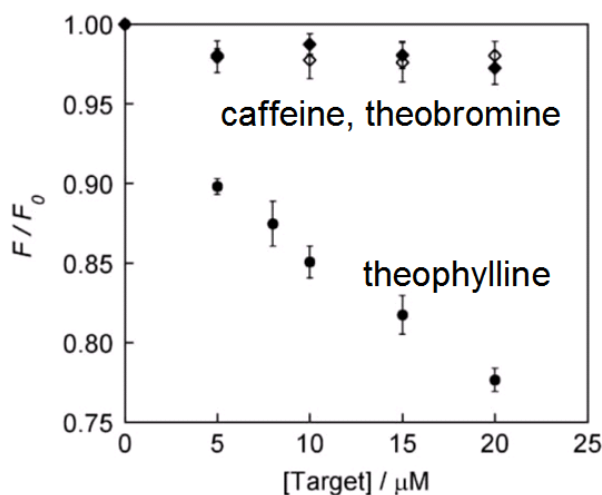
Figure 2-11. Detection of theophylline in horse serum.[60]

The control serum samples (5 μl) containing each ligand were diluted to 50 μl with a buffer solution (pH 7.0, 10 mM sodium cacodylate) containing DNA duplex (5.0 μM), and then the fluorescence measurements were done.

Errors are standard deviations obtained from three independent measurements at each concentration. Other conditions are as same as in Figure 2-10.

19

However, there are some disadvantages for the practical use. First, it's a fluorescence quenching response to theophylline, which is not preferable for clear fluorescence detection. Second, because of the short excitation and emission wavelength of 2-aminopurine (Excitation: 320 nm, Emission: 367 nm), a large background fluorescence is present. Third, need for the modification of the fluorescent nucleotide analogue makes the assay expensive.

2-1-5. Abasic site (AP site)

An abasic site (AP site), also known as an apurinic/apyrimidinic site, is a location in DNA that has neither a purine nor a pyrimidine base, usually due to DNA's damage.

AP sites in DNA arise spontaneously by a hydrolytic process that causes a cleavage of the N-glycosidic bond and leaves the phosphodiester backbone intact, which is markedly accelerated by chemical modification of DNA bases. Approximately 100,000 abasic sites per cell are formed each day.[61] Damaged DNA bases are removed by DNA N-glycosylases, generating AP sites as an intermediate during base excision repair. These lesions may play an important role in spontaneous and chemical mutagenesis.[62] The half-life of an AP site in oligomeric duplex DNA has been measured by the JoAnne's group and the Sheppard's group using five different sequence contexts and ranges from 200 to 900 hours under physiological conditions (pH 7.5, 150 mM NaCl at 37 ℃).[63,64] This means AP site containing DNA duplex has a moderate stability even in biological environment.

The conformation of AP site-containing DNA duplexes' backbones is generally observed as right hand and B-form, but with diversity (**Table 2-2**). Conformational changes due to the presence of the AP site extend to the base pairs adjacent to the lesion site, being dependent on the nature of the flanking and opposite bases.[65]

The structures of DNA oligonucleotides with A, T, G or C opposite an AP site have been investigated by Jingyang Chen et al.[66] by using 2D NMR. Their results indicate that all four kinds of nucleobases opposite the AP site is intrahelical. However, the conformation around the AP site is more perturbed when the unpaired base is a pyrimidine (C or T) than a purine (A or G). The few available studies tend to indicate that the pyrimidine opposite the abasic site may be either stacked inside the helix or expelled outside, or in equilibrium between the two situations, depending on the nature of the flanking bases.[65]

Summary of previous 2D-NMR studies on duplex DNA containing abasic sites (**X**)			
Sequence context	**Anomeric ratio (α:β)**	**Conformation of abasic site**	**Conformation of unpaired base**
5'-CGCGA**X**ACGCC-3' 3'-GCGCT**A**TGCGG-5'	~50:50	α and β: intrahelical	α and β: intrahelical
5'-CGCGA**X**ACGCC-3' 3'-GCGCT**C**TGCGG-5'	0:100	Intrahelical	intrahelical
5'-CGCGA**X**ACGCC-3' 3'-GCGCT**A**TGCGG-5'	~50:50	α: extrahelical β: intrahelical	α and β: intrahelical
5'-CGCATT**X**TTGCG-3' 3'-GCGTAA**A**AACGC-5'	~45:55	α: extrahelical β: intrahelical	α and β: intrahelical
5'-CCAAAG**X**ACTGGG-3' 3'-GGTTTC**A**TGACCC-5'	~60:40	α and β: extrahelical	α and β: intrahelical
5'-CCAAAG**X**ACCGGG-3' 3'-GGTTTC**A**TGGCCC-5'	~60:40	α and β: extrahelical	α and β: intrahelical

Table 2-2. Diversity of structures of AP site-containing DNAs.[66]

Some AP site analogues were developed[65] (**Figure 2-12**) and the two types of AP site used in current study are simply listed here (**Figure 2-13**). dSpacer (a tetrahydrofuranyl residue) is commonly used to mimic an abasic site in an oligonucleotide, because it is not only structurally very similar to the natural site, but also considerably more stable, and thus can tolerate the chemical conditions used in oligo synthesis and purification. The further elimination of the five membered ring, only leaving three backbone carbons gives Spacer C3 (a propylene residue).
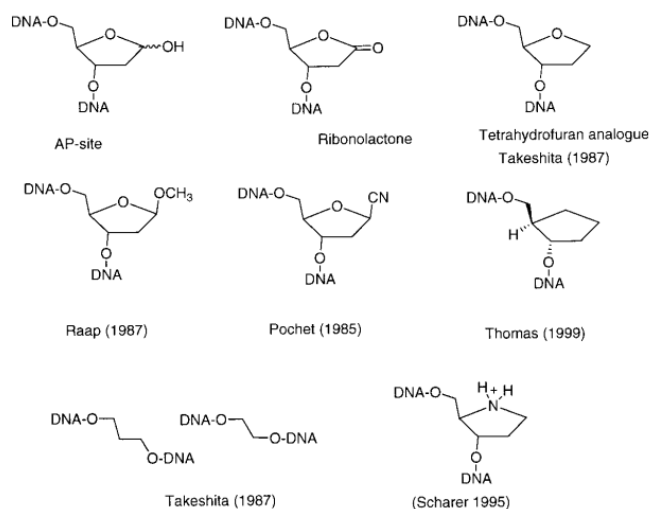
Figure 2-12. Structures of AP site and analogues.[65]
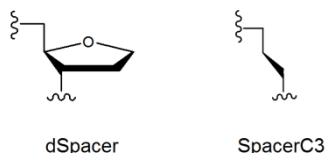
Figure 2-13. Structures of dSpacer and Spacer C3.

Besides internal- or stem-loop structures of aptamer, AP site can also be served as a suitable pocket for the binding event for target molecules. Conformational changes decrease the stability of DNA duplexes with an AP site. In order to form a more chemical stable structure, an idea came out that entering a shape suitable molecule to fill up the lesion by hydrogen bonding with the opposite base, as well as by stacking interaction and molecular shape complementary etc. If it works, this characteristic can be used to specify a certain small molecule. Here is a demonstration of an AP site-containing DNA aptamer to identify riboflavin developed by our labratory.[67]

This aptamer **23T** (23-meric; thymine as receptor nucleobase) is found to show selectivity for riboflavin over flavin mononucleotide (FMN) and flavin adenine dinucleotide (FAD). (**Figure 2-14**)
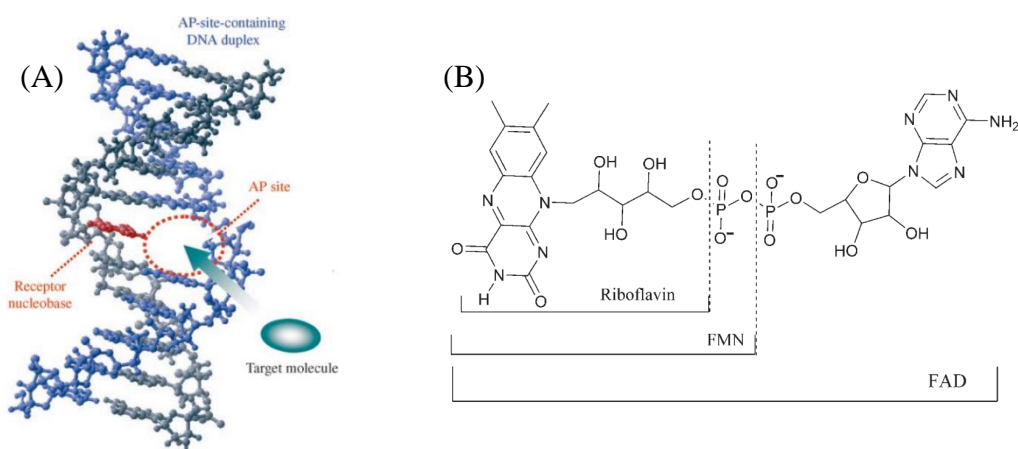
Figure 2-14. (A) Scheme of AP site-containing aptamer and (B) structures of riboflavin and its derivertives.[67]

2-1-6. Serum

Serum, clear, yellowish fluid, as the component that is neither a blood cell (serum does not contain white or red blood cells) nor a clotting factor; it is the blood plasma with the fibrinogens removed. Serum includes all proteins not used in blood clotting (coagulation) and all the electrolytes, antibodies, antigens, hormones, and any exogenous substances (e.g., drugs and microorganisms). Before clotting occurs, the liquid of the blood is called plasma. But plasma also contains the protein fibrinogen and certain other elements necessary for clotting, and it therefore clots as easily as whole blood.

Serum is used in numerous diagnostic tests, as well as in blood typing. But because the composition of serum is too complex, with hundred kinds of compounds, and the batch-to-batch variation effects the consistency of serum products, the exactly gradient and concentration of serum is still variety and under research.

2-2. Design strategy of our AP-aptamer

We designed a new modification-free AP site-containing DNA duplex aptamer (AP-aptamer) for the detection of theophylline in combination with a fluorescent ligand. As schematically shown in **Figure 2-15**, the present method is based on the competitive binding of theophylline and a fluorescent ligand (riboflavin) to the AP site of an AP-aptamer.

Here, we take riboflavin, also known as vitamin B, as the fluorescent ligand due to its binding ability to the AP-aptamer. (It can bind to thymine opposite the AP site in DNA duplexes with strong fluorescence quenching.[67,68]) First, fluorescence of riboflavin ligands bound to the AP site is strongly quenched when the AP site was flanked by guanine bases.[69] And then, when theophylline is in presence, binding of theophylline to the AP site causes the release of the fluorescent ligand from the AP site, resulting in the fluorescence restoration. And this change of signal can be measured by spectrofluorometer.
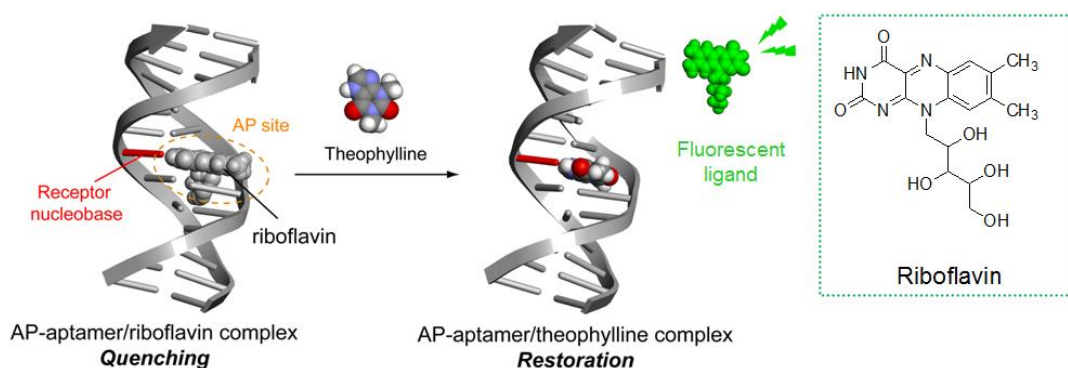
Figure 2-15. Detection scheme for theophylline by using modification-free AP-aptamer.[9]

In our previous study, modification of a DNA strand by a fluorescent nucleotide analogue, 2-aminopurine, was necessary and fluorescence quenching of 2-aminopurine was utilized for the detection of theophylline.[60] In contrast, emissive response becomes to be possible by using modification-free AP-aptamers and AP site-binding ligands according to the scheme shown in **Figure 2-15**.

In addition, riboflavin shows an emission band in the visible region (absorption maximum: 445 nm, emission maximum: 542 nm),[70] and this fluorescent property is preferable for the detection of theophylline in serum samples, since visible light excitation can reduce the background fluorescence from serum, compared to ultraviolet excitation.

2-3. Optimization of abasic site (AP site)-containing DNA duplex aptamer (AP-aptamer)

2-3-1. Abstract

We carried out a series experiments to pick out a most likely suitable AP-aptamer for the detection of theophylline, based on the competitive binding system with the fluorescent molecule-riboflavin.

The consideration of the optimization mainly concerns the following points: the type of receptor nucleobase; the type of AP site; the length of DNA sequence; the selectivity for theophylline over other compounds. And after this process, we also decided the properties of this chosen AP-aptamer, such as, binding affinity with theophylline; and the detection limit for theophylline in buffer and serum samples.

2-3-2. Experimental

2-3-2-1. Materials and instruments

Materials
DNA sequences
11-meric
5'-TCCAG$\underline{X}$GCAAC-3' (X = dSpacer, or SpacerC3), (ε_{260} = 97800 M^{-1}cm^{-1})
3'-AGGTC$\underline{C}$CGTTG-5' (ε_{260} = 105720 M^{-1}cm^{-1})
3'-AGGTC$\underline{T}$CGTTG-5' (ε_{260} = 106160 M^{-1}cm^{-1})
3'-AGGTC$\underline{A}$CGTTG-5' (ε_{260} = 110580 M^{-1}cm^{-1})
3'-AGGTC$\underline{G}$CGTTG-5' (ε_{260} = 108240 M^{-1}cm^{-1})

23-meric
5'-TCTGCGTCCAG$\underline{X}$GCAACGCACAC-3' (X = dSpacer, or SpacerC3), (ε_{260} = 206380 M^{-1}cm^{-1})
3'-AGACGCAGGTC$\underline{C}$CGTTGCGTGTG-5' (ε_{260} = 219980 M^{-1}cm^{-1})
3'-AGACGCAGGTC$\underline{T}$CGTTGCGTGTG-5' (ε_{260} = 220420 M^{-1}cm^{-1})

All of the DNA samples were custom synthesized and HPLC purified (>97%) by Nihon

Gene Research Laboratories Inc. (Sendai, Japan). The extinction coefficients at 25°C were calculated at 260 nm for each strand[71], which was shown in bracket above.

Riboflavin and theophylline were purchased from Aldrich Chemical Co., (Milwaukee, WI) and Wako Pure Chemical Industries, Ltd (Tokyo, Japan), respectively, and they were used as received.

Horse serum was purchased from Kohjin Bio Co., (Saitama, Japan).

The other reagents were commercially available analytical grade and were used without further purification. Water was deionized (≥18.0 MΩ cm specific resistance) by an Elix 5 UV Water Purification System and a Milli-Q Synthesis A10 system (Millipore Corp., Bedford, MA).

Instruments

Fluorescence measurement: Fluorescence spectra were measured with a JASCO model FP-6500 spectrofluorophotometer equipped with a thermoelectrically temperature-controlled cell holder (Japan Spectroscopic Co. Ltd., Tokyo, Japan). It was previously found that the binding affinity of pterin with guanine opposite an AP site increased more than 10 times at 5°C compared to 20°C.[72] Accordingly, fluorescence measurements were carried out at 5°C using a 3 × 3 mm quartz cell. Excitation wavelength for riboflavin was set at 448 nm, which was the maximum absorption wavelength of riboflavin.

UV measurement: JASCO model V-570 spectrophotometer.

Preparation of stock solutions

DNA solutions: The concentrations of DNAs were determined from the molar extinction coefficients at 260 nm. Stock solutions were prepared with miliQ water to 250 μM and stored at 4°C.

Buffer solution: Stock solution was prepared in 100 ml miliQ water and containing sodium cacodylate (1.071g, 50 mM), NaCl (2.935g, 500 mM), EDTA (0.187g, 5.0 mM), and stored at 4°C. When applied it into tubes, it was 5 times diluted, which made the standard buffer solution's concentration as follows: [sodium cacodylate] = 10 mM, [NaCl] = 100 mM, [EDTA] = 1.0 mM.

Sodium cacodylate buffer solution: Stock solution was prepared in 25 ml miliQ water and containing sodium cacodylate (263.47 mg, 50 mM), and stored at 4°C.

(-)-Riboflavin solution: Stock solution was prepared in 50 ml miliQ water and containing riboflavin (1.38 mg, 73.33 μM), and stored at 4°C.

Theophylline solution: Stock solution was prepared in 100 ml miliQ water and containing theophylline (54.9 mg, 3.05 mM), and stored at 4°C.

Caffeine solution: Stock solution was prepared in 50 ml miliQ water and containing caffeine (9.92 mg, 1.02 mM), and stored at 4°C.

Theobromine solution: Stock solution was prepared in 50 ml miliQ water and containing theobromine (9.50 mg, 1.05 mM), and stored at 4°C.

Uric acid solution: Stock solution was prepared in 50 ml miliQ water and containing uric acid (8.78 mg, 1.04 mM), and stored at 4°C.

Creatinine solution: Stock solution was prepared in 50 ml miliQ water and containing creatinine (5.77 mg, 1.02 mM), and stored at 4°C.
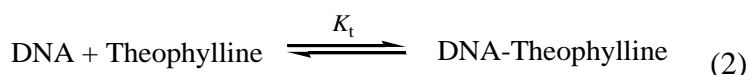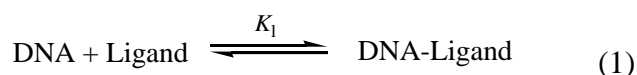
D(+)-glucose solution: Stock solution was prepared in 50 ml miliQ water and containing glucose (9.83 mg, 1.09 mM), and stored at 4°C.

Experiment conditions

In Chapter 2, unless otherwise mentioned, all measurements were performed in standard buffer solution: 10 mM sodium cacodylate buffer solutions (pH 7.0) containing 100 mM NaCl and 1.0 mM EDTA. Before measurements, the sample solutions were annealed as follows: heated at 75°C for 10 min, and gradually cooled to 5°C (3°C/min), after which the solution temperature was raised again to 20°C.

2-3-2-2. Determination of binding constants of DNA-theophylline interactions based on the competitive binding model.

The competitive binding system is considered as the combination of two 1:1 binding events including DNA-riboflavin interactions and DNA-theophylline interactions. Then, the following equilibria are considered to describe the present system.

$$\text{DNA} + \text{Ligand} \xrightleftharpoons{K_l} \text{DNA-Ligand} \qquad (1)$$

$$\text{DNA} + \text{Theophylline} \xrightleftharpoons{K_t} \text{DNA-Theophylline} \qquad (2)$$

$$K_l = [\text{DNA-Ligand}]/[\text{DNA}][\text{Ligand}] \qquad (3)$$

$$K_t = [\text{DNA-Theophylline}]/[\text{DNA}][\text{Theophylline}] \qquad (4)$$

Total concentrations of DNA (C_d), Ligand (C_l), Theophylline (C_t) can be expressed by the following equations:

$$C_d = [\text{DNA}] + [\text{DNA-Ligand}] + [\text{DNA-Target}] \qquad (5)$$

$$C_l = [\text{Ligand}] + [\text{DNA-Ligand}] \qquad (6)$$

$$C_t = [\text{Target}] + [\text{DNA-Target}] \qquad (7)$$

By combining the equations (3)-(7), C_t can be expressed as follows:

$$C_t = (C_l - [\text{Ligand}] - C_d K_l [\text{Ligand}] + C_l K_l [\text{Ligand}] - K_l [\text{Ligand}]^2)/ K_l K_t [\text{Ligand}] ([\text{Ligand}] - C_l) \qquad (8)$$

On the other hand, the fluorescence intensity can be interpreted as the sum of each contribution as follows:

$$F = k_d [\text{DNA}] + k_l [\text{Ligand}] + k_t [\text{Target}] + k_{dl} [\text{DNA-Ligand}] + k_{dt} [\text{DNA-Target}] \qquad (9)$$

where the k represents proportionality constants connecting the fluorescence intensities and concentrations of the species (k_d: free DNA, k_l: free ligand, k_t: free target, k_{dl}: 1:1 DNA-ligand complex, k_{dt}: 1:1 DNA-target complex). In this equation, free DNA, free target, and DNA-target complex are not fluorescent components. In addition, the DNA-ligand complex is also assumed as no contributor based on the fact that this complex shows almost no fluorescence when all riboflavin molecule forms the complex with DNA molecules at the high excess DNA concentration[59,60] and then, equation (9) can be rewritten by the following simple form:

$$F = k_l [\text{Ligand}] \qquad (10)$$

Using the relationship of the fluorescence intensity of a ligand in the absence of DNA

and target ($F_0 = k_1 C_1$), the following equation can be derived.

$$F/F_0 = [\text{Ligand}]/C_1 \qquad (11)$$

Together, equations (8) and (11) describe the present system. And the plot of C_t versus F/F_0 was fitted by the equation combined equations (8) and (11), which gives the value of K_t.

2-3-3. Results and discussions

2-3-3-1. Properties of riboflavin

## 2-3-3-1-1. Basic properties of riboflavin

To determine the fluorescence characteristics of riboflavin, we examined UV and fluorescence excitation / emission spectra under our standard buffer conditions.

We calculated the molar extinction coefficient (11753 $M^{-1}cm^{-1}$) from **Figure 2-16**, and determined the maximum absorption wavelength as 448 nm.
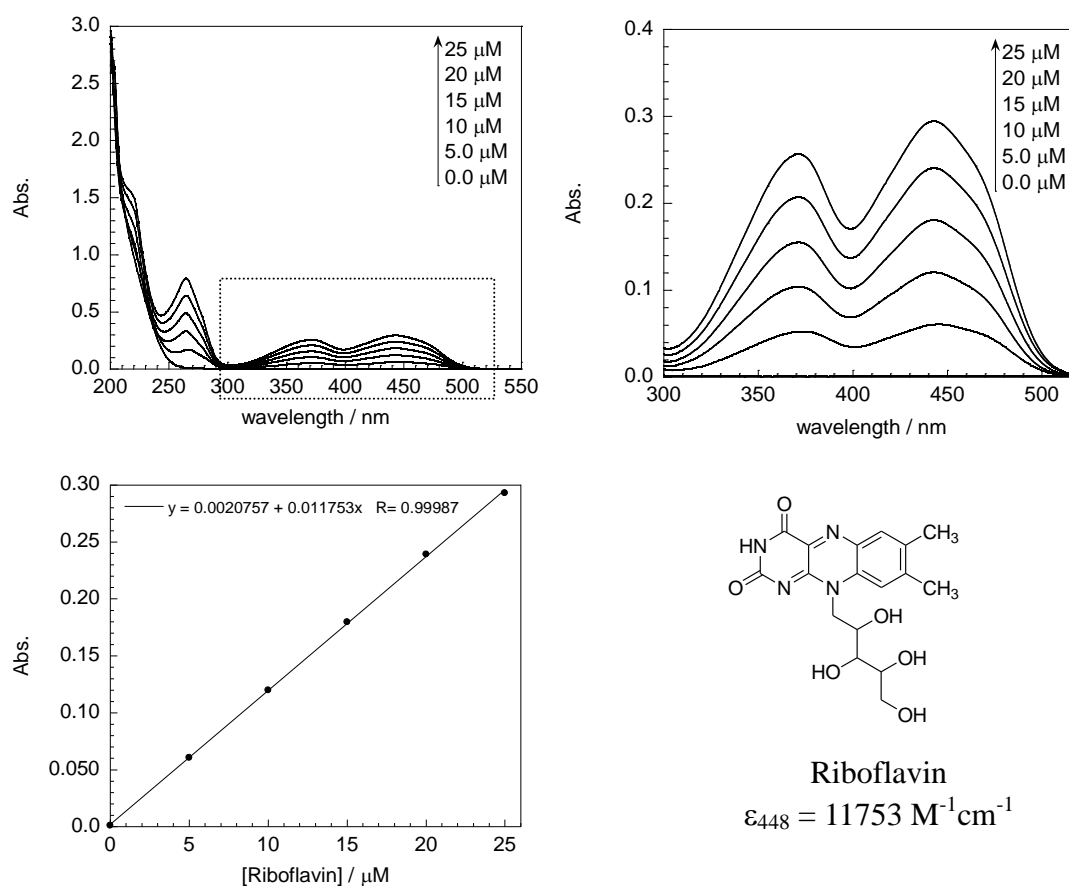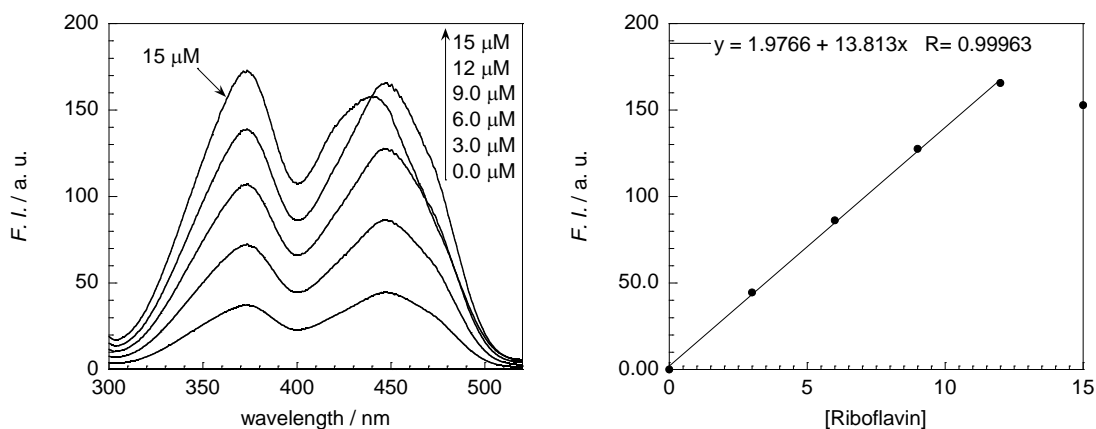

Figure 2-16. UV spectra of riboflavin.

[riboflavin] = 0, 5, 10, 15, 20, 25 μM, buffer, pH 7.0, 20°C, 10×10 mm quartz cell (optical path length: 10 mm), Analysis: 448 nm.
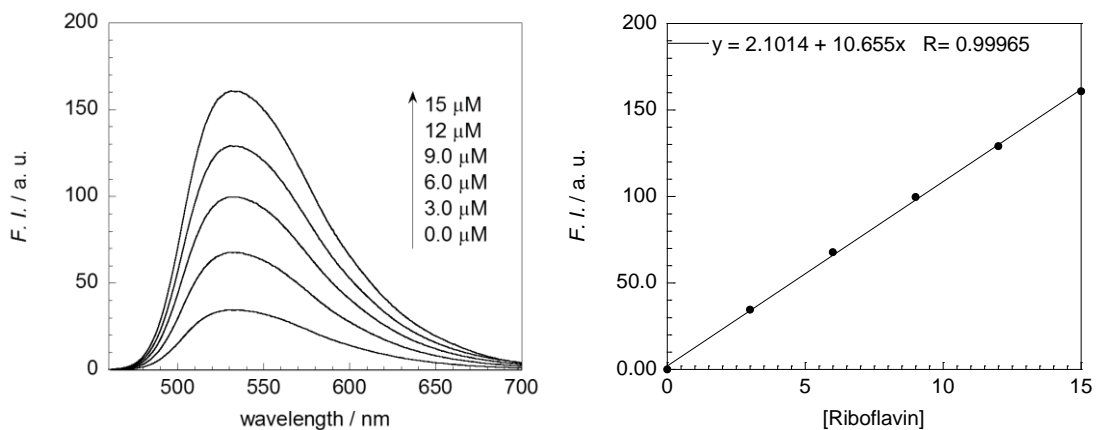
Figure 2-17. Emission spectra of riboflavin.

[riboflavin] = 0, 3, 6, 9, 12, 15 µM, buffer, pH 7.0, 20°C, 3×3 mm quartz cell, Excitation: 448 nm, Analysis: 530 nm.


Figure 2-18. Excitation spectra of riboflavin.

[riboflavin] = 0, 3, 6, 9, 12, 15 µM, buffer, pH 7.0, 20°C, 3×3 mm quartz cell, Excitation: 448 nm, Analysis: 448 nm.

2-3-3-1-2. Comparison of the excitation wavelength

We got an isosbestic point (478nm) by UV spectra (**Figure 2-19**) when adding 11-mer AP-aptamer and theophylline into the riboflavin solution. In order to compare the effect of excitation wavelength, we took fluorescence measurements under the maximum absorption wavelength (448nm, **Figure 2-20**) and the isosbestic point wavelength (478nm, **Figure 2-21**), and the results were listed in **Table 2-3**.
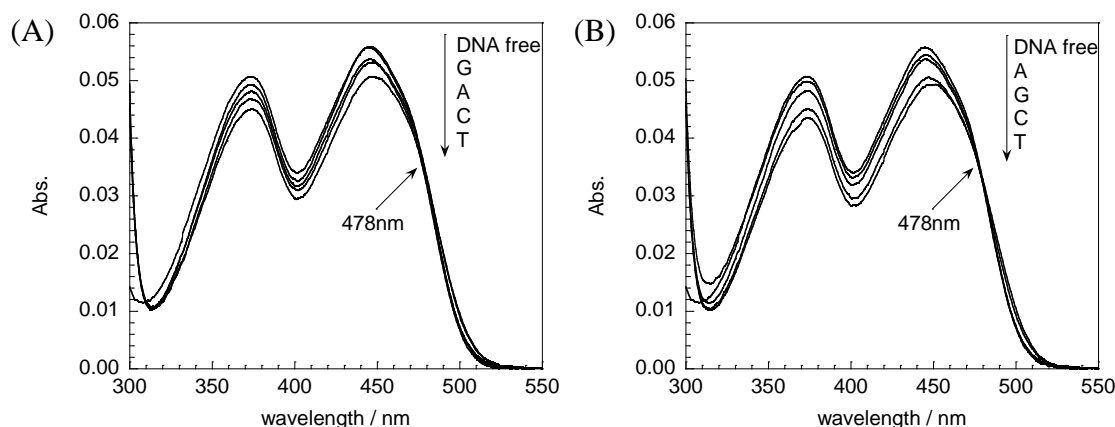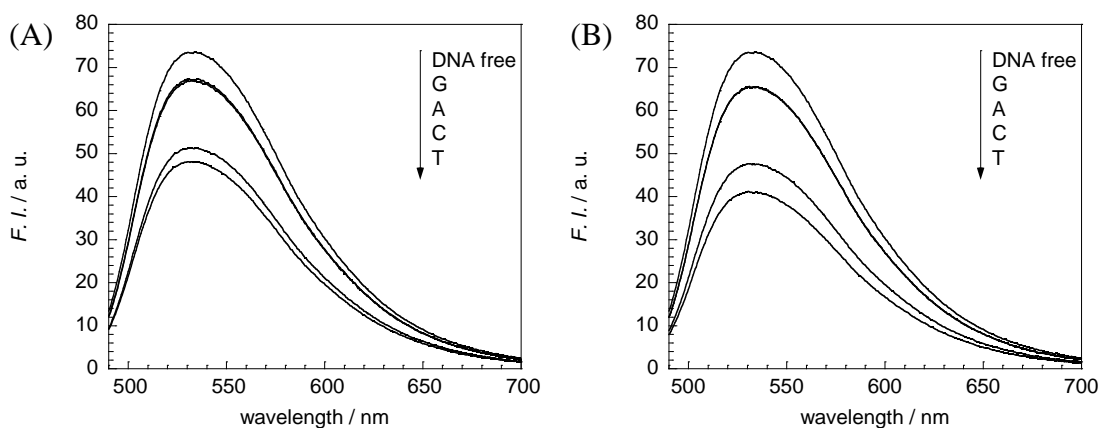

Figure 2-19. UV spectra for AP-aptamer and riboflavin interactions: (A) dSpacer, (B) SpacerC3. [11-mer AP-aptamer] = 5.0 M, [riboflavin] = 5.0 M, buffer, pH 7.0, 20°C, 1×10 mm quartz cell (optical path length: 10 mm).
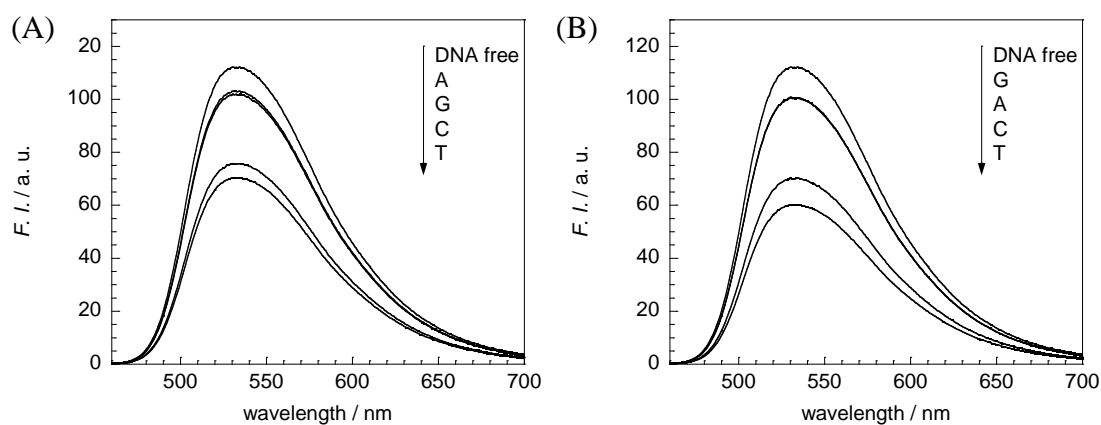
Figure 2-20. Fluorescent spectra excited at 448 nm: (A) dSpacer, (B) SpacerC3. [11-mer AP-aptamer] = 10 μM, [riboflavin] = 10 μM, buffer, pH 7.0, 20°C, 3×3 mm quartz cell, Analysis: 530 nm.

Figure 2-21. Fluorescent spectra excited at 478 nm: (A) dSpacer, (B) SpacerC3.

[11-mer AP-aptamer] = 10 μM, [riboflavin] = 10 μM, buffer, pH 7.0, 20°C, 3×3 mm quartz cell, Analysis: 530 nm.

F/F_0		Ex.448nm	Ex.478nm
dSpacer	G	0.91	0.91
	C	0.67	0.70
	A	0.92	0.91
	T	0.63	0.65
SpacerC3	G	0.90	0.89
	C	0.63	0.65
	A	0.90	0.89
	T	0.54	0.56

Table 2-3. Comparison of the fluorescent ratio excited at maximum absorption wavelength (448nm) and the isosbestic point wavelength (478nm), respectively.

F_0: DNA free in solution (only riboflavin; without AP-aptamers).

From the listed data of **Table 2-3**, we can get the conclusion that there is rarely difference by using these two excitation wavelengths, respectively. We chose the maximum absorption wavelength (448 nm) as the excitation wavelength by tradition.

2-3-3-1-3. Effect of temperature

We took out experiments under room temperature (20°C) and decreased temperature (5°C), and the results turned out the measurements at lower temperature gave out more efficient quenching signals, especially for C and T (**Figure 2-22**). In order to get a clearly quenching, we chose 5°C as the measurement temperature for further experiments. However, it should be pointed out that our system is applicable at various temperatures including room

temperature, but not only at 5°C.

It probably can be explained in this way: At a low temperature, the DNA duplexes are more stable and thus the DNA-riboflavin complexes should be more stable. In contrast, as the temperature rises up, more and more DNA duplexes would have a trend to separate to single strands. As a result, the adoption pockets for riboflavin decreases, which leads to the quenching less efficiency.
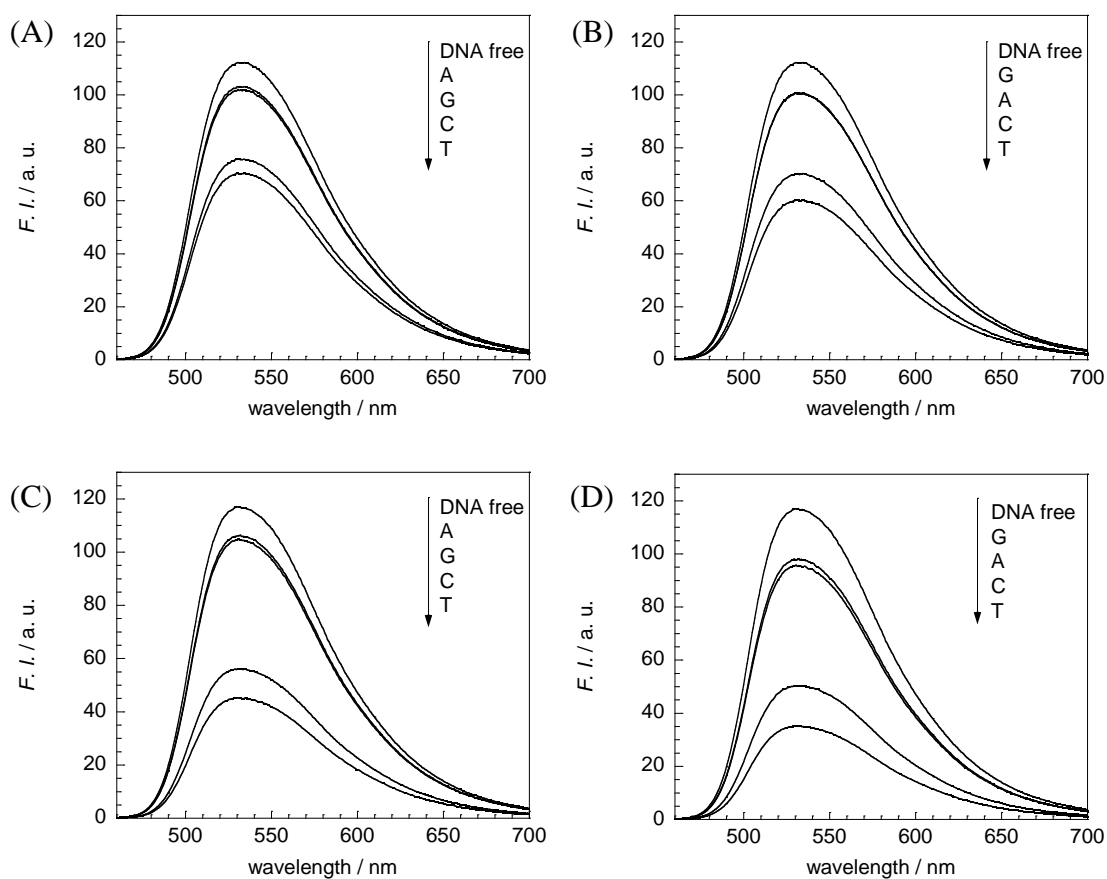
Figure 2-22. Fluorescence spectra at 20°C (A, B) and 5°C (C, D).

(A), (C): dSpacer; (B), (D): SpacerC3.

[11-mer AP-aptamer] = 10 μM, [riboflavin] = 10 μM, buffer, pH 7.0, 20°C or 5°C, 3×3 mm quartz cell, Excitation: 448 nm.

## 2-3-3-2. Optimization of aptamer: the receptor nucleobase

For the optimization of aptamer, first, we examined the fluorescence response of riboflavin (10 μM) upon addition of 11-mer AP-aptamers (10 μM; 5'-TCCAG$\underline{X}$GCAAC-3'/ 3'-AGGTC$\underline{N}$CGTTG-5', $\underline{X}$ = Spacer C3, $\underline{N}$ = G, C, A or T) having guanine (**11G**), cytosine (**11C**), adenine (**11A**), or thymine (**11T**) as a receptor nucleobase in a standard buffer solution of pH 7.0.

As shown in **Figure 2-23** (A)-(D), riboflavin shows fluorescence quenching ability for AP-aptamers with all four kinds of receptor nucleobases. However, the quenching degree various, suggesting the binding of riboflavin at AP site depends on the type of receptor nucleobase.

The fluorescence quenching of riboflavin is most significant for **11T** (**Figure 2-23(D)**), followed with **11C** (**Figure 2-23(B)**), while the response is small for **11G** (**Figure 2-23(A)**) and **11A** (**Figure 2-23(C)**).

The fluorescence restoration was examined by adding 100 μM theophylline. Again, **11C** and **11T** exhibit significant fluorescence restoration upon addition of theophylline, while there are only moderate responses for **11G** and **11A**. This strong response of **11C** and **11T** can be ascribed to the exchange and release of riboflavin from the competitive binding with theophylline.

These results show that the combination of riboflavin with **11C** or **11T** is likely to be suitable for further experiments.
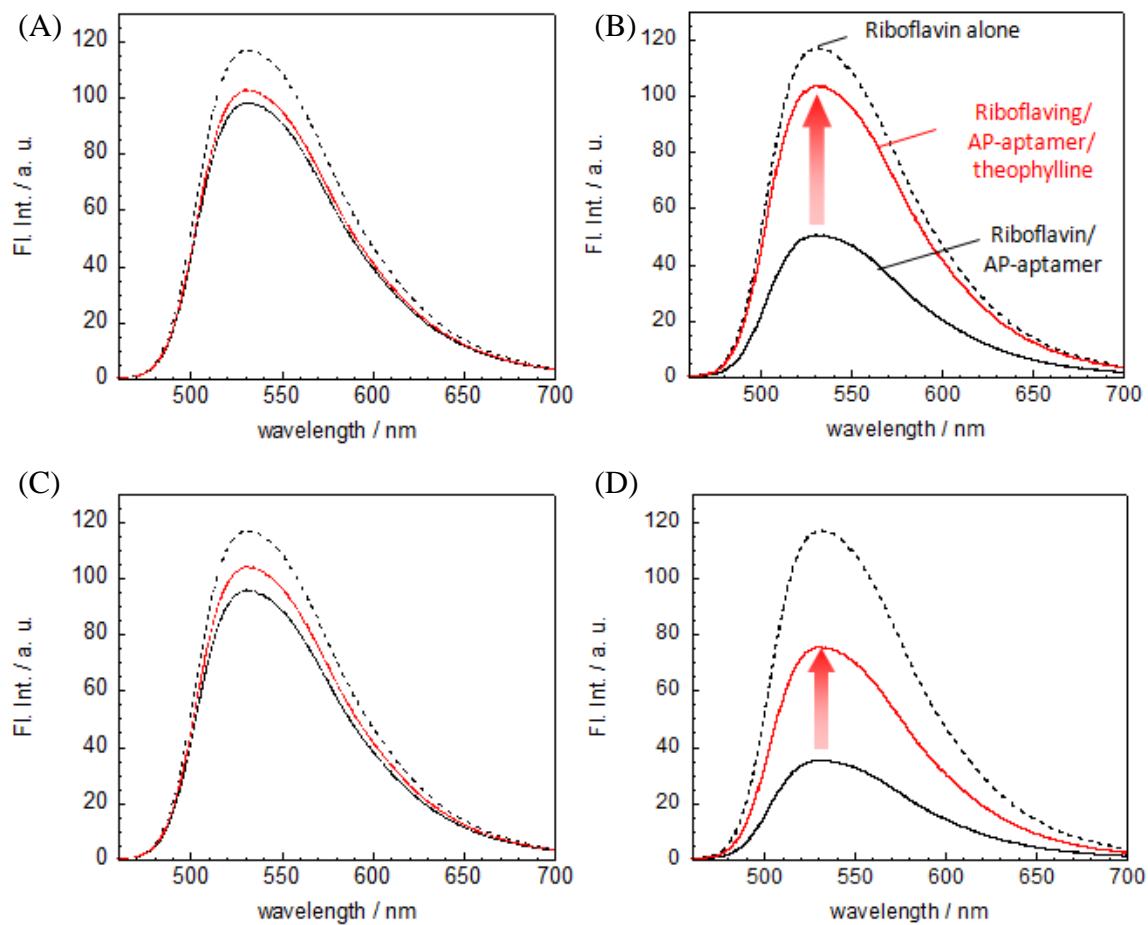
Figure 2-23. Fluorescence spectra of riboflavin in the absence (black dot line) and presence (black solid line) of 11-mer AP-aptamers: (A) **11G**, (B) **11C**, (C) **11A**, and (D) **11T**.
Fluorescence responses of riboflavin with AP-aptamers to theophylline are also shown (red solid line).

[11-mer AP-aptamer] = 10 μM, [riboflavin] = 10 μM, [theophylline] = 100 μM, buffer, pH 7.0, 5°C, Excitation: 448 nm.

We also measured the melting temperatures of 11-mer AP-aptamers (10 μM) with and without theophylline (50 μM). The data was summarized in **Table 2-4**. Although all sequences reached a higher melting temperature after adding theophylline, which means the complexes are more stable than DNA duplexes alone, **11C** and **11T** show a higher ΔT_m comparing to **11G** and **11A**. Therefore, **11C** and **11T** are likely more suitable for further investigation. This result is in accordance with our previous conclusion, which derived from the fluorescence spectra.

		T_m (-)	T_m (+)	ΔT_m
dSpacer	G	30.8 ±0.1	31.6 ±1.1	0.8
	C	26.2 ±0.5	28.2 ±0.2	**2.0**
	A	31.5 ±0.8	32.3 ±0.2	0.8
	T	25.5 ±0.1	28.5 ±0.5	**3.0**
SpacerC3	G	31.0 ±0.7	32.7 ±0.1	1.7
	C	26.0 ±0.4	28.8 ±0.2	**2.8**
	A	30.3 ±0.6	31.2 ±0.6	0.9
	T	23.7 ±0.5	28.4 ±0.2	**4.7**

**Table 2-4.** Melting temperature of 11-mer AP-aptamers and theophylline complex ($n = 3$).

[11-mer AP-aptamer] = 10 μM, [theophylline] = 50 μM, buffer, pH 7.0, 8 cells micro-multicell holder (optical path length: 1 mm), Shimadzu UV-2450 UV/Visible Spectrophotometer.

T_m (-) represents the melting temperature of only 11-mer AP-aptamer, and T_m (+) represents the melting temperature of 11-mer AP-aptamers and theophylline complex. Therefore, ΔT_m shows the changed value, $\Delta T_m = T_m$ (+)-T_m (-).

2-3-3-3. Effect of the type of AP site on the AP-aptamer

When we used dSpacer as the AP site of 11-mer AP-aptamers instead of Spacer C3, the fluorescence response upon addition of theophylline (**Figure 2-24**) was similar to those shown in **Figure 2-23**. But the response is slightly smaller for dSpacer than that for Spacer C3 (**Table 2-5**). Therefore, Spacer C3 was considered to be better in the further experiments.
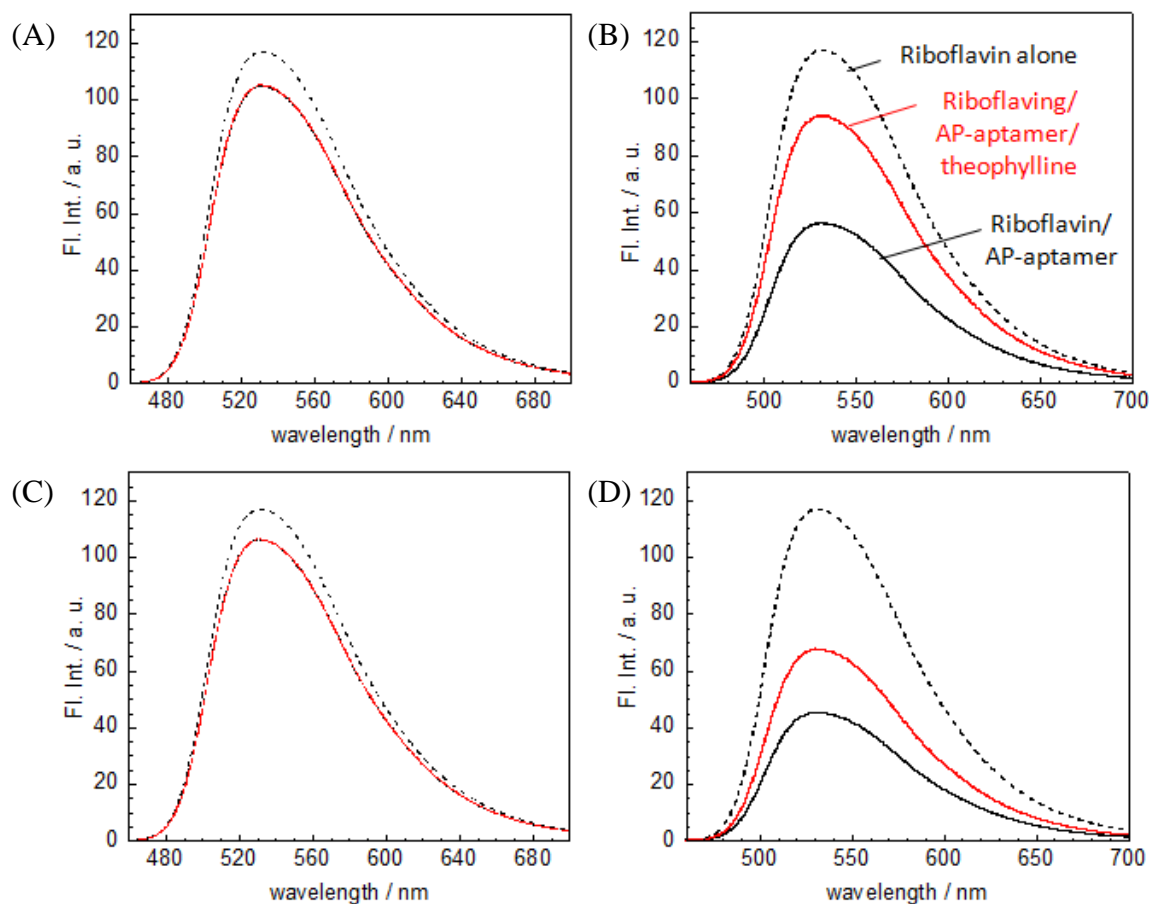
Figure 2-24. Fluorescence spectra by using dSpacer as an AP site.

(A) **11G**, (B) **11C**, (C) **11A**, and (D) **11T**.

All other conditions are as same as given in Figure 2-23.

[11-mer AP-aptamer] = 10 μM, [riboflavin] = 10 μM, [theophylline] = 100 μM, buffer, pH 7.0, 5°C, Excitation: 448 nm.

From **Table 2-5**, it is clear that all four kinds of receptor nucleobases show larger recovery ability when oppositing place is a SpacerC3 type AP site. In addition, C and T show 13% and 15% enlarging by using SpacerC3 than dSpacer, respectively, which cannot be ignored.

	SpacerC3				dSpacer				Recovery ratio %	
	F. I.	Q %	F. I.	R %	F. I.	Q %	F. I.	R %	SpacerC3	dSpacer
G	97.84	83.7	102.70	87.8	104.50	89.4	104.92	89.7	4.1	0.3
C	50.26	43.0	103.52	88.5	55.98	47.9	93.84	80.2	**45.5**	**32.3**
A	95.60	81.7	103.97	88.9	106.05	90.7	106.25	90.9	7.2	0.2
T	35.12	30.0	75.34	64.4	45.14	38.6	67.45	57.7	**34.4**	**19.1**

Table 2-5. Comparison of quenching and restoration efficiency by using SpacerC3 and dSpacer. F.I. represents fluorescence intensity; Q represents quenching efficiency; R represents recovery efficiency, respectively. The percentages come from the fluorescence intensity of each value versus the value when only riboflavin existed in buffer solution. Analysis: 530 nm.

2-3-3-4. Selectivity for theophylline (Comparison with related molecules)

Next, we examined the fluorescence response to the structurally-related methylxanthine derivatives including caffeine and theobromine, and the molecules present in serum (**Figure 2-25**).

Significantly, riboflavin/**11C** shows little response to either caffeine or theobromine and the responses to other molecules such as uric acid, creatinine, and D-glucose that are present in serum are only negligible (**Figure 2-26(A)**).

On the other hand, riboflavin/**11T** exhibits the effective fluorescence response to not only theophylline but also caffeine and theobromine whereas almost no or moderate response are observed for other substrates (**Figure 2-26(B)**).

By now, we successfully obtain a clear and selective response of riboflavin/**11C** for the fluorescence detection of theophylline. Such highly selectivity for theophylline can be ascribed to the possible formation of the hydrogen bonding between theophylline and the receptor cytosine nucleotide at the AP site of **11C**,[60] similarly to the recognition of theophylline by RNA aptamers.[23,43,44] Whereas for caffeine or theobromine, the single methyl group attached to the xanthine ring restricts the forming of hydrogen bondings.
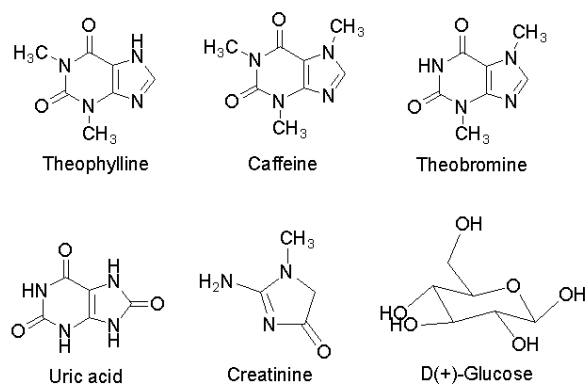
Figure 2-25. Structures of theophylline, caffeine, theobromine and other compounds existed in serum.
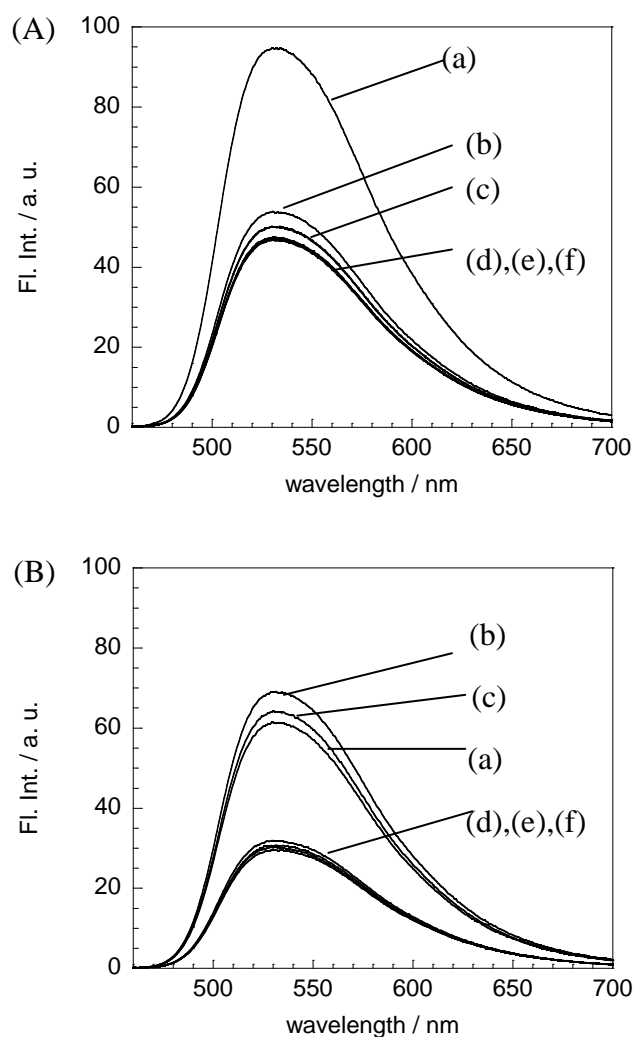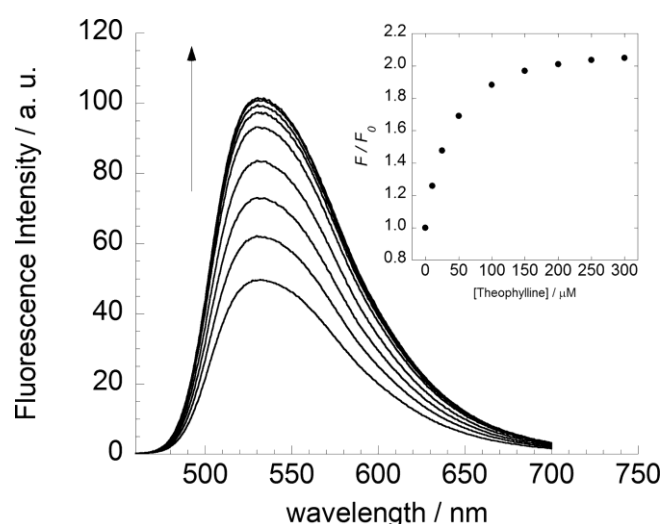

Figure 2-26. Fluorescence responses of (A) riboflavin/**11C** and (B) riboflavin/**11T** to target molecules: (a) theophylline, (b) caffeine, (c) theobromine, (d) uric acid, (e) creatinine, and (f) glucose. [11-mer AP-aptamer] = 10 μM, [riboflavin] = 10 μM, [Target] = 100 μM, buffer, pH 7.0, 5°C, Excitation: 448 nm.

2-3-3-5. Determination of the binding affinity between 11C and theophylline

The binding affinity of **11C** to theophylline was quantitatively assessed by the fluorescence titration experiments, for which changes in the fluorescence intensity of riboflavin/**11C** were measured with increasing the concentration of theophylline. As shown in **Figure 2-27**, the fluorescence response of riboflavin/**11C** to theophylline is concentration-dependent. The resulting titration curve is well analyzed by the competitive binding model including **11C**-riboflavin and **11C**-theophylline interactions (**Figure 2-28**). For this analysis, we used the 1:1 binding affinity of **11C** to riboflavin (K_l) of $(3.6 \pm 0.1) \times 10^5$ M^{-1} (n = 3) that was independently determined from fluorescence titration experiments (**Figure 2-29**). By using this value of K_l, the 1:1 binding affinity of **11C** to theophylline (K_t) was then determined as $(1.1 \pm 0.1) \times 10^5$ M^{-1} (n = 3). This gives the dissociation constant (K_d = $1/K_t$) of 9.1 μM, which is comparable to that of our previous 2-aminopurine modified DNA duplex aptamer (K_d = 10 μM).[60]

Figure 2-27. Fluorescence responses of riboflavin/**11C** to theophylline.[9]

Inset: Fluorescence intensity change at 530 nm of riboflavin/**11C** upon addition of theophylline. F and F_0 denote the fluorescence intensities of riboflavin/**11C** in the presence and absence of theophylline, respectively.
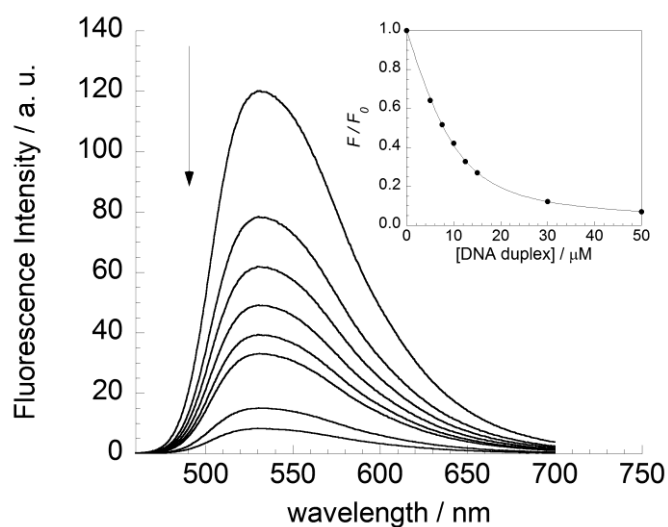
[**11C**] = 10 μM, [riboflavin] = 10 μM, [theophylline] = 0-300 μM, buffer, pH 7.0, 5°C, Excitation: 448 nm, Analysis: 530 nm.
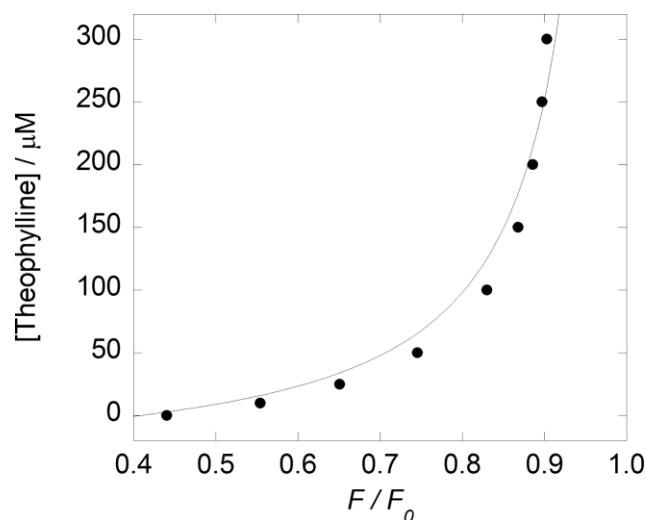
Figure 2-28. Non-linear regression analysis of the changes in the fluorescence intensity ratio at 530 nm of riboflavin/**11C** upon addition of theophylline.[9]

Other solution conditions are the same as those given in Figure 2-27.

F and F_0 denote the fluorescence intensities of riboflavin in the presence and absence of both DNAs and theophylline, respectively.

Figure 2-29. Fluorescence response of riboflavin (10 μM) to **11C**.[9]

Inset: Non-linear regression analysis of the changes in the fluorescence intensity ratio at 530 nm based on a 1:1 binding isotherm model.[73]

F and F_0 denote the fluorescence intensities of riboflavin in the presence and absence of DNA duplexes, respectively.

[**11C**] = 0, 5, 7.5, 10, 12.5, 15, 30, 50 μM, [riboflavin] = 10 μM, buffer, pH 7.0, 5°C, Excitation: 448 nm, Analysis: 530 nm.

2-3-3-6. Optimization of DNA's length

Since the binding affinity of AP site-binding ligands to the receptor nucleotide opposite the AP site depends on the length of DNA duplexes,[3] we examined the fluorescence response to theophylline by utilizing 23-mer (**23C**; 5'-T CTG CGT CCA G$\underline{X}$G CAA CGC ACA C-3'/ 3'-A GAC GCA GGT C$\underline{C}$C GTT GCG TGT G-5', X = SpacerC3), 35-mer (**35C**; 5'-A TAA CGT CTG CGT CCA G$\underline{X}$G CAA CGC ACA CAC GCA T-3'/ 3'-T ATT GCA GAC GCA GGT C$\underline{C}$C GTT GCG TGT GTG CGT A-5', X = SpacerC3), and 47-mer (**47C**; 5'-CAGC CGA TAA CGT CTG CGT CCA G$\underline{X}$G CAA CGC ACA CAC GCA TAT GTGC-3'/ 3'-GTCG GCT ATT GCA GAC GCA GGT C$\underline{C}$C GTT GCG TGT GTG CGT ATA CACG-5' , X = SpacerC3) AP-aptamer having cytosine as the receptor nucleobase.

23C, **35C** and **47C**/riboflavin complexes show stronger fluoresence quenching and restoration ability than **11C**/riboflavin, sugguesing longer DNAs are preferred. However, compared with **23C**, longer DNAs (**35C** and **47C**) didn't show better performance upon addition of theophylline (**Figure 2-30**). Therefore, we consider 23-mer is a proper length of AP-aptamer for further experiments.
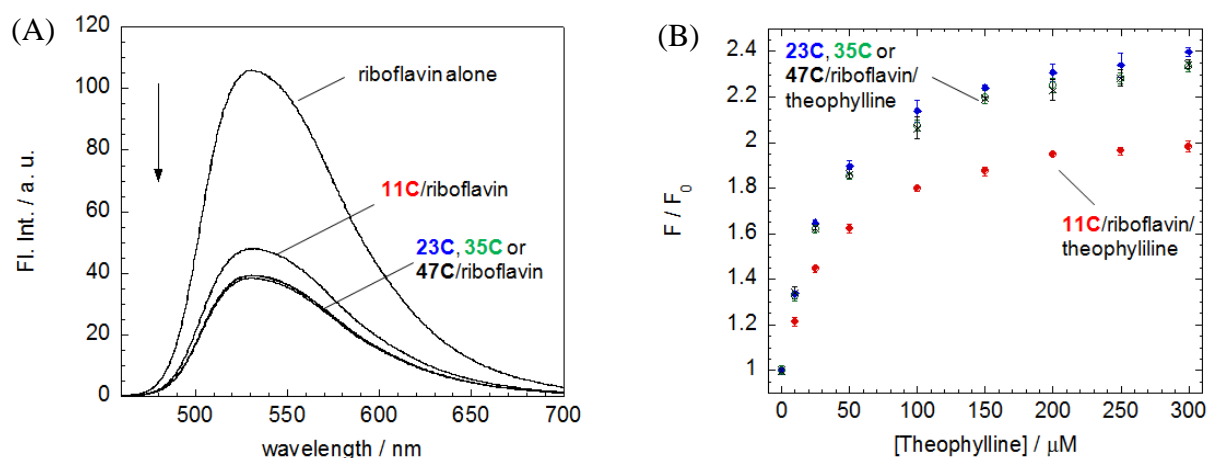

Figure 2-30. (A) Fluorescence quenching spectra of the complex of riboflavin with 11C, 23C, 35C, or 47C; (B) Fluorescence restoration upon addition of theophylline.

[DNA duplex] = 10 μM, [riboflavin] = 10 μM, [theophylline] = (A) 10 μM; or (B) 0, 10, 25, 50, 100, 150, 200, 250, 300 μM, buffer, pH 7.0, 5°C, 3×3 mm quartz cell, Ex band: 3 nm, Em band: 3 nm, Excitation: 448 nm, Analysis:530 nm. F_0 : without target.

2-3-3-7. Determination of the binding affinity between **23C** and theophylline

We examined the affinities of 23-mer AP-aptamers (**23C**) to riboflavin (**Figure 2-31**) and theophylline (**Figure 2-32**) by the fluorescence titration experiments. As compared to the affinity of **11C** to riboflavin, the affinity of **23C** slightly increases ($K_1 = (4.3 \pm 0.2) \times 10^5$ M^{-1}, $n = 3$). And the affinity of riboflavin/**23C** to theophylline ($K_t = (1.2 \pm 0.1) \times 10^5$ M^{-1}, $n = 3$) is comparable with that of **11C** (**Table 2-6**). Although the observed the binding affinity varies not so much, the stronger binding affinity of riboflavin-**23C** leads to the more efficient quenching signaling for a clear detection of theophylline in our assay.
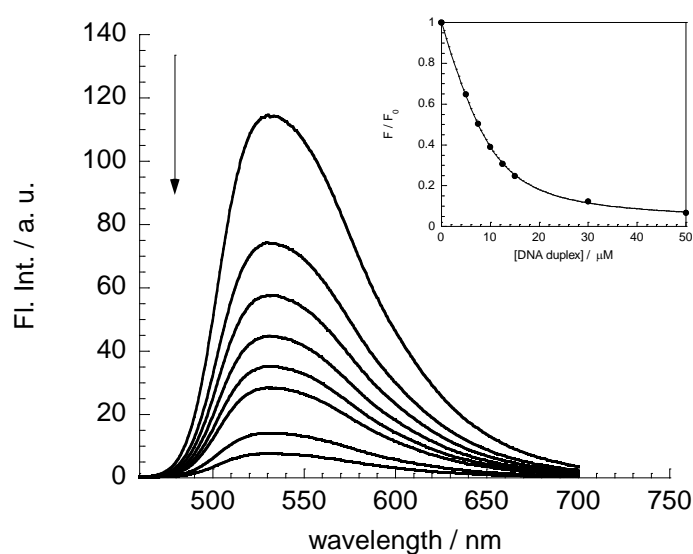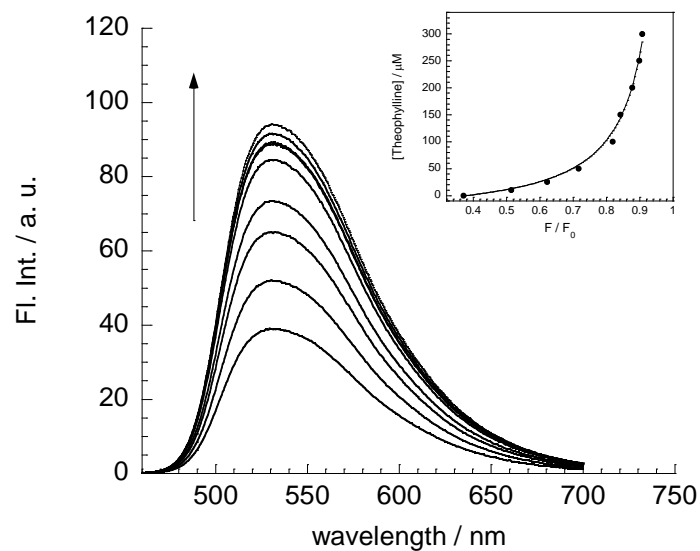

Figure 2-31. Fluorescence response of riboflavin (10 μM) to **23C**.

Inset: Non-linear regression analysis of the changes in the fluorescence intensity ratio at 530 nm based on a 1:1 binding isotherm model.[73]

F and F_0 denote the fluorescence intensities of riboflavin in the presence and absence of DNA duplexes, respectively.

[**23C**] = 0, 5, 7.5, 10, 12.5, 15, 30, 50 μM, [riboflavin] = 10 μM, buffer, pH 7.0, 5°C, Excitation: 448 nm, Analysis: 530 nm.

Figure 2-32. Fluorescence responses of riboflavin (10.0 μM)/**23C** (10.0 μM) to theophylline (0-300 μM). Inset: Non-linear regression analysis of the changes in the fluorescence intensity ratio at 530 nm based on the competitive binding model.

F and F_0 denote the fluorescence intensities of riboflavin in the presence and absence of both DNAs and theophylline, respectively.

[**23C**] = 10 μM, [riboflavin] = 10 μM, [theophylline] = 0, 10, 25, 50, 100, 150, 200, 250, 300 μM, buffer, pH=7.0, 5°C, Excitation: 448 nm, Analysis: 530 nm.

K_{11} ($n = 3$)	**11C**	**23C**
AP-aptamer/riboflavin ($10^5 M^{-1}$)	3.6 ± 0.1	4.3 ± 0.2
AP-aptamer/theophylline ($10^5 M^{-1}$)	1.1 ± 0.1	1.2 ± 0.1

Table 2-6. Binding constants for **11C** and **23C**

2-3-3-8. Binding selectivity and limit of detection of **23C**

Importantly, riboflavin/**23C** shows high selective response to theophylline in the concentration range of 10 to 250 μM (**Figure 2-33**) over caffeine and theobromine, similarly to riboflavin/**11C**. This result indicates that highly selectivity to theophylline is maintained irrespective of the DNA length. Therefore, it can be concluded that **23C** qualifies as a promising DNA duplex for further experiments.
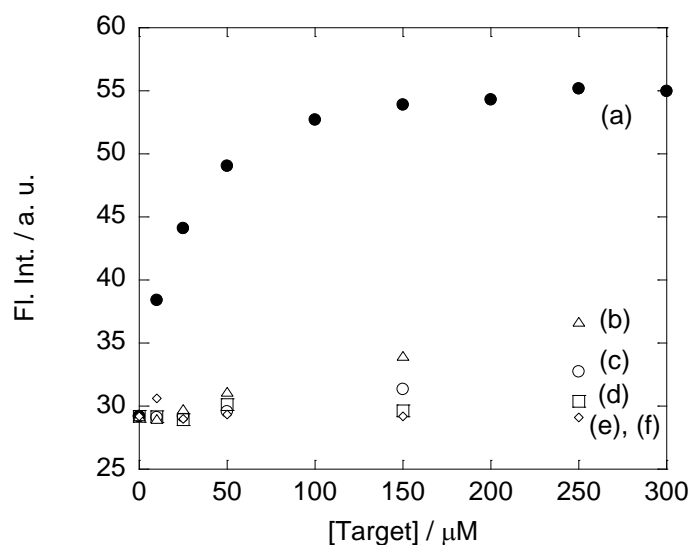
Figure 2-33. Fluorescence responses of riboflavin (5.0 μM)/**23C** (5.0 μM) to target molecules (0-250 μM): (a) theophylline, (b) caffeine, (c) theobromine, (d) uric acid, (e) creatinine, and (f) glucose.
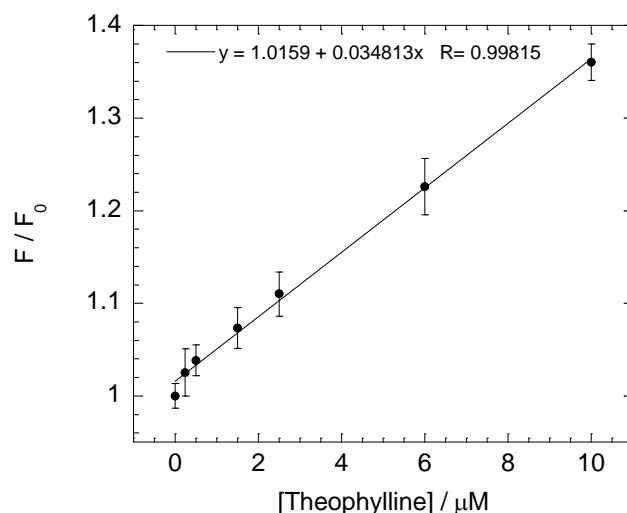F and F_0 denote the fluorescence intensities of riboflavin/**11C** in the presence and absence of target, respectively.
[**23C**] = 5 μM, [riboflavin] = 5 μM, [Target] =0, 10, 25, 50, 150, 250 μM, buffer, pH 7.0, 5°C, Excitation: 448 nm, Analysis: 530 nm.

The examination of the limit of detection (LOD) for theophylline reveals the promising ability of riboflavin/**23C**. The response of riboflavin/**23C** was found to increase linearly as the concentration of theophylline increased from 2.5 μM to 10 μM (**Figure 2-34**). The resulting linear equation was $y = 1.0 + 0.035x$ ($R = 0.9982$). The LOD can be estimated by the following eq (1):

$$\text{LOD} = 3 \times S_{\text{blank}} / m \qquad (1)$$

where S_{blank} and m are the standard deviation of the blank and the slope obatined from the linear fitting, respectively. From three independent experiments, the value of S_{blank} was determined as 0.013. Thus, LOD was estimated as 1.1 μM and this value is almost comparable to that of theophylline-binding RNA aptamer-based methods (0.1-1.2 μM).[24-29]

Figure 2-34. The linear fitting analysis for the determination of detection of limit (LOD) for theophylline based on the response of riboflavin (10.0 μM)/**23C** (10.0 μM).

F and F_0 denote the fluorescence intensities of riboflavin/**23C** in the presence and absence of theophylline, respectively. Error bars represent the standard deviations obtained from three independent experiments. [**23C**] = 10 μM, [riboflavin] = 10 μM, [theophylline] = 0, 0.25, 0.5, 1.5, 2.5, 6, 10 μM, buffer, pH 7.0, 5°C, 3×3 mm quartz cell, Ex band: 3 nm, Em band: 3 nm, Excitation: 448 nm, Analysis: 530 nm.

2-3-3-9. Binding mode

As mentioned earlier, the efficient fluorescence signal of AP-aptamer for theophylline may ascribe to the formation of two hydrogen bondings between theophylline and the receptor nucleobase cytosine. The N-7 hydrogen and C-6 keto oxygen of theophylline are critical.[23,60] The bonding pattern can be illustrated as the following figure:
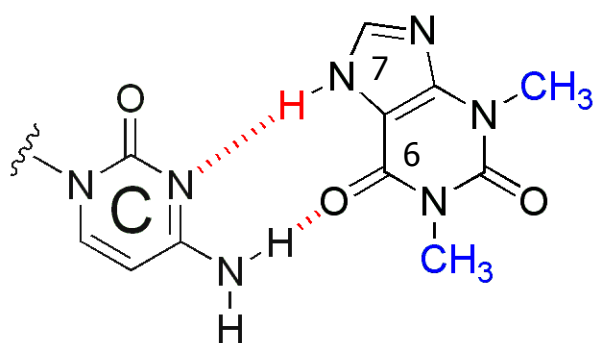

Figure 2-35. Binding mode between theophylline and cytosine.

2-4. Application of the aptamer into biological sample (horse serum)

Finally, we applied our 23-mer AP-aptamer into real serum samples.

2-4-1. Experimental

The preparation procedure of samples is simple and rapid, without pre-purification of serum. This is a significant progress comparing with immunoassays and routine gas/liquid chromatographic methods. A horse serum sample containing theophylline (10 μl) was diluted to 50 μl with a buffer solution (40 μl, pH 7.0) containing **23C** (10 μM) and riboflavin (10 μM). Then, the fluorescence spectra of the resulting solutions (50 μl) can be measured. And the response for caffeine and theobromine were also measured.
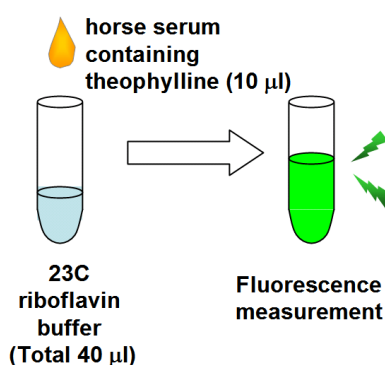
**Figure 2-36**. Sample preparation for fluorescence measurement.

2-4-2. Results and discussion

As shown in **Figure 2-37**, the background fluorescence from serum is negligible under the present conditions, which provides the clear monitoring of the fluorescence signaling of riboflavin/**23C** even in the serum samples. We also compared the inherent background of serum under the same condition with previous 2-aminopurine aptamer[60]. The background nature of serum itself is decreased to nearly one sixth at the analysis wavelength related to each research. The result shows that using riboflavin/**23C** under present condition can significantly avoid the background (**Figure 2-38**, **Table 2-7**). This is one important advantage of our AP-aptamer.

On the other hand, the riboflavin/**23C** complex was found to show the effective response to theophylline whereas almost no response appeared for caffeine and theobromine (**Figure 2-37**), indicating that riboflavin/**23C** can be used for highly selective detection for theophylline in serum samples. In addition, a good linear correlation was obtained between the fluorescence response and the concentration of theophylline ranged from 10 μM to 32.5

μM (**Figure 2-39**), which corresponds to the concentration range from 50 μM to 162.5 μM in the original serum samples. Therefore, riboflavin/**23C** is applicable to the monitoring of serum theophylline in the therapeutic range (60-100 μM).[12]
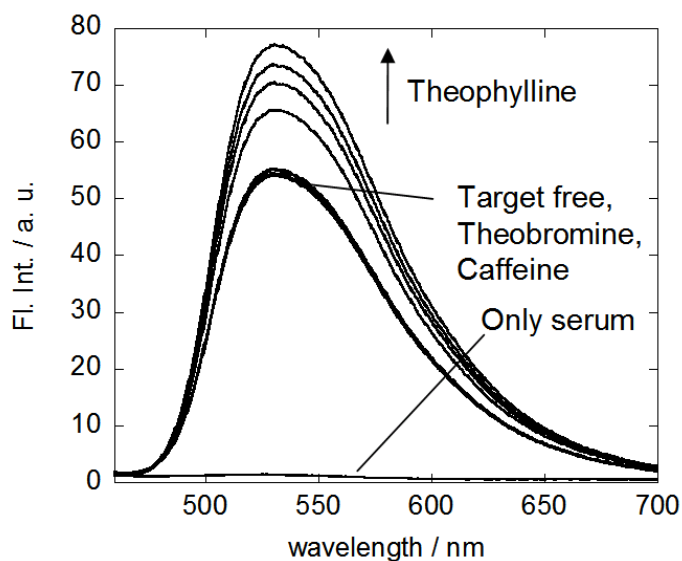
Figure 2-37. Fluorescence response for theophylline, theobromine and caffeine (10-32.5 μM) in horse serum samples.

[**23C**] = 10 μM, [riboflavin] = 10 μM, [theophylline (or theobromine or caffeine) in serum solution] = 10, 17.5, 25, 32.5 μM, horse serum 10 μl, [sodium cacodylate] = 10 mM, pH 7.0, 5°C, Sample volume: 50 μl, Excitation: 448 nm.
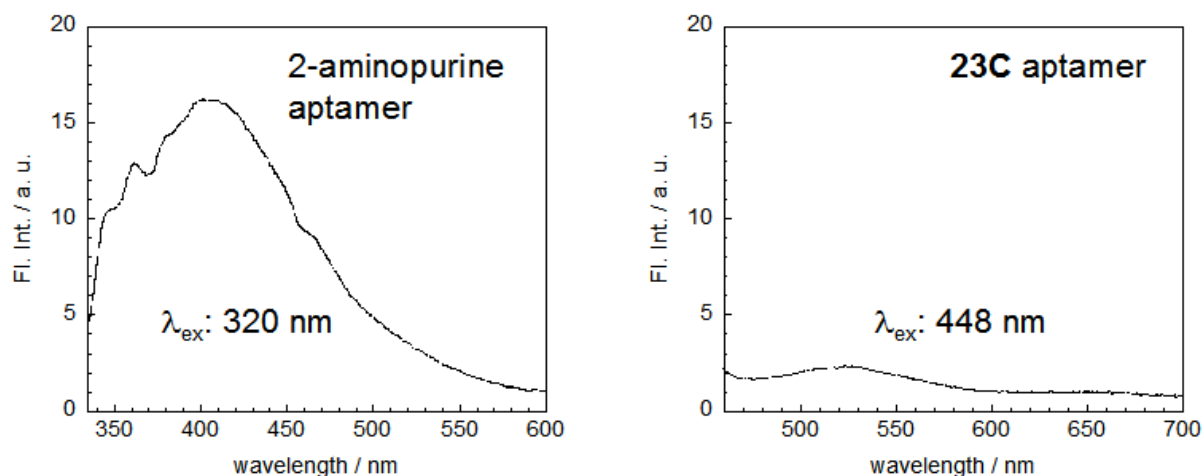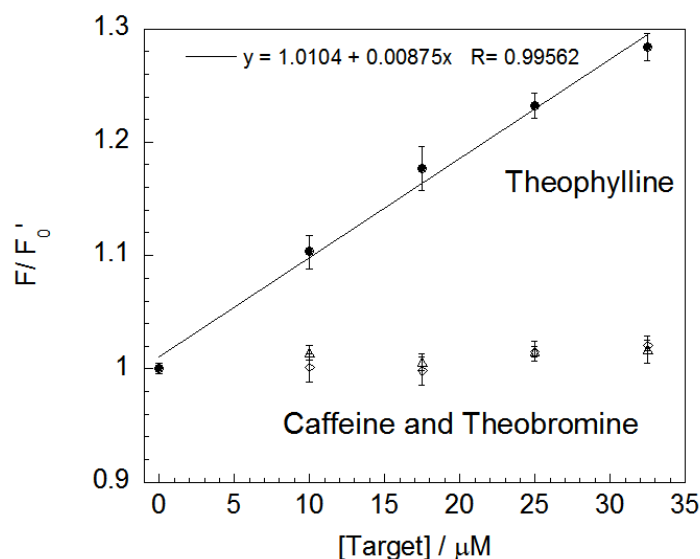

Figure 2-38. Comparison of serum background at different excitation wavelengths.

horse serum 10 μl, [sodium cacodylate] = 10 mM, pH 7.0, 5°C.

	Ex. / nm	Analy./ nm	Fl. Int. / a. u.
2-aminopurine aptamer	320	367	12.396
present AP-aptamer	448	530	2.243

Table 2-7. Comparison of serum background at wavelength related to each research.


Figure 2-39. The linear response for theophylline and the selectivity over caffeine and theobromine by using riboflavin/**23C**.

F and F_0' denote the fluorescence intensities of riboflavin/**23C** in the presence and absence of theophylline, respectively. Experiment conditions are as same as given in Figure 2-37, analysis at 530 nm.

Under the present experimental conditions, LOD for theophylline was determined as 8.0 μM in the original serum samples according to eq (1) in the section 2-3-3-8. As for the response to theophylline, the equation obtained by the linear fitting (**Figure 2-39**) is $y = 1.01 + 0.00875\,x$ ($R = 0.9956$). The standard deviation of blank (S_{blank}) is 0.00456. According to the equation (1), LOD was thus estimated as 1.6 μM, which corresponds to 8.0 μM in the original serum samples.

In order to estimate the response time for riboflavin/**23C** complex after adding theophylline, we carried out another experiment for fluorescence response ratio versus the time by using a same sample (**Figure 2-30**). The result shows the response was soon observed after adding theophylline and it kept for a certain time without significant change although a gradual decrease existed. The gradual decrease in fluorescence intensity may because of photobleaching of riboflavin. In conclusion, the detection can be carried out within a short period and the consistency would keep at least in 90 min.
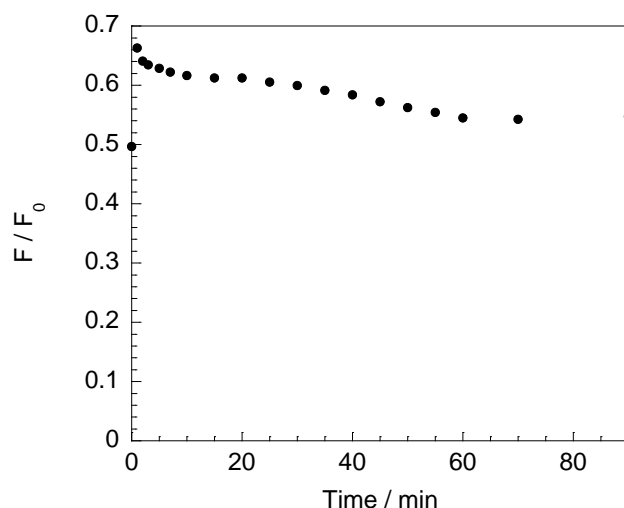
Figure 2-30. Fluorescence response ratio versus the time (0, 1, 2, 3, 5, 7, 10, 15, 20, 25, 30, 35, 40, 45, 50, 55, 60, 70, 90 min).

F and F_0 denote the fluorescence intensities of riboflavin in the presence and absence of both DNAs and theophylline, respectively.

[**23C**] = 10 μM, [riboflavin] = 10 μM, [theophylline in serum solution] = 25 μM, horse serum 10 μl, [sodium cacodylate] = 10 mM, pH 7.0, 5°C, Excitation: 448 nm, Analysis: 530 nm.

When the interfering molecules (theobromine and caffeine) are coexisted in serum, the response to theophylline is not influenced (**Figure 2-31**). This result strongly supported the applicability for riboflavin/**23C** to biological samples.
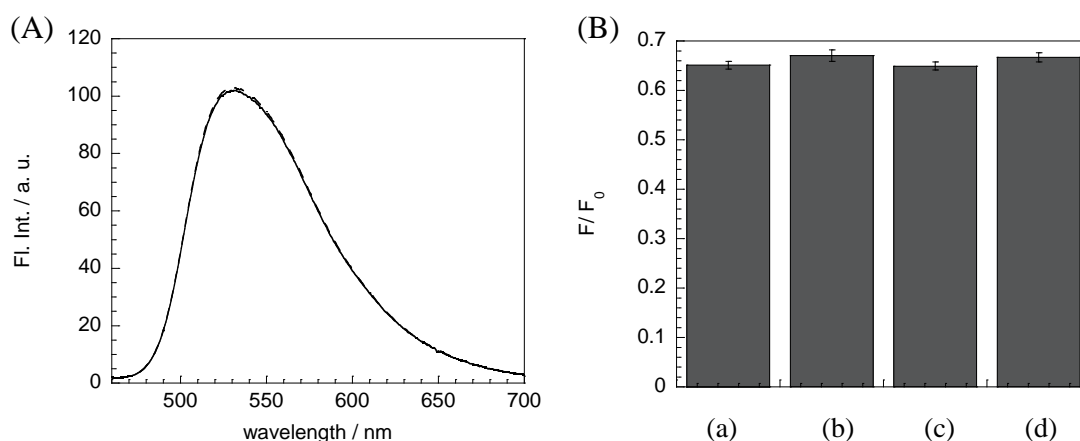
Figure 2-31. Effect of interfering molecules to the response

(A) Fluorescence spectra for theophylline alone and theophylline with theobromine or caffeine;

(B) Bar figure for (a) theophylline alone, (b) theophylline with theobromine, (c) theophylline with caffeine, and (d) theophylline with both theobromine and caffeine.

[**23C**] = 10 μM, [riboflavin] = 10 μM, [theophylline or theobromine or caffeine in serum solution] = 25 μM, horse serum 10 μl, [sodium cacodylate] = 10 mM, pH 7.0, 5°C, Excitation: 448 nm, Analysis: 530 nm

As is demonstrated here, theophylline in serum samples is ready to be analyzed in serum based on the fluorescence response of riboflavin/**23C** without any cumbersome pretreatment such as deproteinization and solvent extraction, which is significantly advantageous with a view toward development of new aptamer-based methods suitable for practical use by choosing a suitable combination of AP-aptamers and ligands for specific targets.

2-5. Conclusion

In conclusion, we developed a new competitive assay for fluorescent detection of theophylline based on a modification-free AP site-containing DNA duplex aptamer (AP-aptamer) in combination with an AP site-binding ligand, riboflavin. By the competitive binding of theophylline and riboflavin at the AP site in the AP-aptamer, quenched fluorescence of riboflavin bound to the AP site was restored due to the release of riboflavin from the AP site to the solution phase.

Fluorescence response showed a good linear correlation to the concentration of theophylline ranged from 10 μM to 32.5 μM in horse serum samples, and little response was observed for caffeine and theobromine. Importantly, this range corresponds to the concentration range from 50 μM to 162.5 μM in the original serum samples, which covers the therapeutic range (60-100 μM).

Due to the high selectivity for theophylline, the present method could be successfully applicable to detect serum theophylline in a therapeutic concentration range. Since neither the covalent labeling with signal transduction units nor the modification with the fluorescent nucleotide analogues is required, the proposed assay is simpler, easier, and more cost-effective than typical assays based on theophylline-binding RNA-aptamers. These characteristics of the proposed method are clearly advantageous for practical use.

Compared with 2-aminopurine modified DNA aptamer, our AP-aptamer gives a missive response to theophylline with low background fluorescence from serum, and the modification free character makes the assay much cheaper.

We expect that such characteristics allow the design of the label- and modification-free AP-aptamer-based assays targeting various kinds of small molecules. We are now undertaking further studies in this direction.

Acknowledgement and References

9. Parts of the materials including figures and text extracts are reproduced by permission of John Wiley and Sons (License Number: 3562940963969).
Y. Sato, Y. Zhang, S. Nishizawa, T. Seino, K. Nakamura, M. Li, and N. Teramae, *Chem. Eur. J.*, **2012**, 18, 12719-12724.

10. M. Kawai, M. Kato, *Methods Find. Exp. Clin. Pharmacol.*, **2000**, 22, 309-320.

11. D. J. F. Rowe, I. D. Watson, J. Williams, D. J. Berry, *Ann. Clin. Biochem.*, **1988**, 25, 4-26.

12. L. Hendeles, M. Weinberger, *Pharmacotherapy*, **1983**, 3, 2-44.

13. Eshleman, S. H. S., Shaw, L. M., *Clin. Chem.*, **1990**, 36, 398-399.

14. T. E. B. Leakey, *J. Chromatogr.*, **1990**, 507, 199-220.

15. H. Kanazawa, R. Atsumi, Y. Matsushima, J. Kizu, *J. Chromatogr. A*, **2000**, 870, 87-96.

16. S. Riahi, M. F. Mousavi, S. Z. Bathaie, M. Shamsipur, *Anal. Chim. Acta*, **2005**, 548, 192-198.

17. F. Beaudry, J.-P. Lavoie, P. Vachon, *Biomed. Chromatogr.*, **2005**, 19, 643-648.

18. J. Wang, E. Dempsey, M. Ozsoz, M. R. Smyth, *Analyst*, **1991**, 116, 997-999.

19. C. J. McNeil, J. M. Cooper, J.A. Spoors, *Biosens. Bioelectron.*, **1992**, 7, 375-380.

20. E. E. Ferapontova, L. Gorton, *Bioelectrochemistry*, **2005**, 66, 55-63.

21. E. E. Ferapontova, S. Shipovskov, L. Gorton, *Biosens. Bioelectron.*, **2007**, 22, 2508-2515.

22. S. Shipovskov, E. E. Ferapontova, *Biocat. Biotrans.*, **2008**, 26, 508-518.

23. R. D. Jenison, S. C. Gill, A. Pardi, B. Polisky, *Science*, **1994**, 263, 1425-1429.

24. E. E. Ferapontova, E. M. Olsen, K. V. Gothelf, *J. Am. Chem. Soc.*, **2008**, 130, 4256-4257.

25. E. E. Ferapontova, K. V. Gothelf, *Electroanalysis*, **2009**, 21, 1261-1266.

26. G.-C. Zhao, X. Yang, *Electrochem. Commun.*, **2010**, 12, 300-302.

27. C. J. Rankin, E. N. Fuller, K. H. Hamor, S. A. Gabarra, T. P. Shields, *Nucleosides, Nucleotides Nucleic Acids*, **2006**, 25, 1407-1424.

28. M. N. Stojanovic, D. M. Kolpashchikov, *J. Am. Chem. Soc.*, **2004**, 126, 9266-9270.

29. R. Pei, M. N. Stojanovic, *Anal. Bioanal. Chem.*, **2008**, 390, 1093-1099.

30. R. Pernites, R. Ponnapati, M. J. Felipe, R. Advincula, *Biosens. Bioelectron.*, **2011**, 26, 2766-2771.

31. Teresa Mairal, Veli Cengiz Özalp, Pablo Lozano Sánchez, Mònica Mir, Ioanis Katakis, Ciara K. O'Sullivan, *Anal. Bioanal. Chem.*, **2008**, 390, 989-1007.

32. Hermann, T.; Patel, D. J. *Science*, **2000**, *287*, 820.

33. Harada, K.; Frankel, A. D. *EMBO J.* **1995**, *14*, 5798.

34. Famulok, M.*J. Am. Chem. Soc.* **1994**, *116*, 1698.

35. Jhaveri, S. D.; Kirby, R.; Conrad,R.; Maglott, E. J.; Bowser, M.; Kennedy, R. T.; Glick, G.; Ellington, A. D.*J. Am. Chem. Soc.* **2000**, *122*, 2469.

36. Jhaveri, S.; Rajendran, M.; Ellington,A. D. *Nat. Biotechnol.* **2000**, *18*, 1293.

37. Merino, E. J.; Weeks, K. M., *J. Am. Chem. Soc.* **2003**, *125*, 12370.

38. Nagatoshi, S.; Nojima, T.;Juskowiak, B.; Takenaka, S. *Angew. Chem., Int. Ed.* **2005**, *44*, 5067.

39. Lin, C.; Katilius, E.; Liu, Y.; Zhang, J.; Yan, H. *Angew. Chem., Int. Ed.*, **2006**, *45*, 5296.

40. Burgstaller, P.; Famulok, M. *Angew. Chem., Int. Ed.* **1994**, *33*, 1084.

41. Lauhon, C. T.; Szostak, J. W. *J. Am. Chem. Soc.* **1995**, *117*, 1246.

42. Roychowdhury-Saha, M.; Lato, S. M.; Shank, E. D.; Burke, D. H.*Biochemistry* **2002**, *41*, 2492.

43. Zimmermann, G. R.; Jenison, R. D.; Wick, C. L.; Simorre, J. P.;Pardi, A. *Nat. Struct. Biol.* **1997**, *4*, 644.

44. Anderson, P. C.; Mecozzi, S.*J. Am. Chem. Soc.* **2005**, *127*, 5290.

45. Jayasena SD, *Clin. Chem.*, **1999**, 45, 1628-1650.

46. Ellington, A.D., Szostak, J.W., 1990. Nature 346, 818-822.

47. Tuerk, C., Gold, L., *Science*, **1990**, 249, 505-510.

48. S. Tombelli, M. Minunni, M. Mascini, *Biosensors and Bioelectronics*, **2005**, 20, 2424-2434.

49. Geiger, A., Burgstaller, P., Von der Eltz, H., Roeder, A., Famulok, M., *Nucl. Acids Res.*, **1996**. 24, 1029-1036.

50. Zhan LS, Shao NS, Peng JC, Sun HY, Wang QL, *Prog Biochem Biophys*, **2003**, 30, 151-155.

51. Drolet DW, Jenison RD, Smith DE, Pratt D, Hicke BJ, *Comb Chem High Throughput Screen*, **1999**, 2, 271-278.

52. Subash Chandra Bose Gopinath, *Anal Bioanal Chem*, **2007**, 387, 171-182

53. Famulok, M., Mayer, G., Blind, M., *Acc. Chem. Res.*, **2000**, 33, 591-599.

54. Bernard Juskowiak, *Anal Bioanal Chem*, **2011**, 399, 3157-3176.

55. Razvan Nutiu, Lieven P. Billen and Yingfu Li, *Nucleic Acid Switches and Sensors (Chapter 4)*, **2006**, ISBN: 0-387-37491-4.

56. http://en.wikipedia.org/wiki/Förster_resonance_energy_transfer

57. Hamaguchi N, Ellington A, Stanton M, *Anal Biochem*, **2001**, 294,126-131.

58. Stojanovic MN, de Prada P, Landry DW, *J Am Chem Soc*, **2001**, 123, 4928-4931.

59. Nutiu R, Li Y, *J Am Chem Soc*, **2003**, 125, 4771–4778.

60. M. Li, Y. Sato, S. Nishizawa, T. Seino, K. Nakamura, N. Teramae, *J. Am. Chem. Soc.*, **2009**, 131, 2448-2449.

61. Lindahl T, Nyberg B., *Biochemistry*, **1972**, 11, 3610-7.

62. Loeb LA, Preston BD. *Ann Rev Genet*, **1986**, 20, 201-30.

63. Chen J, Stubbe J, *Biochemistry,* **2004**, 43, 5278-5286.

64. Zheng Y, Sheppard TL, *Chem. Res. Toxicol.*, **2004**, 17, 197-207.

65. Lhomme J, Constant JF, Demeunynck M., Biopolymers. **1999**, 52, 65-83.

66. Jingyang Chen, Fran çois-Yves Dupradeau, David A. Case, Christopher J. Turner and JoAnne Stubbe, *Nucl. Acids Res*., **2008**, 36, 253-262.

67. N. B. Sankaran, S. Nishizawa, T. Seino, K. Yoshimoto, N. Teramae, *Angew. Chem. Int. Ed.*, **2006**, 45, 1563-1568.

68. S. Nishizawa, N. B. Sankaran, T. Seino, Y.-Y. Cui, Q. Dai, C.-Y. Xu, K. Yoshimoto, N. Teramae, *Anal. Chim. Acta*, **2006**, 556, 133-139.

69. N. B. Sankaran, Y. Sato, F. Sato, B. Rajendar, K. Morita, T. Seino, S. Nishizawa, N. Teramae, *J. Phys. Chem. B*, **2009**, 113, 1522-1529.

70. P. Zirak, A. Penzkofer, T. Mathes, P. Hegemann, *Chem. Phys.*, **2009**, 358, 111-122.

71. Puglisi, J. D.; Tinoco, I. *Method Enzymol.* **1989**, *180*, 304-325.

72. Q. Dai, C.-Y. Xu, Y. Sato, K. Yoshimoto, S. Nishizawa, N. Teramae, *Anal. Sci.* **2006**, 22, 201-203

73. Connors, K. A. *Binding constants*, John Wiley & Sons, New York, **1987**, pp. 339-343.

Chapter 3: Development of a highly selective ligand binding with cytosine opposite an abasic site in DNA duplexes[74]

3-1. Introduction

3-1-1. SNPs

Single Nucleotide Polymorphisms (SNPs, pronounced 'snips') are the most common happened DNA sequence mutation, occurring with a single nucleotide (A, T, C or G) in the genome. For example, a SNP may replace the nucleotide adenosine (A) with the nucleotide guanine (G) in a certain location of DNA.

All humans have almost the same sequence of 3 billion DNA nucleotides distributed between their 23 pairs of chromosomes. But there may be up to 0.1% of our DNA various at certain locations, what makes individuals different from one another. This means in our genome, there are about 3 million SNPs existing, which is a huge amount of variation deserving to be studied. On the other hand, we can also use the mutation of SNP as biological markers, helping scientists locate genes that are associated with disease.[75,76]

SNPs become important to study because of their ability to influence disease risk, drug efficacy and side-effects. For example, a single base mutation in the APOE (apolipoprotein E) gene is associated with a higher risk for Alzheimer disease.[77] Furthermore, SNPs are probably the most important category of genetic changes influencing common diseases. In terms of common diseases, 9 of the top 10 leading causes of death have a genetic component and thus most likely one or more SNPs influence your disease risk.[78]

In conclusion, SNPs in human genome is crucial important to study for the fields of genetics, diagnostics and disease research.

3-1-2. Existent small ligands for SNPs detection by using AP site-containing DNA duplex

A series of small ligands have been found with highly selective binding ability to a nucleobase opposite an abasic site (AP site) in DNA duplexes. These ligands have been designed intentionally with a fluorescent emit signal upon the binding with DNA duplexes. This strategy of small ligand-based fluorescence assay for SNPs detection has been proposed as shown in **Figure 3-1**.
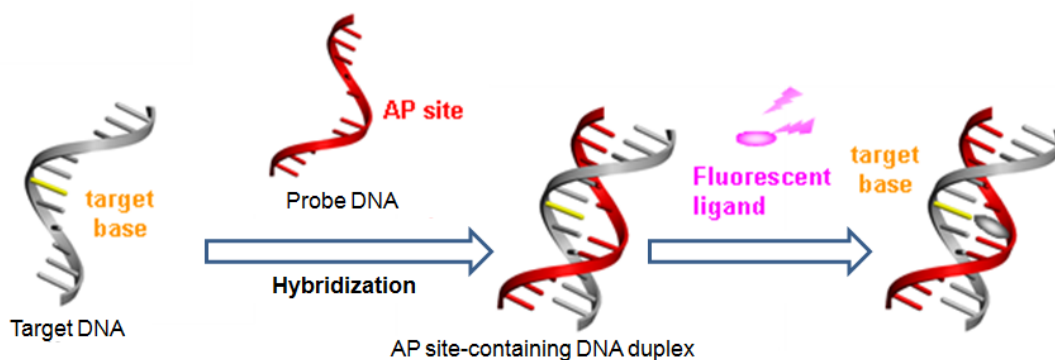
Figure 3-1. Schematic illustration of the ligand binding to nucleobases opposite an AP site in a DNA duplex.

As different with canonical DNA-small ligand binding, such as intercalation[79] or groove binding[80], it is characteristic of ligands to bind to non-Watson–Crick base-pairing sites in DNA duplexes, where the binding is selectively promoted by a pseudo-base pairing along the Watson–Crick edge of the intrahelical target nucleobases.[81] A classic example is the mismatch-binding ligands developed by Nakatani and co-workers, and a surface plasmon resonance (SPR) assay has been proposed based on forming of these pseudo-base pairs.[82-84]

In our approach, we chose AP site to be the binding pocket. As introduced in chapter 2, AP site can serve as a chemically stable binding cavity in a probe DNA, and provide a target nucleobase in the opposite position after hybridization with the target DNA strand. The AP site is hydrophobic and allows a direct contact of the small ligand to target nucleobase via hydrogen bonding, where the ligand is further stacked with two nucleobases flanking the AP site. This makes AP site a suitable binding location in the duplex.[81]

In fact, some ligands have been already proved to have useful affinity and selectivity for target nucleobases opposite the AP sites, including cytosine selective 2-amino-7-methyl-1,8-naphthyridine (AMND[85,86]), guanine selective 2-amino-6, 7-dimethyl-4-hydroxypteridine[87], adenine selective alloxazine[88] and thymine selective amiloride[89] (**Figure 3-2**). All of these ligands show a complexation induced fluorescent signal, and SNP genotype of samples can be clearly distinguished by binding with ligands.
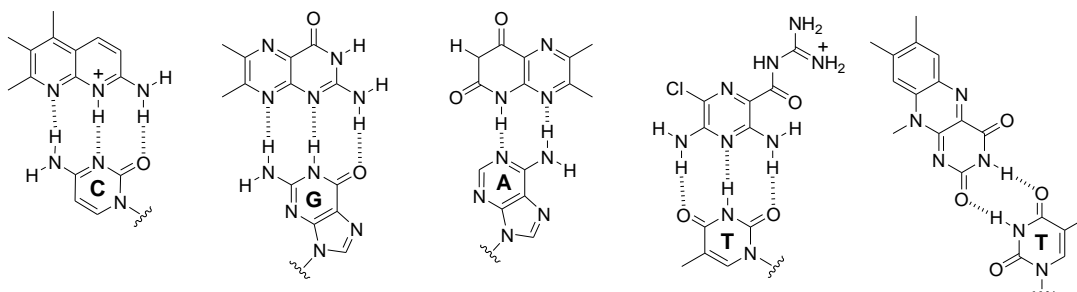

Figure 3-2. AP site-binding ligands developed by our group with specific nucleobase selectivity.

This method needn't to modify the target and/or probe DNA strands, and measured easily by fluorescence spectrophotometer, so as to be cost effective. In addition, the

measurement can be carried out rapidly without controlling a precise temperature, which is great advantageous in practical use.

3-1-3. Insufficient of AMND for C selective detection

Focus on one of the C selective ligands—AMND, we realized it was insufficient of the selectivity between pyrimidine C and T. Indeed, the difference in the binding affinity of AMND derivatives for C over T is only two- or three-fold.[74,81] The estimated value of binding affinity for C was 1.5 μM in previous literature 86. As shown in **Figure 3-3**, the proposed hydrogen bonding of AMND can be formed not only with C, but also with T (two possible patterns). Therefore, a better exclusive selective ligand for C over T is needed to be developed.
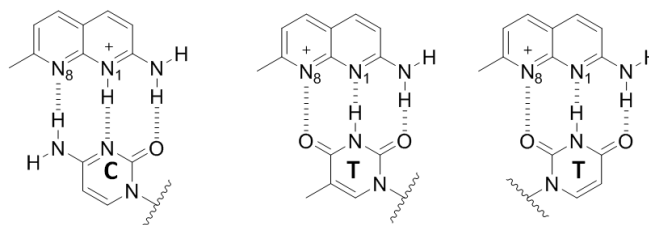
Figure 3-3. Proposed binding modes of AMND with C and T (two possible patterns).[74]

3-2. Design strategy of CF$_3$-AMND

Our design strategy is straight forward and simple. Since the protonation at the N8 position of AMND is feasible, which is preferable for formation of a fully complementary hydrogen bonding to T, we proposed to add a strong electron withdraw group to the naphthyridine ring.

The position of CF$_3$ group was calculated by computer before synthesizing compound. (Data not shown.)

3-3. Experimental

3-3-1. Materials and experiments

CF$_3$-AMND has been synthesized and purified by Dr. Takehiro Seino, who was a previous member of our group. He has reported CF$_3$-AMND in his doctor's thesis, but more detail information of properties about this ligand is still lack of research.

Synthesis of CF$_3$-AMND[74,90]
2,6-Diaminopyridine (1.1 g, 10.5 mmol) in phosphoric acid (50 mL) were added to 1,1,1-trifluoro-2,4-pentanedione (1.6 g, 10.2 mmol) and the reaction mixture was stirred at 90 ℃ for 26 h. After neutralization with NaOH, the mixture was filtered. The brown residue was extracted three times with 200 mL of CHCl$_3$ each time and the organic phase was dried over Na$_2$SO$_4$. The solvent was evaporated in vacuo to give the mixture of CF$_3$ substituent-modified AMND molecules at 5 position and 7 position. Mixture was dissolved in 10 mL of chloroform, and filtrated. Filtrate was evaporated, dissolved in 20 mL of ethyl acetate, and 2 mL of HCl (0.1 M) was dropped in the solution. Filtration of the residue gave CF$_3$-AMND as pale yellow needle (25 mg, 0.11 mmol, 1.1 %).

1H NMR (DMSO-d_6, 600 MHz): δ = 8.17 (d, 1H, J = 11 Hz), 7.65 (s, 1H), 7.08 (d, 1H, J = 11 Hz), 2.68 (s, 3H). HRMS (ESI) for C$_{10}$H$_8$N$_3$F$_3$: calcd: ([M +H]$^+$), 228.0743; found, 228.0742.

Materials
DNA sequences
5'-GCTCCTCTGG<u>X</u>GCCCTCGACG-3' (X = dSpacer), (ε_{260} = 176200 M^{-1}cm^{-1})
5'-GCTCCTCTGG<u>G</u>GCCCTCGACG-3' (ε_{260} = 185440 M^{-1}cm^{-1})
3'-CGAGGAGACC<u>C</u>CGGGAGCTGC-5' (ε_{260} = 208440 M^{-1}cm^{-1})
3'-CGAGGAGACC<u>T</u>CGGGAGCTGC-5' (ε_{260} = 208880 M^{-1}cm^{-1})
3'-CGAGGAGACC<u>A</u>CGGGAGCTGC-5' (ε_{260} = 213300 M^{-1}cm^{-1})
3'-CGAGGAGACC<u>G</u>CGGGAGCTGC-5' (ε_{260} = 210960 M^{-1}cm^{-1})

All of the DNA samples were custom synthesized and HPLC purified (>97%) by Nihon Gene Research Laboratories Inc. (Sendai, Japan). The extinction coefficients at 25°C were calculated at 260 nm for each strand[63], which was shown in bracket above.

The other reagents were commercially available analytical grade and were used without further purification. Water was deionized (≥18.0 MΩ cm specific resistance) by an Elix 5 UV Water Purification System and a Milli-Q Synthesis A10 system (Millipore Corp., Bedford, MA).

Instruments
Fluorescence measurement: Fluorescence spectra were measured with a JASCO model FP-6500 spectrofluorophotometer equipped with a thermoelectrically temperature-controlled

cell holder (Japan Spectroscopic Co. Ltd., Tokyo, Japan). Fluorescence measurements were carried out at 20°C using a 3 × 3 mm quartz cell. Excitation wavelength was set at 346 nm for CF$_3$-AMND, and 350 nm for AMND.

UV measurement: JASCO model V-570 spectrophotometer.

Preparation of stock solutions

DNA solutions: The concentrations of DNAs were determined from the molar extinction coefficients at 260 nm. Stock solutions were prepared with miliQ water to 250 μM and stored at 4°C.

Buffer solution: Stock solution was prepared in 100 mL miliQ water and containing sodium cacodylate (1.071g, 50 mM), NaCl (2.935g, 500 mM), EDTA (0.187g, 5.0 mM), and stored at 4°C. When applied it into tubes, it was 5 times diluted, which made the standard buffer solution's concentration as follows: [sodium cacodylate] = 10 mM, [NaCl] = 100 mM, [EDTA] = 1.0 mM.

Buffer solutions at various pH: Prepare sodium cacodylate solution and NaCl/EDTA solution separately. The amount of NaCl/EDTA is as two times as pH 7.0 buffer solution. And sodium cacodylate (2.14g, 100 mM) in miliQ water, adjusted with HCl or NaOH to the total volume as 100 mL. When applied them to samples, combine the two kinds of solutions and will give out the concentration as follows: [sodium cacodylate] = 10 mM, [NaCl] = 100 mM, [EDTA] = 1.0 mM, pH various.

In Chapter 3, unless otherwise mentioned, all measurements were performed in standard buffer solution: 10 mM sodium cacodylate buffer solutions (pH 7.0) containing 100 mM NaCl and 1.0 mM EDTA. Before measurements, the sample solutions were annealed as follows: heated at 75°C for 10 min, and gradually cooled to 5°C (3°C/min), after which the solution temperature was raised again to 20°C.

3-3-2. Determination of binding constants obtained from fluorescence titration.

The changes in fluorescence intensity of the ligand were monitored as a function of the concentration of DNA duplex. The resulting titration curve was analyzed by nonlinear least-squares regression based on a 1:1 binding isotherm[65]:

$$F / F_0 = \{1 + kK_{11}[D]\}/\{1 + K_{11}[D]\} \qquad (1)$$

where F and F_0 are the observed fluorescence intensities of amiloride in the presence and absence of duplexes, respectively, and k ($= k_{11}/k_L$) represents the ratio of proportionality constants connecting the fluorescence intensities and concentrations of the molecules (1:1 complex: k_{11}, free ligand: k_L). The concentration of the free duplex, [D], can be related to known total concentrations of the duplex (D_0) and ligand (L_0), by the following equation:

$$D_0 = [D] + \{L_0 K_{11}[D]\}/\{1 + K_{11}[D]\} \qquad (2)$$

Together, eqs. (1) and (2) describe the system.

3-3-3. Salt dependence of the binding constants[74,91]

The effect of different NaCl concentrations on the 1:1 binding constants (K_{11}) of CF_3-AMND to C and T was examined at 20 $^{\circ}$C (pH 7.0) by fluorescence titration experiments, and analyzed according to the polyelectrolyte theory proposed by Record *et al.*[91]. The observed salt dependence of the binding constants is explained by eq. (3).

$$\delta \log K_{11}/\delta \log [Na^+] = -Z\psi = SK \qquad (3)$$

where Z is the apparent charge on the ligand and ψ (0.88 for B-type DNA) is the proportion of counterions associated with each DNA phosphate group. The slope (SK) of the plot, which is equivalent to the number of counterions released from the duplex upon ligand binding, was obtained from the regression lines of best linear least squares fit, by which the values of Z were estimated.

3-3-4. Analysis of PCR products

Asymmetric PCR was performed as described in the literature 81. After PCR amplification, an aliquot (40 μL) of PCR products was buffered to pH 5.5 with 100 mM sodium cacodylate. Then, CF_3-AMND (0.1 μM) and a 20-mer AP site-containing probe DNA (2.0μM; for sense strand analysis; 5'-CCT ACG CCA <u>X</u>CA GCT CCA AC -3', for antisense strand analysis; 5'-GTT GGA GCT G<u>X</u>T GGC GTA GG-3', X = AP site; dSpacer (a tetrahydrofuranyl residue)) were added.

Fluorescence spectra of the resulting solutions (50 μL) were then measured at 20°C with FP-6500 spectrofluorophotometer equipped with the thermoelectrically temperature-controlled cell holder using 3×3 mm quartz cells.

3-4. Results and discussion

3-4-1. Selectivity of CF$_3$-AMND for receptor nucleobase's type

First, we examined the selectivity of CF$_3$-AMND toward different kinds of target nucleobases (5'-GCT CCT CTG G<u>X</u>G CCC TCG ACG-3'/ 3'-CGA GGA GAC C<u>N</u>C GGG AGC TGC-5', X = dSpacer, N = A, G, T or C). As shown in **Figure 3-4**, the addition of a fully-matched DNA duplex (X/N = G/C) without AP sites does not cause of any fluorescence quenching to CF$_3$-AMND, indicating negligible intercalative binding of CF$_3$-AMND.

Also, almost no response can be observed for A, G and T in the AP site containing DNA duplexes. In contrast, significant fluorescence quenching is observed for C, where the fluorescence intensity at 403 nm decreases by as much as 75%.
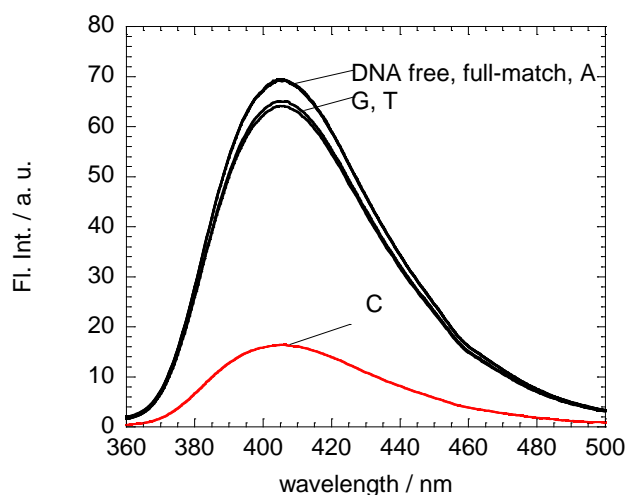
Figure 3-4. Fluorescence spectra of CF$_3$-AMND to the target nucleobase in 21-mer AP site-containing DNA duplexes.

[CF$_3$-AMND] = 1 μM, [DNA duplex] = 5 μM , buffer, pH 7.0, 20°C, Excitation: 346 nm.

The high selectivity for C is consistent with the results observed for UV-visible absorption spectral changes (**Figure 3-5**). The absorption intensity of CF$_3$-AMND remarkably decreases upon addition of the AP site-containing DNA duplexes carrying C whereas the absorption changes are slight for fully-matched DNA duplexes and AP site-containing DNA duplexes carrying the G, A, or T target.
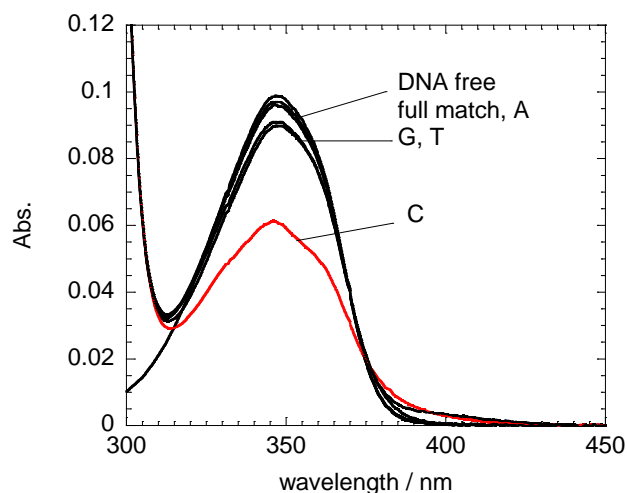
Figure 3-5. UV-visible absorption spectra of CF_3-AMND in the absence and presence of 21-mer AP site-containing DNA duplex.

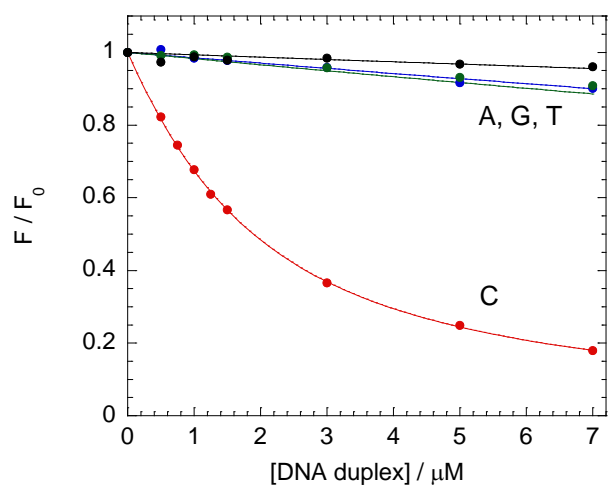[CF_3-AMND] = 10 μM, [DNA duplex] = 10 μM , buffer, pH 7.0, 20°C.

3-4-2. Determination of the binding affinity

The binding affinity of CF_3-AMND to target nucleobases opposite the AP site was examined by fluorescence titration experiments. Fluorescence quenching response of CF_3-AMND (1.0 μM) was monitored upon addition of AP site-containing DNA duplexes in the concentration range from 0 to 7.0 μM (**Figure 3-6**). The resulting titration curves (**Figure 3-7**) were well analyzed by non-linear least-squares regression based on a 1:1 binding model and the binding constant (K_{11}) for C was determined as $(7.1 \pm 0.2) \times 10^5 \text{ M}^{-1}$ ($n = 3$) by three times of independent experiments (**Figure 3-8**). Since the present concentration condition was not suitable for accurate determination of K_{11} for T, A, and G due to the weak binding, K_{11} values for these nucleobases were independently obtained in the high concentration conditions ([CF_3-AMND] = 10 μM, [DNA duplexes] = 0-70 μM; **Figure 3-9**).
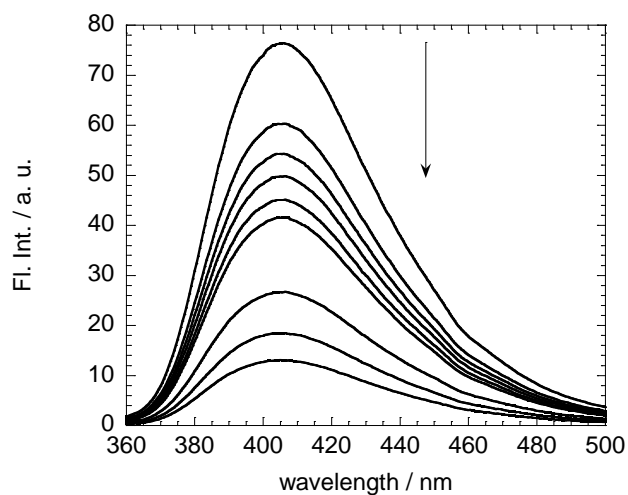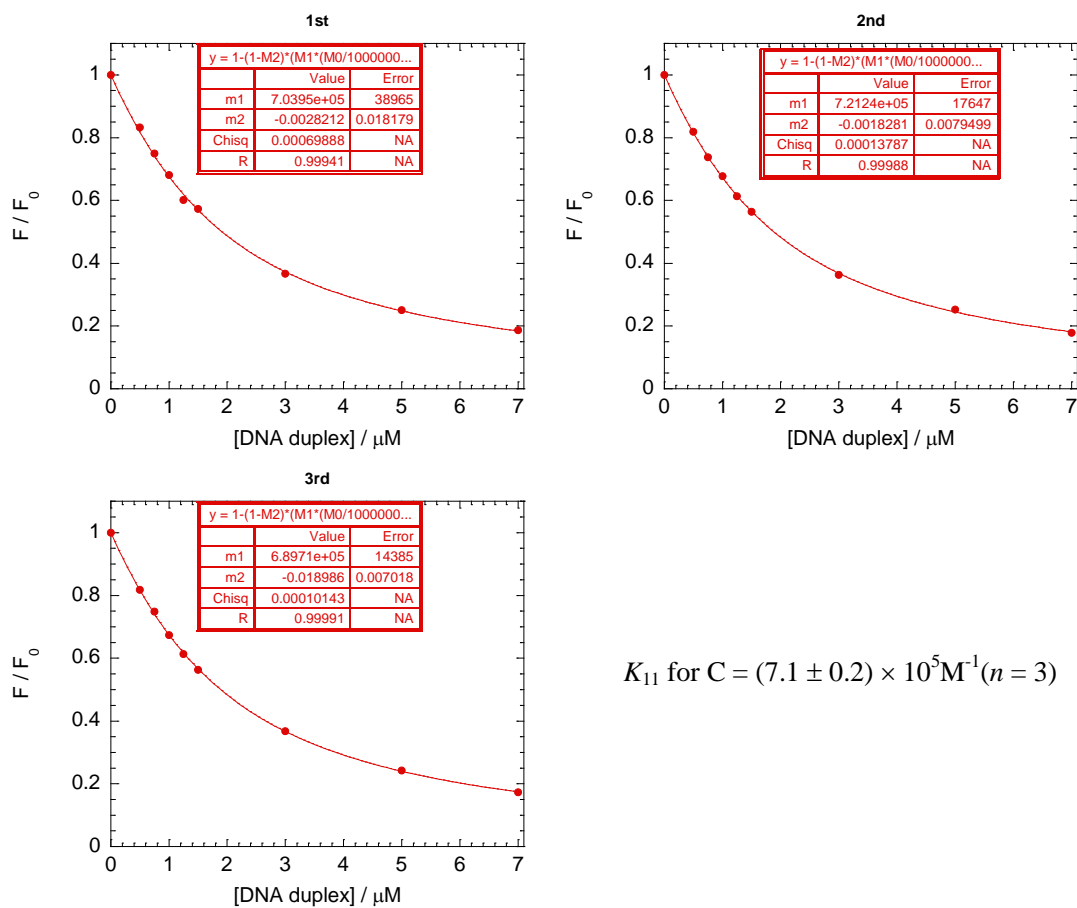
Figure 3-6. Fluorescence response of CF₃-AMND (1.0μM) to C in 21-mer AP site-containing DNA duplexes.

Other solution conditions are the same as given in Figure 3-4.

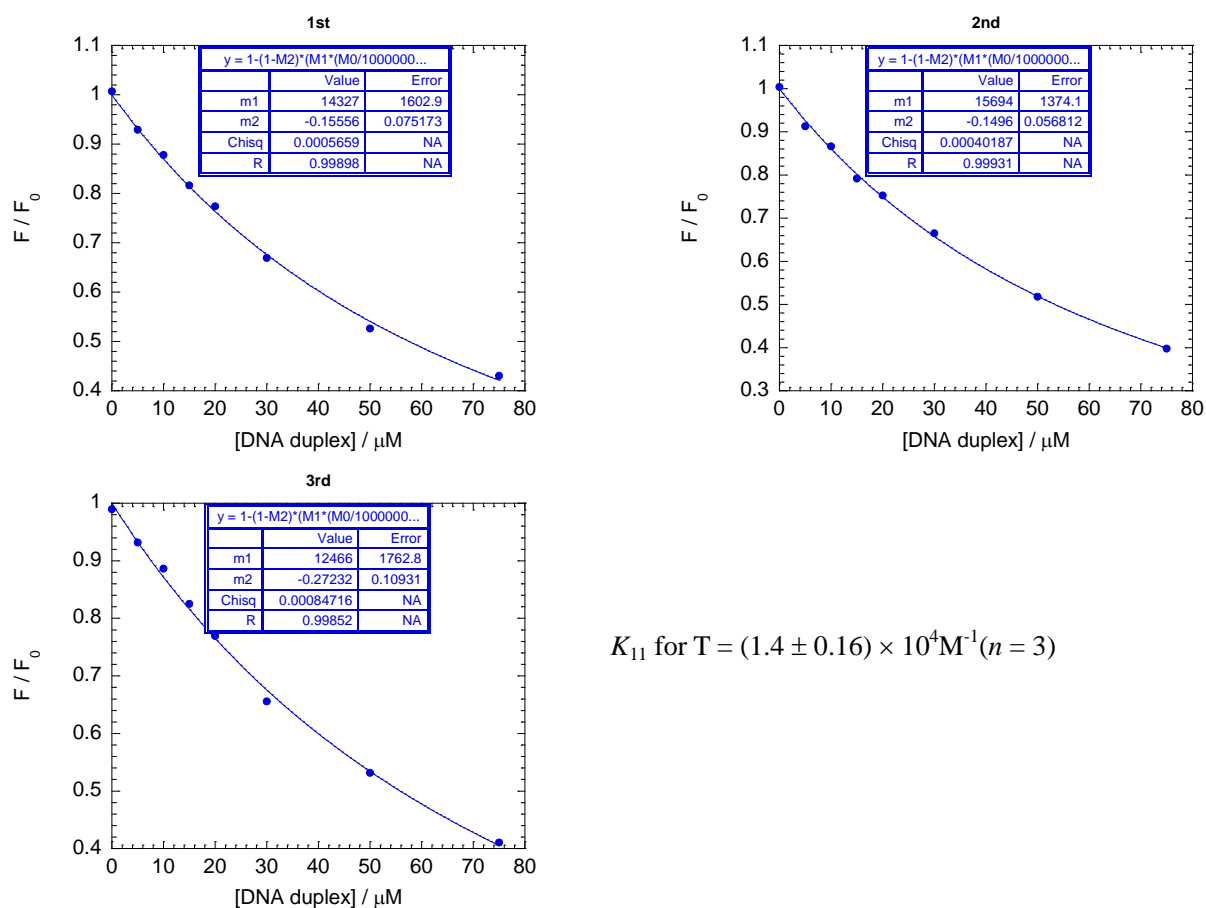**Figure 3-7.** Fluoresence titration curves for the binding of CF₃-AMND to the target nucleobases.
[CF₃-AMND] = 1 μM, [DNA duplex] = 0, 0.5, 0,75, 1.0, 1.25, 1.5, 3, 5, 7 μM, buffer, pH 7.0, 20°C, Excitation: 346 nm, Analysis:403 nm.

1st

y = 1-(1-M2)*(M1*(M0/1000000...		
	Value	Error
m1	7.0395e+05	38965
m2	-0.0028212	0.018179
Chisq	0.00069888	NA
R	0.99941	NA

2nd

y = 1-(1-M2)*(M1*(M0/1000000...		
	Value	Error
m1	7.2124e+05	17647
m2	-0.0018281	0.0079499
Chisq	0.00013787	NA
R	0.99988	NA

3rd

y = 1-(1-M2)*(M1*(M0/1000000...		
	Value	Error
m1	6.8971e+05	14385
m2	-0.018986	0.007018
Chisq	0.00010143	NA
R	0.99991	NA

K_{11} for C $= (7.1 \pm 0.2) \times 10^5 \mathrm{M}^{-1} (n = 3)$

Figure 3-8. Fluorescence titration curves for the binding of CF_3-AMND to C (Three times of independent experiments). Other solution conditions are the same as given in Figure 3-7.

Figure 3-9. Fluoresence titration curves for the binding of CF$_3$-AMND to T (Three times of independent experiments). Other solution conditions are the same as given in Figure 3-7.

Significantly, the binding constant for C is found to be more than 50-fold larger than those for the other three nucleobases ($K_{11}/10^5$ M−1 (n = 3): T, 0.14 ± 0.016; G, 0.16 ± 0.029; A, <0.10). Such a difference in the binding constants for C over T (K_{11} (C)/ K_{11} (T)) is much superior to those of the C-binding ligands developed previously.[81,84,92,93] These results clearly show that CF$_3$-AMND shows the strongest binding to C with high selectivity.

Then, the binding affinity of parent AMND was determined by fluorescence titration experiment in the same way. The binding constant is (5.4 ± 0.5) × 10^6 M−1 (n = 3) for C, and (1.3 ± 0.1) × 10^6 M−1, (n = 3) for T, which leads to the relatively low selectivity of AMND for C over T (K_{11} (C)/ K_{11} (T) = 4.2) compared to CF$_3$-AMND.

K_{11} (n = 3)	C	T	K_{11}(C)/K_{11}(T)
AMND /10^{6}M^{-1}	5.35 ± 0.46	1.29 ± 0.06	4.2
CF$_3$-AMND /10^{5}M^{-1}	7.05 ± 0.16	0.142 ± 0.016	51

Table 3-1. List of binding constants of AMND/CF$_3$-AMND to the target nucleobases C and T.

3-4-2. Effect of pH

Since 2-amino-1,8-naphthyridine derivatives can bind to the pyrimidine nucleobases in their protonated states,[81,84,92,93] we examined the pH dependence of the absorption spectra of CF$_3$-AMND to determine the pKa value and it was determined as 5.1 (Data not shown). The decrease in pKa compared to the parent AMND (pKa = 6.8)[81] is ascribed to the increase in the acidity of the aza-nitrogen of the AMND ring by attaching the CF$_3$ group. Thus, almost all of the CF$_3$-AMND molecules are in a neutral form at pH 7.0 in solution. However, in order to form hydrogen bonding with C or T, the protonation of CF$_3$-AMND is necessary. This is probably the reason for the binding affinity of CF$_3$-AMND to C or T is smaller than that of AMND at pH 7.0.

We found that the binding affinity of CF$_3$-AMND to C is remarkably increased under the acidic solution condition with pH lower than 7.0 (**Figure 3-10**). Significantly, the K_{11} value at pH 5.5 is $(1.3 \pm 0.1) \times 10^7$ M-1 ($n = 3$), which is two orders of magnitude larger than that at pH 7.0. The observed increase in the affinity can be explained by the increased amount of the N1 protonated CF$_3$-AMND species suitable for C-binding at pH 5.5. We did not do any of the experiments in the pH range lower than 5.0 considering the possible protonation of nucleobases. Importantly, high selectivity of CF$_3$-AMND for C is maintained at pH 5.5 (**Figure 3-11**), where the value of K_{11} (C)/ K_{11} (T) is 58-fold. Moreover, CF$_3$-AMND shows high selective response for C compared to T at pH 5.5 regardless of the nucleobases flanking the AP sites in the DNA duplexes (**Figure 3-12**). Therefore, CF$_3$-AMND can work as an effective and versatile ligand for detection of the C-related single-base mutation in DNAs.
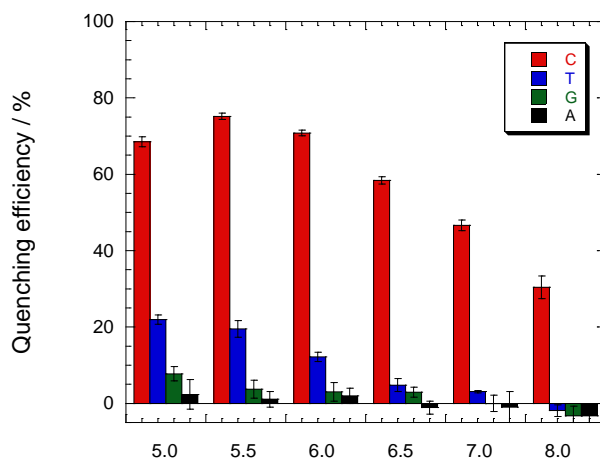

Figure 3-10. pH dependence of the quenching efficiency of CF$_3$-AMND (1.0 μM) upon binding to the target nucleobase (C, red; T, blue; G, green; A, black) in 21-mer AP site-containing DNA duplexes (1.0 μM).

Quenching efficiency (%) was calculated by $(F_0\text{-}F)/F \times 100$, where F and F_0 denote the fluorescence intensities of CF$_3$-AMND in the presence and absence of DNA duplexes, respectively.

Error bars represent the standard deviations obtained from three independent experiments.

[CF$_3$-AMND] = 1 μM, [DNA duplex] = 1 μM, buffer, pH = 5.0~8.0, 20°C, 3×3 mm quartz cell, Ex band: 3 nm, Em band: 5 nm, Excitation: 346 nm, Analysis: 403 nm.
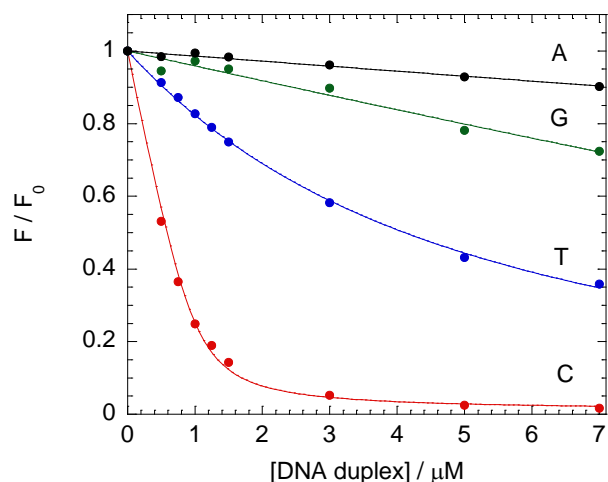
Figure 3-11. Fluorescence titration curves for the binding of CF$_3$-AMND (1.0 μM) to 21-mer AP site-containing DNA duplexes, obtained in solutions buffered to pH 5.5 (10 mM sodium cacodylate) containing 100 mM NaCl and 1.0 mM EDTA.

The changes in the fluorescence intensities at 403 nm were analyzed based on a 1:1 binding isotherm model.

F and F_0 denote the fluorescence intensities of CF$_3$-AMND in the presence and absence of DNA duplexes, respectively.

[CF$_3$-AMND] = 1 μM, [DNA duplex] = 0, 0.5, 0.75, 1.0, 1.25, 1.5, 3, 5, 7 μM, buffer, pH = 5.5, 20°C, 3×3 mm quartz cell, Ex band: 3 nm, Em band: 5 nm, Excitation: 346 nm, Analysis: 403 nm.

K_{11} ($n = 3$)	C	T	$K_{11}(C)/K_{11}(T)$
AMND at pH 7.0 / M^{-1}	$(5.35 \pm 0.46) \times 10^6$	$(1.29 \pm 0.06) \times 10^6$	4.2
CF$_3$-AMND at pH 7.0 / M^{-1}	$(7.05 \pm 0.16) \times 10^5$	$(1.42 \pm 0.16) \times 10^4$	51
CF$_3$-AMND at pH 5.5 / M^{-1}	$(1.30 \pm 0.13) \times 10^7$	$(2.23 \pm 0.08) \times 10^5$	58

Table 3-2. List of binding constants of AMND/CF$_3$-AMND to the target nucleobases C or T at pH 7.0 and pH5.5.
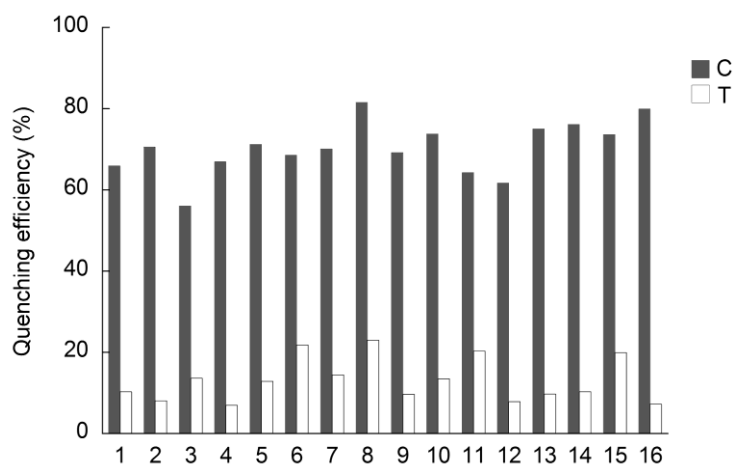
Figure 3-12 Effect of flanking nucleobases on the fluorescence quenching efficiency of CF_3-AMND (0.5 μM) to C (gray bars) and T (white bars) in the 21-mer AP site-containing DNA duplexes (1.0 μM; 5'-GCT CCT CTG WXW' CCC TCG ACG-3'/3'-CGA GGA GAC Z**N**Z' GGG AGC TGC-5', **X** = AP site (Spacer C3) or G, **N** = C, or T). W, W' represent the nucleobases flanking the AP site and Z, Z' represent complementary nucleobases flanking the target nucleobase; W**X**W'/Z**N**Z' = 1) T**X**T/A**N**A, 2) G**X**T/C**N**A, 3) C**X**T/G**N**A, 4) A**X**T/T**N**A, 5) T**X**G/A**N**C, 6) C**X**G/G**N**C, 7) A**X**G/T**N**C, 8) G**X**G/C**N**C, 9) T**X**C/A**N**G, 10) G**X**C/C**N**G, 11) C**X**C/G**N**G, 12) A**X**C/T**N**G, 13) T**X**A/A**N**T, 14) G**X**A/C**N**T, 15) C**X**A/G**N**T, 16) A**X**A/T**N**T. Other solution conditions are the same as those given in Figure 3-11. Quenching efficiency (%) was calculated by $(F_0-F)/F \times 100$, where F and F_0 denote the fluorescence intensities of CF_3-AMND in the presence and absence of DNA duplexes, respectively. Excitation, 346 nm. Analysis, 403 nm. Temperature, 20°C.

3-4-3. Determination of apparent charge (*Z*)

Protonated CF$_3$-AMND can bind to C and T at the AP site, as revealed by the examination of the salt dependence of the binding constants K_{11} based on Record's polyelectrolyte theory[91]. The binding constants of CF$_3$-AMND for C and T were determined at different salt concentrations using fluorescence titration experiments (**Figure 3-13**). K_{11} values for C and T remarkably decrease as the salt concentration increases (**Table 3-3**). The estimated apparent charges (Z) of CF$_3$-AMND were estimated as 1.47 and 1.02 when binding to C and T, respectively, as obtained from the linear regression analysis of a double logarithmic plot of K_{11} versus the Na$^+$ concentration (**Figure 3-14**).

These results indicate that the protonation of the bound CF$_3$-AMND at pH 7.0 would be facile compared to the protonation in the free state, and this is consistent with the previously reported results.[81,84,92,93]
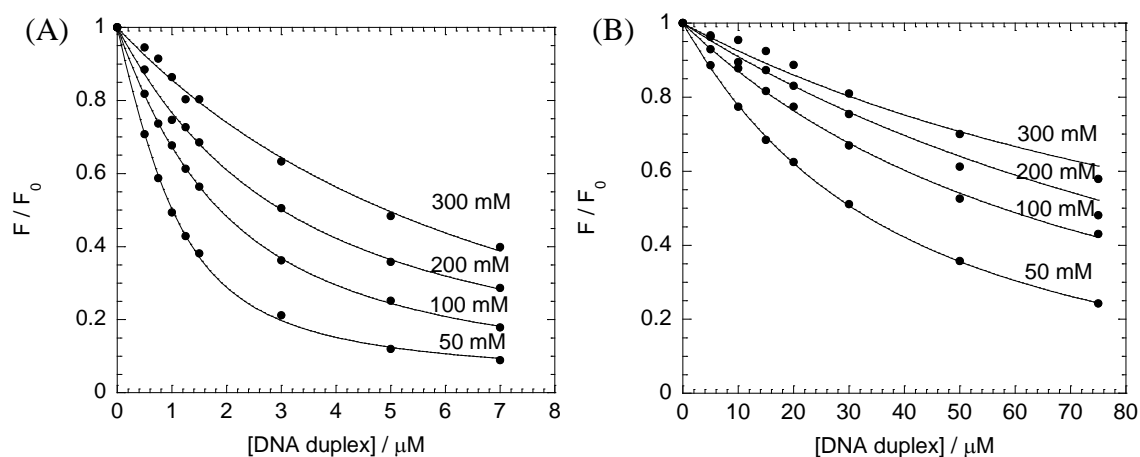
Figure 3-13. Fluorescent titration experiments at different salt concentrations for (A) cytosine, and (B) thymine.

	[Na$^+$] = 60 mM[a]	[Na$^+$] = 110 mM[b]	[Na$^+$] = 210 mM[a]	[Na$^+$] = 310 mM[a]
C	2.1 ($\pm$ 0.1) $\times$ 10^6	7.2 ($\pm$ 0.2) $\times$ 10^5	3.9 ($\pm$ 0.3) $\times$ 10^5	1.3 ($\pm$ 0.2) $\times$ 10^5
T	4.0 ($\pm$ 0.1) $\times$ 10^4	1.4 ($\pm$ 0.2) $\times$ 10^4	1.2 ($\pm$ 0.1) $\times$ 10^4	8.7 ($\pm$ 0.4) $\times$ 10^3

Table 3-3. Binding constants of CF$_3$-AMND to C and T at different salt concentrations

a) Errors are the fitting errors.

b) Errors are the standard deviations obtained from three independent experiments.
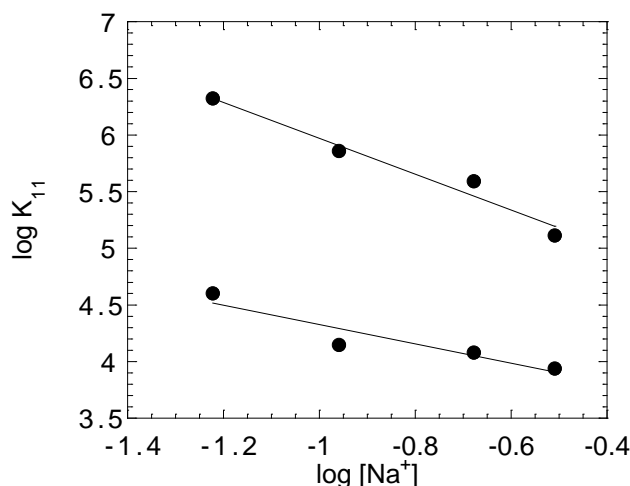
Figure 3-14. Salt dependence of the binding constants (K_{11}) of CF$_3$-AMND to C (upper) and T (lower). The obtained linear equation: y = 4.70 + 1.29 x (r = 0.9859) for C, y = 3.46 + 0.898 x (r = 0.9859) for T.

<u>Calculation procedure of apparent charge:</u>

$\delta \log K_{11}/\delta \log [Na^+] = -Z\psi = SK$

Z: the apparent charge on the ligand; ψ: the proportion of counterions associated with each DNA phosphate group (0.88 for B-type DNA); SK: the slope of the plot, which is equivalent to the number of counterions released from the duplex upon ligand binding.

Thus, for C: $Z = -SK/\psi = 1.29/0.88 = 1.47$; for T: $Z = -SK/\psi = 0.898/0.88 = 1.02$

3-3-4. Effect of the type of binding site

We tried to apply other kinds of active sites instead of AP site for the binding event. However, only moderate selectivity for C can be obtained by gap site, and almost no selectivity by bulge site. This result indicates our ligand is only applicable for AP site as the active binding site, which is a restriction to widely apply this ligand.

DNA sequences

AP site: 5'-GCTCCTCTGG**X**GCCCTCGACG-3', X = AP-site (dSpacer);
             3'-CGAGGAGACC**N**CGGGAGCTGC-5', N = C, T, G or A

Gap site: 5'-GCTCCTCTGG-3' 5'-GCCCTCGACG-3'
             3'-CGAGGAGACC**N**CGGGAGCTGC-5', N = C, T, G or A

Bulge site: 5'-GCTCCTCTGGGCCCTCGACG-3'
             3'-CGAGGAGACC**N**CGGGAGCTGC-5', N = C, T, G or A
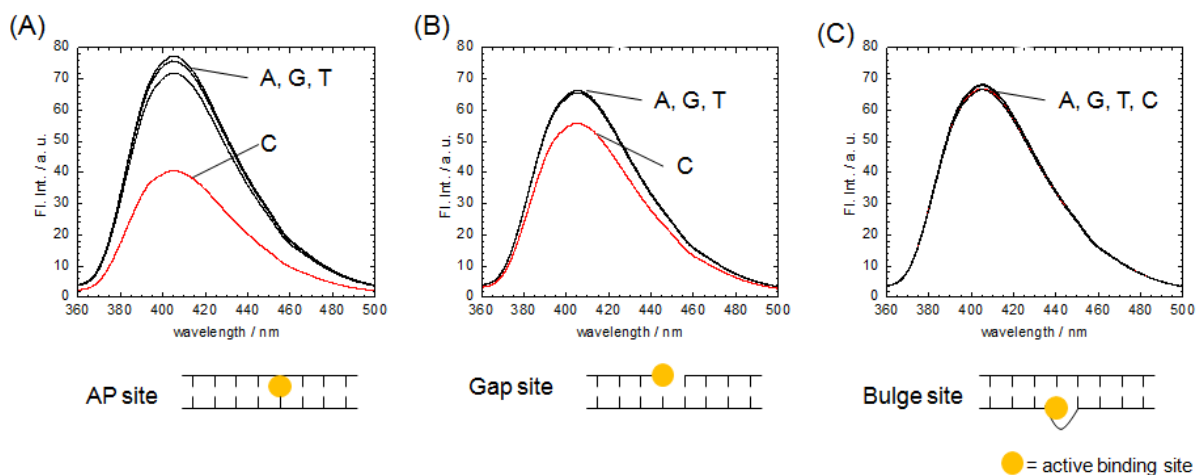
Fig. 3-15. Fluorescence spectra by using different kinds of binding sites; and schematic drawing of these sites .

## 3-4-5. Explanation of the improved selectivity of CF$_3$-AMND compared to AMND

As shown in **Figure 3-16**, CF$_3$-AMND binds to C and T in N1 and N8-protonated forms, respectively. Although further studies such as NMR analysis are required to examine the binding behaviors in detail, it is conceivable that the observed high selectivity of CF$_3$-AMND for C over T (**Figure 3-7**) arises from more favorable protonation at the N1 position than the N8 position due to the electron-withdrawing effect of the CF$_3$ group, which then enables the effective pseudo-base pairing with C through hydrogen bonding.

CF$_3$-AMND: R = CF$_3$
AMND: R = H
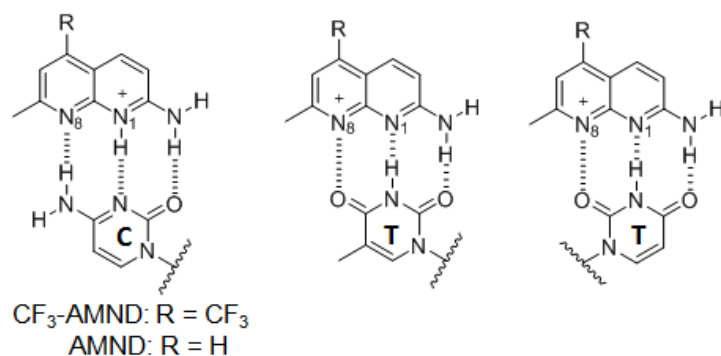
Figure 3-16. Possible binding modes of AMND or CF$_3$-AMND with C and T (two possible patterns).[74]

3-4-6. Application of CF$_3$-AMND to C-related singlebase mutation in K-ras gene

CF$_3$-AMND was applied to the analysis of singlebase mutation in 107-mer DNAs (K-ras gene; codon 12, sense strand)[81] amplified by asymmetric PCR. **Figure 3-16** shows fluorescence responses of 0.1 μM CF$_3$-AMND to the amplified DNAs carrying different target nucleobases measured at 5 ℃ in a solution buffered to pH 5.5 containing 2.0 μM AP sitecontaining probe DNA (5'-CCT ACG CCA XCA GCT CCA AC-3', X = AP site (dSpacer)). As is clearly seen, CF$_3$-AMND exhibits significant fluorescence quenching for C-containing DNA sequences whereas moderate responses are observed for DNAs containing G, T, and A targets. Therefore, CF$_3$-AMND is applicable to highly selective detection of C compared to other nucleobases in PCR products, which will facilitate the accurate analysis of C-related single-base mutation in practical use.
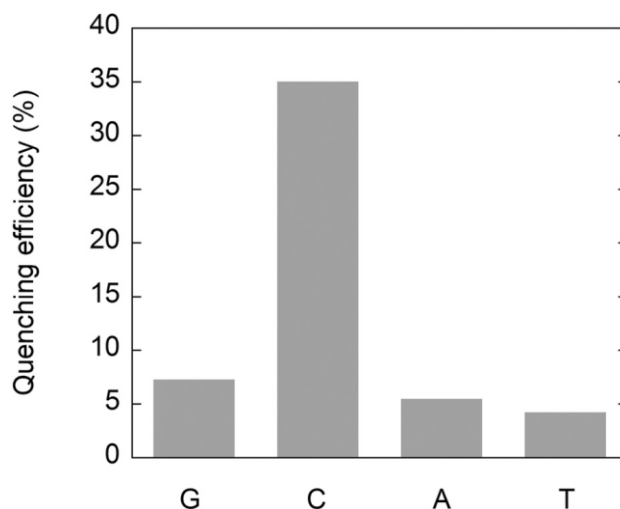
Figure 3-16. Analysis of a single-base mutation in 107-mer DNAs (K-ras gene, codon 12, sense strand) amplified by PCR, measured in solutions buffered to pH 5.5 (100 mM sodium cacodylate) containing 2.0 μM AP site-containing probe DNA and 0.1 μM CF$_3$-AMND. Quenching efficiency (%) was calculated by $(F_0 - F)/F \times 100$, where F and F_0 denote the fluorescence intensities of CF$_3$-AMND in the presence and absence of DNA duplexes, respectively. Excitation: 346 nm. Analysis: 403 nm. Temperature: 5 ℃.

3-5. Conclusion

In summary, we successfully developed CF_3-AMND as a C-specific binding ligand based on AMND. It shows highly selective binding to C in AP site-containing DNA duplexes. The introduction of a CF_3 substituent into the parent AMND significantly improved the binding selectivity for C. We expect that high C-selectivity of CF_3-AMND will be able to provide accurate analysis of C-related single-base mutation in DNAs.

On the other hand, we noted that the binding affinity of CF_3-AMND to C is relatively moderate at the physiological pH condition, and not applicable by using other type of binding sites. Therefore, further efforts to conquer these disadvantages are needed towards practical gene analysis.

Acknowledgement and References

74. Parts of the materials including figures and text extracts are reproduced by permission of The Royal Society of Chemistry.
Y. Sato, Y. Zhang, T. Seino, T. Sugimoto, S. Nishizawa and N. Teramae, *Org. Biomol. Chem*, **2012**, 10, 4003-4006.
Link: http://pubs.rsc.org/en/Content/ArticleLanding/2012/OB/c2ob25513h#!divAbstract

75. http://en.wikipedia.org/wiki/Single-nucleotide_polymorphism

76. http://ghr.nlm.nih.gov/handbook/genomicresearch/snp

77. Wolf, A. B.; Caselli, R. J.; Reiman, E. M.; Valla, *J. Neurobiology of Aging*, **2013**, 34, 1007-1017.

78. http://www.who.int/mediacentre/factsheets/fs310/en/

79. Ren J, Jenkins TC, Chaires JB, *Biochemistry*, **2000**, 39(29), 8439-8447.

80. Haq I, Ladbury JE, Chowdhry BZ, Jenkins TC, Chaires JB, *J. Mol. Biol*, **1997**, 271(2), 244-257.

81. Y. Sato, S. Nishizawa, K. Yoshimoto, T. Seino, T. Ichihashi, K. Morita, and N. Teramae, *Nucleic Acids Res.*, **2009**, 37(5), 1411-1422.

82. Nakatani K, Sando S, Saito I., *Nat. Biotechnol.*, **2001**, 19, 51-55.

83. Hagihara S, Kumasawa H, Goto Y, Hayashi G, Kobori A, Saito I, Nakatani K., *Nucleic Acids. Res.*, **2004**, 32, 278-286.

84. Kobori A, Horie S, Suda H, Saito I, Nakatani K., *J. Am. Chem. Soc.*, **2004**, 126, 557–562.

85. Yoshimoto K, Nishizawa S, Minagawa M, Teramae N, *J Am Chem Soc.*, **2003**, 30, 125, 8982-8983.

86. S. Nishizawa, K. Yoshimoto, T. Seino, CY. Xu, M. Minagawa, H. Satake, A. Tong, N. Teramae, *Talanta.*, **2004**, 63, 175-179.

87. Q. Dai, CY. Xu, Y. Sato, K. Yoshimoto, S. Nishizawa, N. Teramae, *Anal Sci.*, **2006**, 22, 201-203.

88. B. Rajendar, S. Nishizawa, N. Teramae, *Org Biomol Chem.*, **2008**, 6, 670-673.

89. C. Zhao, Q. Dai, T. Seino, YY. Cui, S. Nishizawa, N. Teramae, *Chem. Commun.*, **2006**, (11), 1185-1187.

90. E. V. Brown, *J. Org. Chem.*, **1965**, 30, 1607-1610.

91. Puglisi, J. D.; Tinoco, I. *Method Enzymol.*, **1989**, 180, 304-325.

92. Connors, K. A. *Binding constants*, John Wiley & Sons, New York, **1987**, 339-343.

93. H. Suda, A. Kobori, J. Zhang, G. Hayashi and K. Nakatani, *Bioorg. Med. Chem.*, **2005**, 13, 4507-4512.

Chapter 4: Development of peptide nucleic acid-thiazole orange conjugates for discrimination of terminal mismatches in DNA/RNA

4-1. Introduction

4-1-1. Routine method for the detection of terminal mismatch

As introduced in last chapter, mismatches of DNA/RNAs will be formed when mutations occur, and study of mismatches is clinically important for diagnostics, prognostics, risk assessment and disease prevention. Such as SNPs, where a single nucleobase mismatch formed, will relate to diseases. (ref. introduction in Chapter 3)

Usually, detection of mismatches relies on the method based on the thermal stability of duplex hybridization, and the hybridization property can be evaluated by determining their melting temperature (T_m). The melting temperature is defined as the temperature at which 50% of the DNA strands are in the random coil or single-stranded state; thus meanwile, 50% of the DNA strands and their perfect complements are in duplex. It's the temperature of a middle state between DNA single strands and duplexes.[94]

However, T_m values, measured from melting temperature experiments, are different by only a few degrees (0.5~3°C)[95] between perfectly matched duplexes and terminal mismatched ones.

Particularly, when the mismatches happen at the terminal positions of DNA/RNAs' strand, it's more difficult to be detected than at the internal positions. This is because a mismatch at internal position of DNA/RNA duplex is easier to be destabilized than a terminal mismatch in general, so as to be easier tested by melting temperature experiments.[96] It becomes much more difficult to be discriminated for short duplexes.[97]

## 4-1-2. DNA-TO and PNA-TO ligands for the detection of (terminal) mismatch

Ulysse Asseline and coworkers have proposed a method by measuring fluorescent signal for the detection of terminal mismatch. They synthesized a series of complementary oligo-DNA strands conjugated with thiazole orange (TO) as fluorescent markers. To the target single nucleobase, if mismatch forms, the fluorescence response will be stronger (**Figure 4-1**). Thus the mismatches can be detected successfully.[98]

However, in the result they have shown, it was only related to the 3rd or 4th mismatches counted from the terminal of DNA strand, which are not so much the terminal positions. And the need of modification of probe DNA makes it inconvenient and time consuming, especially when the DNA strand is longer.
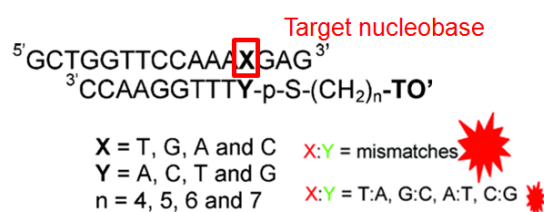
Figure 4-1. DNA sequences used in developing ODN-TO' conjugate experiments for terminal mismatch detection.[98]

Instead of oligo-DNA strands, peptide nucleic acids (PNAs) are often used for its better stability compared with corresponding DNAs (Thermal stable to hybridize with DNA/RNA by lack of electrostatic repulsion; enzymatic stable for not easily recognized by either nucleases or proteases).[99,100] Structurally, PNAs are neutral artificial nucleic acids with backbones composed of repeating N-(2-aminoethyl)-glycine units linked by peptide bonds (**Figure 4-2**).
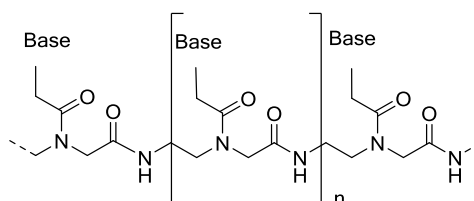
Figure 4-2. Structure of PNA's backbone

Oliver Seitz and coworkers developed a PNA-TO conjugate for internal mismatch detection.[101] It showed good selectivity between perfect match sequence and the mismatched ones (**Figure 4-3**).
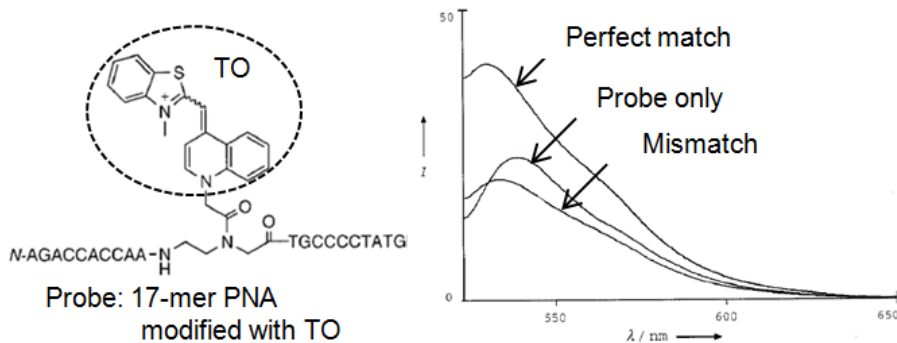
Figure 4-3. PNA-TO conjugate for internal mismatch detection.[101]

To combine the results of their research, we realized that the PNA-TO conjugate might be a promising candidate for the detection of mismatches at terminal positions.

In our group, a series of PNA-TO conjugates has been devoloped recently for siRNA's delivery imaging, even in living cells.[102] **Figure 4-4** shows the possible binding mode of PNA-TO to siRNA duplex's terminal position. Here, PNA unit is synthesized to recognize the terminal overhang two nucleobases, and TO unit works as a fluorescence light-up intercalator.
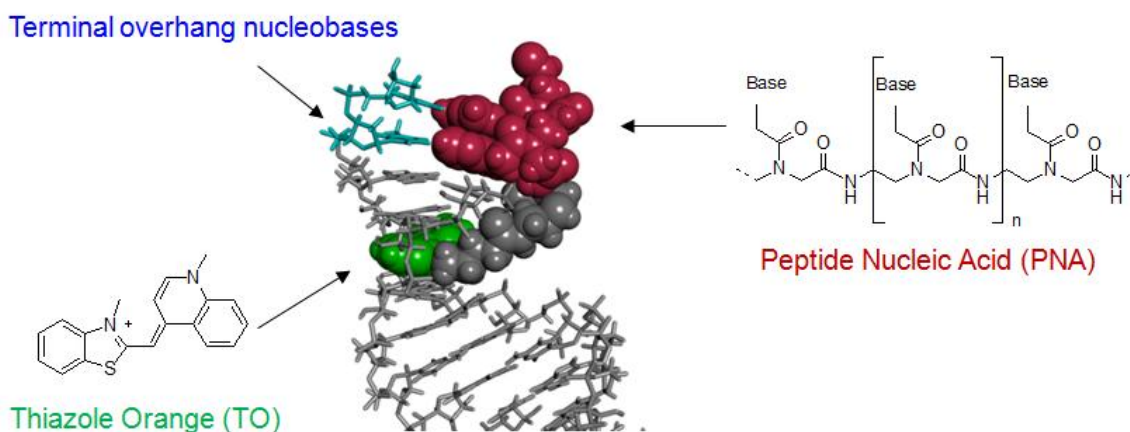
Figure 4-4. Possible binding mode of PNA-TO to siRNA duplex's terminal position (Energy-minimized structure by MacroModel ver. 9.0).[102]

Moreover, this **AA-TO** ligand for the purpose of siRNA's imaging, also showed a good selective fluorescence response for perfect match sequence over terminal mismatched ones (**Figure 4-5**). It indicates the using of PNA-TO would be promising for selective binding to the overhang nucleobases.

However, this result related to only two nucleobases which is obviously not enough for the purpose of a single-base mismatch detection. And we showed mutations detection only in the internal part of DNA/RNA strands in SNPs so far (ref. Chapter 3). As a supplement, we also hope to develop the technique not only related to the internal positions, but also the terminal positions. Therefore, method for the detection of a single-base mismatch at terminal position of nucleic acids is needed to be developed.
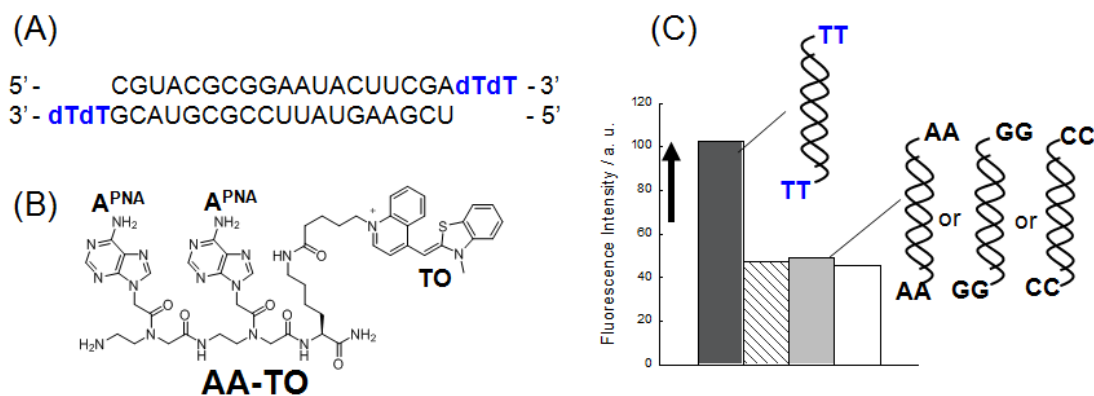
Figure 4-5. (A) Sequence of siRNA; (B) Structure of the PNA-TO ligand (AA-TO);
(C) Fluorescence response for perfect match sequence (TT), and mismatched ones (AA, GG, and CC). [102]

4-1-3. Let-7 microRNA family

The lethal-7 (let-7) gene was first discovered in the nematode Caenorhabditis elegans as a key developmental regulator by controling the timing of stem-cell division and differentiation, and became one of the first two known microRNAs (the other one is lin-4). Let-7 and its family members are highly conserved across species in sequence and function, and misregulation of let-7 leads to a less differentiated cellular state and the development of cell-based diseases such as cancer.[103]

Numerous reports have shown that the expression levels of let-7 are frequently low and the chromosomal clusters of let-7 are often deleted in many cancers.[104] Let-7 is expressed at higher levels in more differentiated tumors, which also have lower levels of activated oncogenes. Therefore, expression levels of let-7 could be prognostic markers in several cancers associated with differentiation stages. In lung cancer, for example, reduced expression of let-7 is significantly correlated with reduced postoperative survival.[105-107]

However, the detection and describe of the members of let-7 family is a challenge as the sequences of members is similar that differ by only a few nucleobases. Such sequences will hybridize similarly to the complementary probes and the signal will not be specific anymore.

Let-7d in the let-7 family, which has been implicated in cocaine addiction and other neurological disorders, targets the neural stem cell regulator TLX. Overexpression of let-7d in vivo reduced neural stem cell proliferation and promoted premature neuronal differentiation and migration.[108] Thus, development of the detection method for let-7d becomes useful.

Here, by using the PNA-TO conjugates, we hope that let-7d with a single nucleobase mismatch at the 5'- terminal position compared to other let-7 family members can be recognized.

4-2. Design strategy

PNA's backbone is composed of repeating N-(2-aminoethyl)-glycine units linked by peptide bonds. Higher thermal stability and specificity than the corresponding DNAs in order to make sure it will hybridize with complementary probe smoothly, regardless of its short length. TO was chosen as an intercalator in order to stabilize the duplex. In addition, TO can act as fluorescence marker to give out a fluorescent signal so as to be measured by fluorescence spectrometer.

Our detection scheme is quite simple. First, put the target strand and probe strand together and let the hybridization happen, so as to form a duplex and leave the target terminal nucleobases exposed. Then put PNA-TO ligands into the solution. If a perfect match formed at the terminal position, it will emit a fluorescent signal. But if mismatches exist, PNA would be restricted to recognize the target nucleobases, thus a small signal can be obtained. By this process, the selective recognition between match and mismatch sequences can be achieved (**Figure 4-6**).

Higher ability to discriminate terminal mismatch by giving a stronger fluorescent signal is expected compared to the two PNA-TO conjugate[102], because of the increased number of PNA should contribute to stabilize the binding.

However, we also didn't chose PNA sequences for more than three nucleobases. It's because an ultra-shot PNA strand is expected more sensitive than the longer ones when binding to target strands. They should be easier to be destabilized by mismatches, so as to be easier to give out signaling.
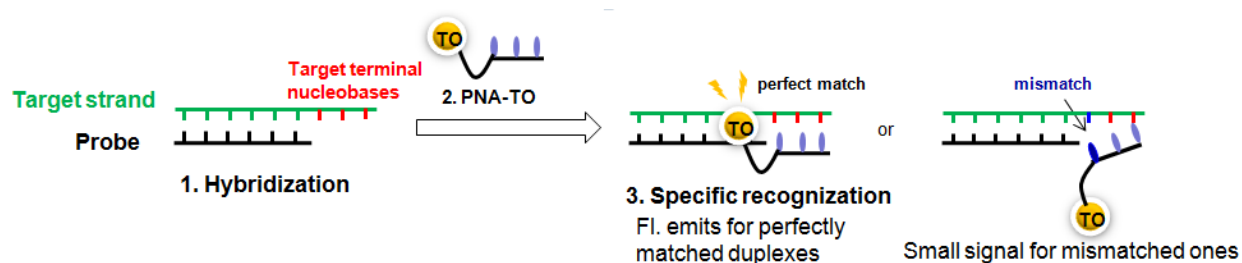
Figure 4-6. Detection scheme of our PNA-TO ligand for terminal mismatch.

4-3. Experimental

Synthesis procedure of peptide nucleic acid -thiazole orange conjugates (PNA-TO).[102]

All probes examined in this study were synthesized on an Endeavor 90 peptide synthesizer (Apptec, Louisville, KY, USA) based on Fmoc/Bhoc chemistry. Briefly, Fmoc-Lys(Alloc)-OH was first loaded onto Rink Amide AM resin and Fmoc/Bhoc-protected PNA monomers were then coupled. For pyrene-containing conjugates, pyrene derivative was coupled to N-terminal of the PNA-lysine assembly directly or through a glycine spacer. The assembly on the resin was performed by repetitive cycles of Fmoc deprotecting (20% piperidine in DMF), coupling with DIC/HOBt activation, and capping (acetic anhydride/pyridine). The completion of the coupling reactions was confirmed by the Kaiser test. After the selective deprotection of the Alloc group by treating with tetrakis(triphenylphosphine) palladium (0) and dimethylamine borane in dichloromethane, carboxylate-terminated butyl spacer-containing TO derivative[109] was coupled to the ε-amino group of Lys. After the Fmoc group was deprotected, deprotection of Bhoc groups in PNA nucleotides and cleavage from the resin were carried out using a mixture of trifluoroacetic acid (TFA)/triisopropylsilane/water (95/2.5/2.5). After the resulting solution was filtered to remove the resin, the probes were then precipitated in cold diethyl ether. The crude products were purified by a reverse-phase HPLC system (pump, PU-2086 Plus x2; mixer, MX 2080-32; column oven, CO-1565 (40°C); detector, UV-2070 plus and UV-1570M (Japan Spectroscopic Co. Ltd., Tokyo, Japan)) equipped with a C18 column (Inertsil ODS3: GL Sciences Inc., Tokyo, Japan) using a gradient of water/acetonitrile containing 0.05% TFA. All probes used in this study were verified for 90% by MALDI-TOF-MS (4800 Plus MALDI TOF/TOF analyzer: AB Sciex, Tokyo, Japan).

A2 (AAA-C2-TO): MALDI-TOF-MS for $C_{60}H_{71}N_{26}O_8S$ $[M]^+$; calcd 1315.57, found 1315.48.

A4 (AAA-C4-TO): MALDI-TOF-MS for $C_{62}H_{76}N_{26}O_8S$ $[M]^+$; calcd 1343.60, found 1343.92.

A6 (AAA-C6-TO): MALDI-TOF-MS for $C_{64}H_{79}N_{26}O_8S$ $[M]^+$; calcd 1371.63, found 1371.92.

C6 (CCC-C6-TO): MALDI-TOF-MS for $C_{61}H_{79}N_{20}O_{11}S$ $[M]^+$; calcd 1299.60, found 1299.53.

Py-C4 (Pyrene-CCC-C4-TO): MALDI-TOF-MS for $C_{78}H_{86}N_{21}O_{13}S$ $[M]^+$; calcd 1556.64, found 1557.13.

Py-TCT-TO (Pyrene-TCT-C4-TO): MALDI-TOF-MS for $C_{80}H_{88}N_{19}O_{15}S$ $[M]^+$; calcd 1586.64, found 1587.24.

These PNA-TO ligands were dissolved into water to prepare the stock solutions. Stock solutions of pyrene-containing probes were prepared using water or water/DMSO (for Py-TCT-TO only) mixtures. These stock solutions were kept at 4°C in the dark before their use. Sample solutions of pyrene-containing probes used for the experiments contain a small amount of these organic solvents (< 0.2%).

DNA and RNA sequences

5'-TTT: 5'-TTTGACCTAGTAGGCTGC-3' (ε_{260} = 171320 $M^{-1}cm^{-1}$)

5'-ATT: 5'-ATTGACCTAGTAGGCTGC-3' (ε_{260} = 176940 $M^{-1}cm^{-1}$)

5'-TAT: 5'-TATGACCTAGTAGGCTGC-3' (ε_{260} = 176640 $M^{-1}cm^{-1}$)

5'-TTA: 5'-TTAGACCTAGTAGGCTGC-3' (ε_{260} = 177200 $M^{-1}cm^{-1}$)

3'-TTT: 5'-GACCTAGTAGGCTGCTTT-3' (ε_{260} = 171800 $M^{-1}cm^{-1}$)

3'-ATT: 5'-GACCTAGTAGGCTGCTTA-3' (ε_{260} = 178140 $M^{-1}cm^{-1}$)

3'-TAT: 5'-GACCTAGTAGGCTGCTAT-3' (ε_{260} = 177120 $M^{-1}cm^{-1}$)

3'-TTA: 5'-GACCTAGTAGGCTGCATT-3' (ε_{260} = 176800 $M^{-1}cm^{-1}$)

5'-GGG: 5'-GGGGACCTAGTAGGCTGC-3' (ε_{260} =179140 $M^{-1}cm^{-1}$)

5'-CGG: 5'-CGGGACCTAGTAGGCTGC-3' (ε_{260} = 175060 $M^{-1}cm^{-1}$)

5'-GCG: 5'-GCGGACCTAGTAGGCTGC-3' (ε_{260} =175140 $M^{-1}cm^{-1}$)

5'-GGC: 5'-GGCGACCTAGTAGGCTGC-3' (ε_{260} = 175140 $M^{-1}cm^{-1}$)

3'-GGG: 5'-GACCTAGTAGGCTGCGGG-3' (ε_{260} = 179620 $M^{-1}cm^{-1}$)

3'-CGG: 5'-GACCTAGTAGGCTGCGGC-3' (ε_{260} = 175140 $M^{-1}cm^{-1}$)

3'-GCG: 5'-GACCTAGTAGGCTGCGCG-3' (ε_{260} = 175620 $M^{-1}cm^{-1}$)

3'-GGC: 5'-GACCTAGTAGGCTGCCGG-3' (ε_{260} = 176360 $M^{-1}cm^{-1}$)

No overhang: 5'-GACCTAGTAGGCTGC-3' (ε_{260} = 147040 $M^{-1}cm^{-1}$)

Probe: 3'-CTGGATCATCCGACG-5' (ε_{260} = 144000 $M^{-1}cm^{-1}$)

let-7a: 5'- UGAGGUAGUAGGUUGUAU AGUU-3' (ε_{260} = 244510 $M^{-1}cm^{-1}$)

let-7b: 5'- UGAGGUAGUAGGUUGUGUGGUU-3' (ε_{260} = 237310 $M^{-1}cm^{-1}$)

let-7c: 5'- UGAGGUAGUAGGUUGUAUGGUU-3' (ε_{260} = 240730 $M^{-1}cm^{-1}$)

let-7f : 5'- UGAGGUAGUAGAUUGUAUAGUU-3' (ε_{260} = 246670 $M^{-1}cm^{-1}$)

let-7d: 5'- AGAGGUAGUAGGUUGCAUAGU-3' (ε_{260} = 234650$M^{-1}cm^{-1}$)

let-7e: 5'- UGAGGUAGGAGGUUGUAUAGU-3' (ε_{260} = 234290 $M^{-1}cm^{-1}$)

let-7g: 5'- UGAGGUAGUAGUUUGUACAGU-3' (ε_{260} = 229780 $M^{-1}cm^{-1}$)

let-7i: 5'- UGAGGUAGUAGUUUGUGCUGU-3' (ε_{260} = 221510 $M^{-1}cm^{-1}$)

DNA probe: 3'-CCATCATCCTTCGTATCA-5' (ε_{260} = 172080 $M^{-1}cm^{-1}$)

RNA probe: 3'-CCAUCAUCCUUCGUAUCA-5' (ε_{260} = 177580 $M^{-1}cm^{-1}$)

All of the DNA samples were custom synthesized and HPLC purified (>97%) by Nihon Gene Research Laboratories Inc. (Sendai, Japan). RNAs were custom synthesized and PAGE purified (>97%) by Sigma-Genosys (Hokkaido, Japan). The extinction coefficients at 25°C were calculated at 260 nm for each strand [63], which was shown in bracket above.

Rink Amide AM resin, Fmoc-protected amino acid derivative were purchased from Aapptec (Luisville, KY, USA).

Fmoc/Bhoc protected PNA monomers were purchased from ASM Research Chemicals (Hannover, Germany).

The other reagents were commercially available analytical grade and were used without further purification. Water was deionized (≥18.0 MΩ cm specific resistance) by an Elix 5 UV

Water Purification System and a Milli-Q Synthesis A10 system (Millipore Corp., Bedford, MA).

Instruments

Fluorescence measurement: Fluorescence spectra were measured with a JASCO model FP-6500 spectrofluorophotometer equipped with a thermoelectrically temperature-controlled cell holder (Japan Spectroscopic Co. Ltd., Tokyo, Japan). Fluorescence measurements were carried out at 20°C using a 3×3 mm quartz cell. Excitation wavelength was set at 514 nm for PNA-TO ligands.

UV measurement: JASCO model V-570 spectrophotometer.

Preparation of stock solutions

DNA and RNA solutions: The concentrations of DNAs were determined from the molar extinction coefficients at 260 nm. Stock solutions were prepared with miliQ water to 250 μM or 100 μM and stored at 4°C for DNA; -20°C for RNA.

Buffer solution: Stock solution was prepared in 100 ml miliQ water and containing sodium cacodylate (1.071g, 50 mM), NaCl (2.935g, 500 mM), EDTA (0.187g, 5.0 mM), and stored at 4°C. When applied it into tubes, it was 5 times diluted, which made the standard buffer solution's concentration as follows: [sodium cacodylate] = 10 mM, [NaCl] = 100 mM, [EDTA] = 1.0 mM.

In Chapter 4, unless otherwise mentioned, all measurements were performed in standard buffer solution: 10 mM sodium cacodylate buffer solutions (pH 7.0) containing 100 mM NaCl and 1.0 mM EDTA. Before measurements, the sample solutions were annealed as follows: heated at 75°C for 10 min, and gradually cooled to 5°C (3°C/min), after which the solution temperature was raised again to 20°C.

4-4. Results and discussion

4-4-1. Optimization of PNA-TO conjugates

4-4-1-1. Abstract

We carried out a series experiments to determine the most likely useful PNA-TO conjugate to recognize terminal mismatches in DNA duplexes. Since the similarity of DNAs and RNAs, and the better stability and inexpensive property, we used DNAs for the preliminary experiments. For PNA-TO ligands, we first surveyed the selectivity for terminal mismatch at both 5' and 3' end. Then, we synthesized a series PNA-TO conjugates with different lengths of the linker between PNA moiety and TO moiety (**A2**, **A4**, and **A6**), and compared the effect of linker's length to selectivity. Next, we also synthesized a different kind of ligand (**C6**) targeting another type of terminal mismatch, and tried to prove that our approach is workable without relationship of the sequence. Finally, we showed a demonstration of microRNA's terminal mismatch recognition.

4-4-1-2. Discrimination ability of PNA-TO for terminal mismatch

We synthesized A^{PNA}-A^{PNA}-A^{PNA}-$(CH_2)_6$-TO (**A6**) first, and measured fluorescence spectra of **A6** with or without DNA duplex. As shown in **Figure 4-6**, the ligand **A6** alone has almost negligible fluorescence response. However, upon addition of DNA duplexes, strong fluorescence signal can be observed. For both 5' and 3' ends, selective response for perfect match sequence over mismatched sequences can be obtained. And obviously, the discrimination ability relates to the mismatch formed position: the fluorescence intensity of perfect match sequences are larger than 1st terminal mismatches, followed by 2nd and 3rd terminal mismatches, and followed by no overhang sequences.

The N- end of PNA corresponds to 5' end of DNA, and C- end of PNA corresponding to 3' end of DNA. In general, antiparallel forms (two strands with opposite alignments) of nucleic acid duplexes are canonical form (**Figure 4-7**). Interestingly, the result shows fluorescence intensity of 5' end is comparable with 3' end for perfect match strand in our system, which means parallel formation can be formed in this case.

DNA sequences used in this section:
5'-TTT: 5'-TTTGACCTAGTAGGCTGC-3'
5'-ATT: 5'-ATTGACCTAGTAGGCTGC-3'
5'-TAT: 5'-TATGACCTAGTAGGCTGC-3'
5'-TTA: 5'-TTAGACCTAGTAGGCTGC-3'
3'-TTT: 5'-GACCTAGTAGGCTGCTTT-3'

3'-ATT: 5'-GACCTAGTAGGCTGCTTA-3'

3'-TAT: 5'-GACCTAGTAGGCTGCTAT-3'

3'-TTA: 5'-GACCTAGTAGGCTGCATT-3'

No overhang: 5'-GACCTAGTAGGCTGC-3'

Probe:　　　　3'-CTGGATCATCCGACG-5'
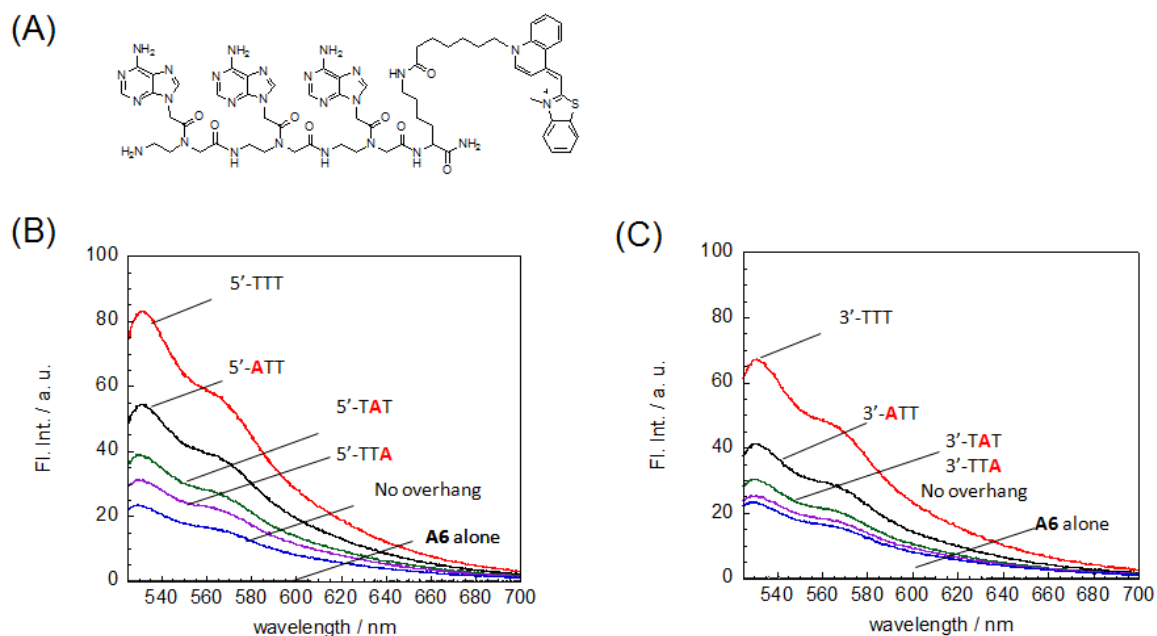
Figure 4-6. (A) Structure of A^{PNA}-A^{PNA}-A^{PNA}-$(CH_2)_6$-TO (**A6**);

(B) Fluorescence spectra of **A6** to DNA duplexes at 5' ends;

(C) Fluorescence spectra of **A6** to DNA duplexes at 3' ends.

[DNA duplex] = [**A6**] = 200 nM, buffer, pH 7.0, 20°C, Sensitivity: medium, Ex band: 3 nm, Em band: 5 nm, 3×3 quartz cell, Excitation: 514 nm.
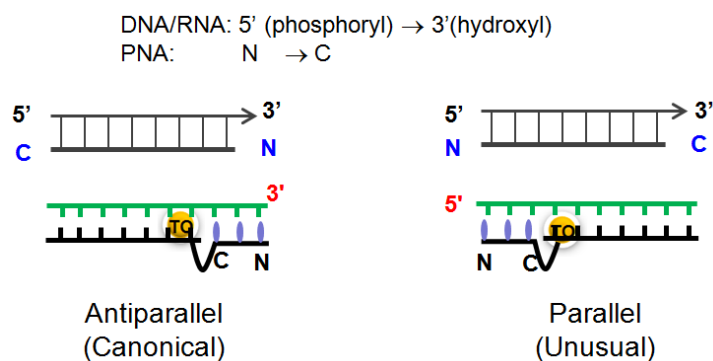
Figure 4-7. Illustration of antiparallel and parallel form of DNA/PNA-TO duplex

4-4-1-3. Effect of the linker's length in PNA-TO ligands

In order to investigate the effect of linker's length in PNA-TO ligands, we further synthesized AAA-C2-TO (**A2**) and AAA-C6-TO (**A6**). As shown in **Figure 4-8**, for all ligands, selective response for perfect match sequence over mismatched sequences can be obtained at 3' end. And the degree of light-up response, however, depends on the linker's length (**A6**, **A4** > **A2**), suggesting longer linker would be better for the effective fluorescent response. The same selectivity and tendency can be observed for 5' end too (Data not shown).
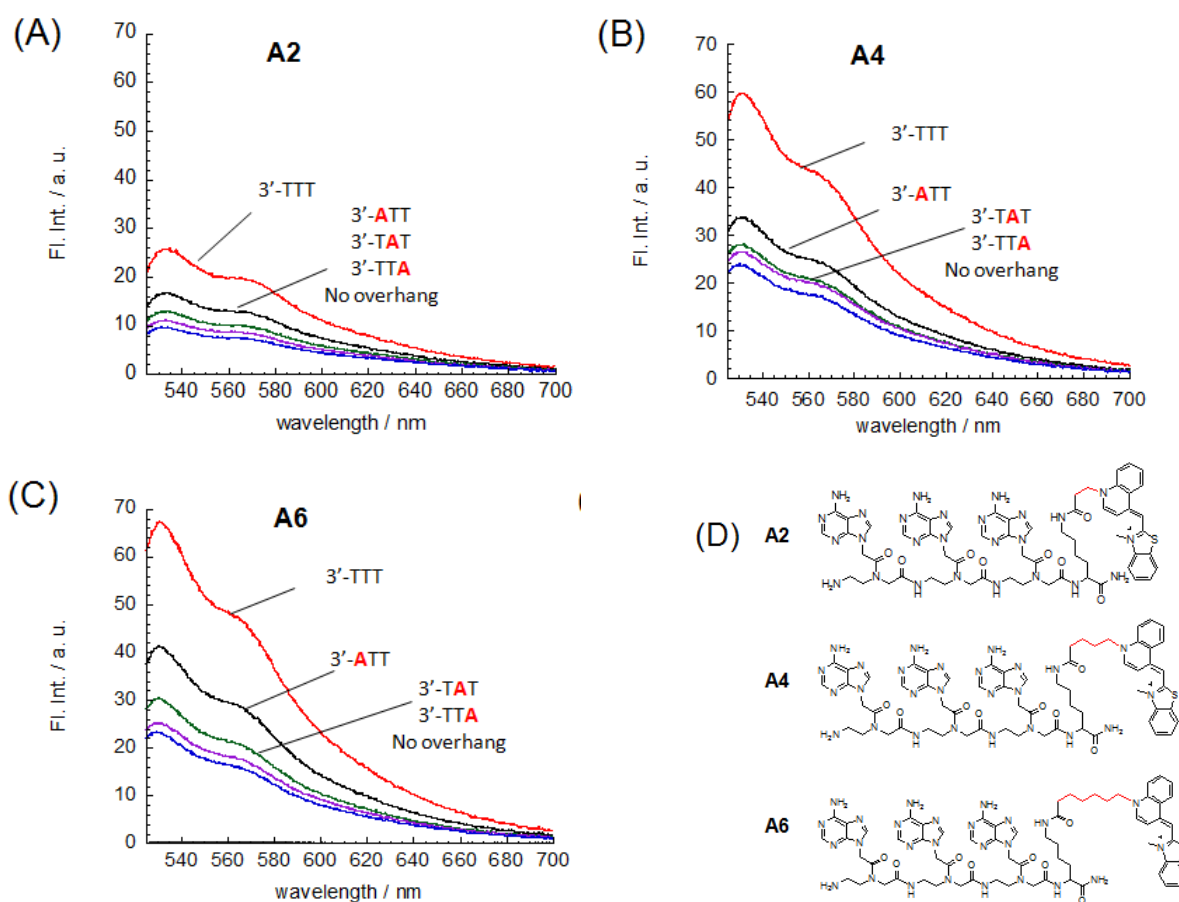
Figure 4-8. (A), (B) and (C) Fluorescence spectra of **A2**, **A4**, and **A6** to DNA duplexes at 3' ends, respectively; (D) Structure of A^{PNA}-A^{PNA}-A^{PNA}-$(CH_2)_6$-TO (**A6**).

[DNA duplex] = [**A2**, **A4** or **A6**] = 200 nM, buffer, pH 7.0, 20°C, Sensitivity: medium, Ex band: 3 nm, Em band: 5 nm, 3×3 quartz cell, Excitation: 514 nm.

4-4-1-4. Ligand design for another sequence

We wanted to prove the universal of our ligand design strategy. Therefore, we synthesized another PNA-TO ligand (**Figure 4-9(A)**) for different target sequences. The linker's length is determined as 6, so the ligand is C^{PNA}-C^{PNA}-C^{PNA}-$(CH_2)_6$-TO (**C6**). The result shows the discrimination ability maintains for perfect match sequence over terminal mismatches, irrespective of the type of nucleobases (purine of pyrimidine). This implies the ligand design would have flexibility for any kind of terminal sequences, which is a great advantageous of our method.

DNA sequences used in this section:

5'-GGG:	5'-GGGGACCTAGTAGGCTGC-3'
5'-CGG:	5'-CGGGACCTAGTAGGCTGC-3'
5'-GCG:	5'-GCGGACCTAGTAGGCTGC-3'
5'-GGC:	5'-GGCGACCTAGTAGGCTGC-3'
3'-GGG:	5'-GACCTAGTAGGCTGCGGG-3'
3'-CGG:	5'-GACCTAGTAGGCTGCGGC-3'
3'-GCG:	5'-GACCTAGTAGGCTGCGCG-3'
3'-GGC:	5'-GACCTAGTAGGCTGCCGG-3'
No overhang:	5'-GACCTAGTAGGCTGC-3'
Probe:	3'-CTGGATCATCCGACG-5'
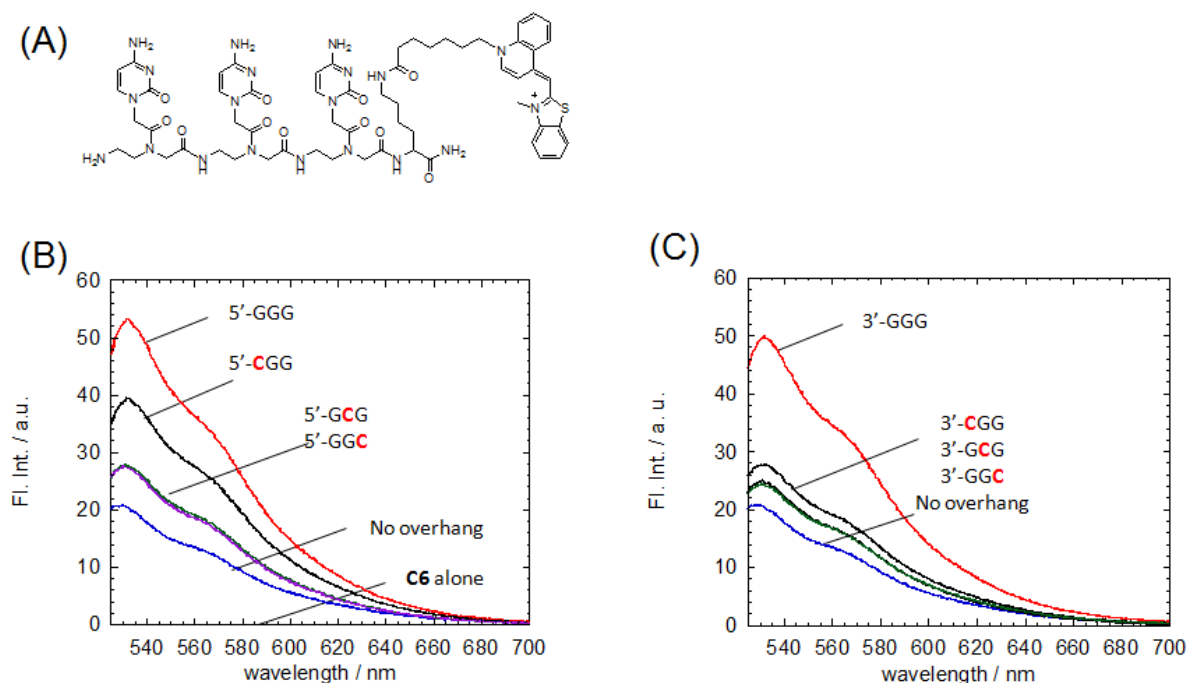
Figure 4-9. (A) Structure of C^{PNA}-C^{PNA}-C^{PNA}-$(CH_2)_6$-TO (**C6**);
(B) Fluorescence spectra of **C6** to DNA duplexes at 5' ends;
(C) Fluorescence spectra of **C6** to DNA duplexes at 3' ends.
Other solution conditions are the same as given in Figure 4-6.

4-4-1-5. Comparison of the binding selectivity for the target terminal overhang sequences with A (purine) and C (pyrimidine)

We summarized the data for the ligand **A6** and **C6**, and compared them. For 3' end, both ligands show good selectivity for perfect match sequences, where the fluorescence intensities are ca. 40%~60% larger than mismatches. However, the selectivity for 5' end shoud be improved, especially for the 1st terminal mismatches (**Figure 4-10**; marked with red rectangle).
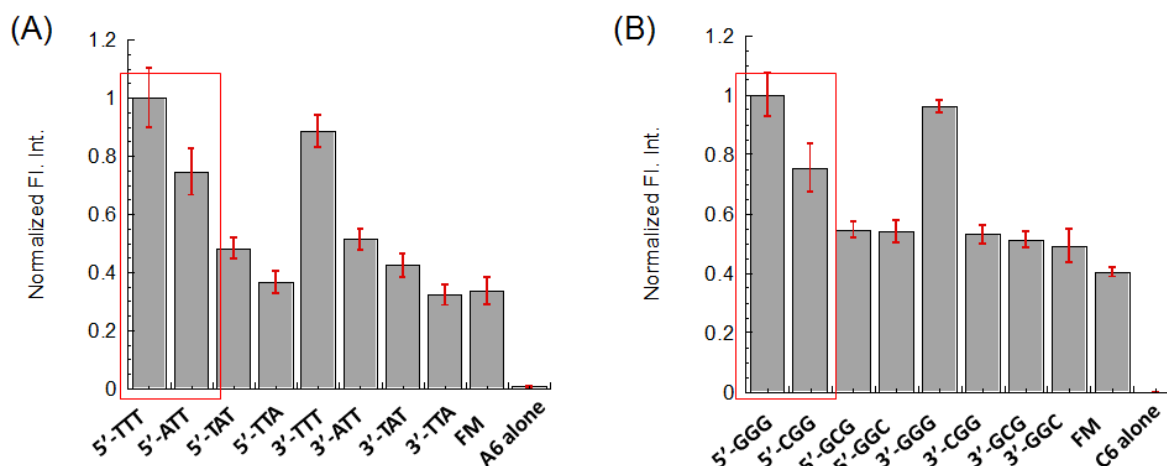
Figure 4-10. Bar figures of normalized fluorescence intensity for (A) **A6**, and (B) **C6**. Other solution conditions are the same as given in Figure 4-6.

The binding affinities have been measured by fluorescent titration experiments, and the results are shown in **Table 4-1**.

K_{11} ($n = 3$)	**A6** / $10^6 M^{-1}$	**C6** / $10^6 M^{-1}$
5'- perfect match (5'-TTT or 5'-GGG)	4.6 ± 0.1	10.5 ± 2.5
5'- 1st mismatch (5'-ATT or 5'-CGG)	1.9 ± 0.5	10.7 ± 2.3
3'-perfect match (3'-TTT or 3'-GGG)	2.6 ± 0.3	7.5 ± 0.9
3'- 1st mismatch (3'-ATT or 3'-CGG)	1.8 ± 0.1	2.3 ± 0.4

Table 4-1. Binding constants for **A6** and **C6** to perfect match sequences and 1st terminal mismatches. (Errors are the fitting errors.)

4-4-2. Enhancement of the selectivity at 5'- end

From the fluorescence spectra of **A6** (**Figure 4-6**) and **C6** (**Figure 4-9**), we noticed the response to no overhang strands also existed (5'-GACCTAGTAGGCTGC-3'/ 3'-CTGGATCATCCGACG-5'). It's probably come from the nonspecific intercalation of TO unit to the DNA duplex, without complementary recognition of PNA unit to the terminal target bases. Accordingly, the key to high selectivity for the overhanging nucleobases is to suppress such non-selective intercalation.[102]

We took the same strategy as ref. 102, which is to introduce pyrene as a cap structure at N-terminal of PNA-TO (**Py-PNA-TO**) because the high propensity of pyrene for π-π stacking can promote the intramolecular stacking of the probe in the absence of target DNAs (**Figure 4-11**). Therefore, it restricts the nonspecific intercalation of TO unit to the stem of DNA duplex. Moreover, after binding with the DNA duplex, pyrene will also provide terminal stacking interactions which benefit a more stable binding, and a hydrophobic environment, which benefit to form hydrogen bonds.
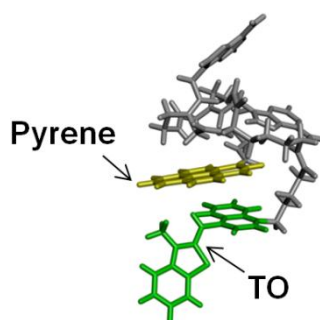
Figure 4-11. The possible initial conformation of **Py-PNA-TO**

The results are listed in **Figure 4-12**. The left side figure (B) presents the spectra by using **C6** (CCC-C6-TO), and the right side figure (C) presents the spectra by using **Py-C** (Pyrene-CCC-C4-TO). **Py-C** shows an incredibly good selectivity for terminal mismatches, regardless of the mismatch formed position. Especially for 1st terminal mismatch, the selectivity has been improved as compared to the ligand without pyrene moiety. This means pyrene cap is significantly effective in the improvement of binding selectivity for terminal mismatches at 5' end.
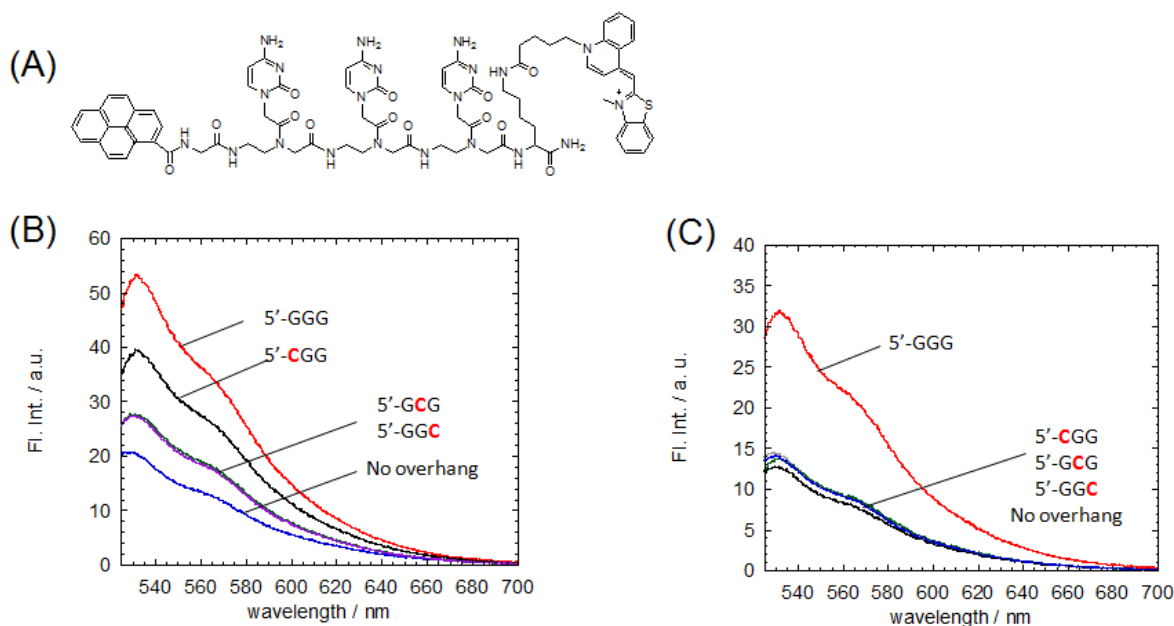
Figure 4-12. (A) Structure of Pyrene-C^{PNA}-C^{PNA}-C^{PNA}-(CH$_2$)$_4$-TO (**Py-C4**);

(B) Fluorescence spectra of **C6** to DNA duplexes at 5' ends;

(C) Fluorescence spectra of **Py-C4** to DNA duplexes at 5' ends.

Other solution conditions are the same as given in Figure 4-6.

In fact, we also tried to synthesize the ligand with the linker's length as C6 (Pyrene-CCC-C6-TO). However, almost no obviously improvement of selectivity can be achieved (Figure not shown). It probably can be explained by considering the possible initial conformation of this ligand (**Figure 4-11**). If the linker's length increases, it would be longer distance between PNA unit and TO unit, so as to be harder to form the intramolecular stacking formation as shown in **Figure 4-11**. Thus, the non-specific binding of TO unit will increase, and lead to the low selectivity of this ligand.

4-4-3. A demonstrate application by using let-7 family microRNAs

Finally, we apply our Py-PNA-TO ligand into the detection of microRNAs. As mentioned in the introduction section, let-7 microRNAs are tumer-related with highly similar sequences. The sequences are listed as follows:

let-7a:　5'- UGAGGUAGUAGGUUGUAU AGUU-3'
let-7b:　5'- UGAGGUAGUAGGUUGUGUGGUU-3'
let-7c:　5'- UGAGGUAGUAGGUUGUAUGGUU-3'
let-7f :　5'- UGAGGUAGUAGAUUGUAUAGUU-3'
let-7d:　5'- **A**GAGGUAGUAGGUUGCAUAGU-3'
let-7e:　5'- UGAGGUAGGAGGUUGUAUAGU-3'
let-7g:　5'- UGAGGUAGUAGUUUGUACAGU-3'
let-7i:　5'- UGAGGUAGUAGUUUGUGCUGU-3'
DNA probe:　3'-CCATCATCCTTCGTATCA-5'
RNA probe:　3'-CCAUCAUCCUUCGUAUCA-5'

The 1st terminal nucleobase of let-7d is adenosine (A), while all the others are urine (U). Therefore, we chose let-7d as the target and therefore synthesized Pyrene-TCT-C4-TO (**Py-TCT-TO**, **Figure 4-12 (A)**) for it. Successfully, a clear selectivity for let-7d out of all the let-7 sequences was obtained (**Figure 4-12 (B)**). By taking three times independent experiments, a figure with error bars was also obtained, suggesting the experiment result is repeatable (**Figure 4-12 (C)**). Also, by using RNA probe to complementarily form duplexes with let-7 microRNAs, can get a similar result (**Figure 4-13**).

It's exciting that in this demonstration, the very 1st terminal mismatch can be recognized with Py-TCT-TO, where is the most difficult to discrimination position. In addition, the success also indicates this PNA-TO ligand can be used for not only DNA duplex, but also DNA/RNA hybrid, or RNA duplex.
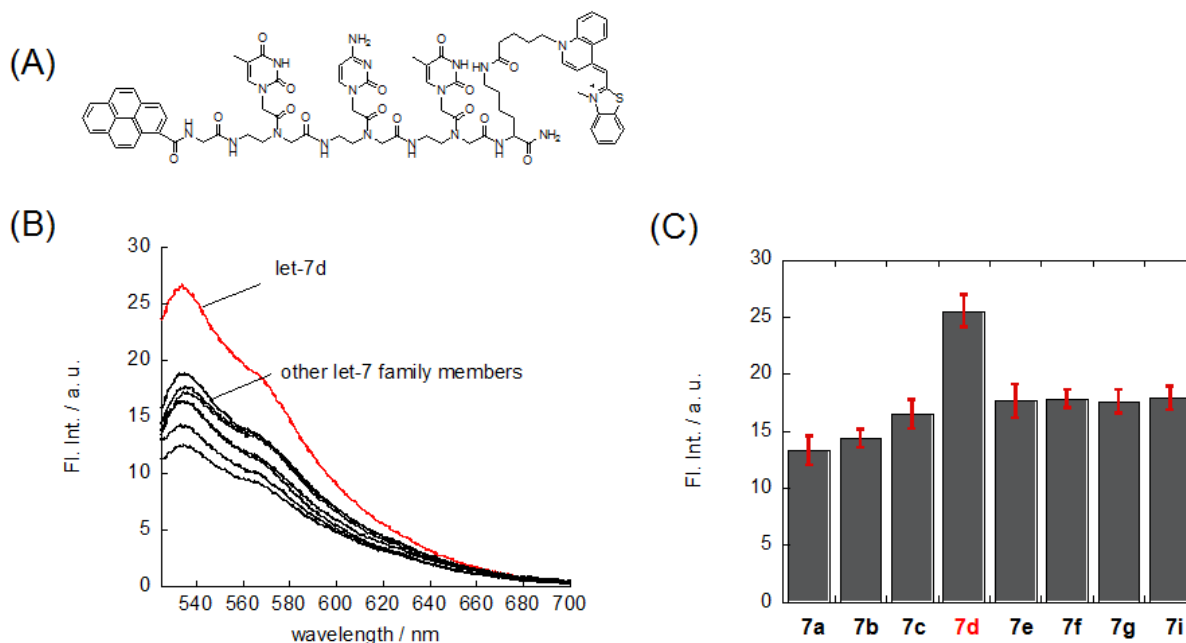
Figure 4-12. (A) Structure of Pyrene-T^{PNA}-C^{PNA}-T^{PNA}-(CH$_2$)$_4$-TO (**Py-TCT-TO**);

(B) Fluorescence spectra of **Py-TCT-TO** for let-7d;

(C) Bar figures of let-7 family microRNAs.

[let-7 RNA/DNA hybrid] = [Py-CCC-C4TO] = 200 nM, buffer, pH 7.0, 20°C, Sensitivity: medium, Ex band: 3 nm, Em band: 5 nm, 3×3 quartz cell, Excitation: 514 nm, Analysis at 531 nm.
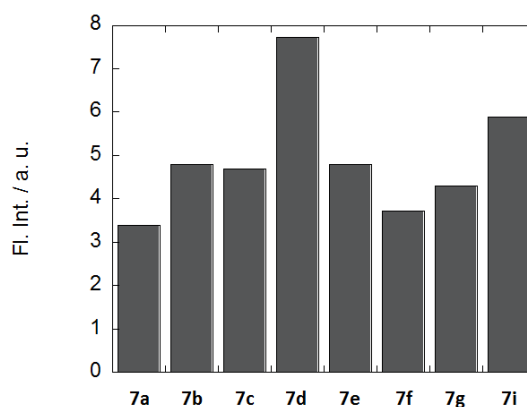
Figure 4-13. Bar figures of let-7 family microRNAs by using RNA probe.

[let-7 RNA/RNA duplex] = [Py-CCC-C4TO] = 200 nM. Other solution conditions are the same as given in Figure 4-12.

Under the present experimental conditions, LOD for let-7d was determined as 18 nM (0.9 nmol in 50µL sample) according to eq (1) in Chapter 2. As for the response to let-7d, the equation obtained by the linear fitting (**Figure 4-14**) is $y = 0.31776 + 0.12697\ x$ ($R = 0.99946$). The standard deviation of blank (S_{blank}) is 0.75403. According to the equation (1), LOD was thus estimated as 18 nM, which is comparable with Northern blotting.
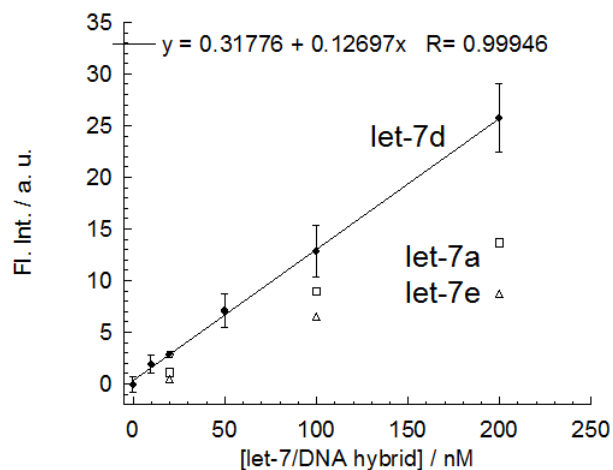
Figure 4-14. The linear fitting analysis for the determination of detection of limit (LOD). [let-7 RNA/DNA hybrid] = 0, 10, 20, 50, 100, 200 nM, [Py-CCC-C4TO] = 50 nM.

4-5. Conclusion

We successfully developed a series of PNA-TO ligands with high selectivity for perfect match sequence over terminal mismatched ones, even for a single mismatch at the very 1st terminal position. It's effective at both 5' and 3' terminals, and introducing pyrene to the ligand as a molecular cap has improved the specificity for the 1st terminal position mismatch at 5' end. In addition, it's applicable to microRNA detection with high selectivity and sensitivity.

Since we used both DNA and RNA strands in our study, the PNA-TO ligands probably can be utilized in both DNAs and RNAs and the type of target nucleobases are not limited. Furthermore, it's a method which is real modification-free of DNA/RNAs for SNPs detection at terminal positions.

However, we have to admit the limitations of our method. Such as, the synthesis of ligands is a time cost work. And the fluorescence stability of the binding PNA-TO/DNA or RNA complex is not that good. After preparation of examples, measurement should be soon taken in case of the quenching of fluorescence.

References

94. http://www.entelechon.com/2008/08/dna-melting-temperature/

95. Yong You, Bernardo G. Moreira, Mark A. Behlke, and Richard Owczarzy, *Nucleic Acids Research*, **2006**, 34(8), e60**.**

96. Stahl, D. A., and R. Amann. **1991**. Development and application of nucleic acid probes, p. 205-248. In E. Stackebrandt and M. Goodfellow (ed.), *Nucleic acid techniques in bacterial systematics.*, John Wiley & Sons Ltd., Chichester, United Kingdom.

97. Hidetoshi Urakawa, Peter A. Noble, Said El Fantroussi, John J. Kelly, and David A. Stahl, *Appl. Environ. Microbiol.*, **2002**, 68, 235-244.

98. Ulysse Asseline, Marcel Chassignol, Yves Aubert, and Victoria Roig, *Organic & Biomolecular Chemistry*, **2006**, 4(10), 1949-1957.

99. http://en.wikipedia.org/wiki/Peptide_nucleic_acid

100. Giovanni N. Roviello, Ettore Benedetti, Carlo Pedone, Enrico M. Bucci, *Amino Acids*, **2010**, 39, 45-57.

101. O. Seitz, F. Bergmann and D. Heindl, *Angew. Chem., Int. Ed.,* **1999**, 38, 2203-2006.

102. T. Sato, Y. Sato, K. Iwai, S. Kuge, S. Nishizawa, N. Teramae, *Chem. Commun.*, **2015**, 51, 1421-1424.

103. Sarah Roush, Frank J. Slack, *Tends in cell biology*, **2008**, Volume 18, Issue 10, 505-516.

104. Calin; Sevignani, C; Dumitru, CD; Hyslop, T; Noch, E; Yendamuri, S; Shimizu, M; Rattan, S; Bullrich, F et al., *PNAS*, **2003**, 101 (9), 2999-3004.

105. Shell S; Park SM; Radjabi AR et al., *PNAS*, **2007**, 104 (27), 11400-11405.

106. Takamizawa J; Konishi H; Yanagisawa K et al., *Cancer Res.*, 2004, 64, 3753-3756.

107. http://en.wikipedia.org/wiki/Let-7_microRNA_precursor

108. Chunnian Zhao, GuoQiang Sun, Peng Ye, Shengxiu Li and Yanhong Shi, *Scientific Reports*, **2006**, 3, 1329.

109. Carreon, J. R., Stewart, K. M., Mahon, Jr. K. P., Shin, S. Kelly, S. O., *Bioorg. Med. Chem. Lett.*, **2007**, 17, 5182-5185.

Chapter 5: Conclusion

In summary, we have developed three systems by utilizing the interactions between small ligand and DNA/RNAs.

In chapter 2, we developed an AP site-containing AP-aptamer without modification with fluorescent probes. It was based on the competitive binding of theophylline with riboflavin at the AP site. In the absence of theophylline, riboflavin binds to the receptor nucleobase opposite the AP site, and this is accompanied by fluorescence quenching. Upon addition of theophylline, the competitive binding of theophylline with riboflavin occurs, which results in the effective fluorescence restoration due to the release of riboflavin from the AP site.

Fluorescence response showed a good linear correlation to the concentration of theophylline ranged from 10 μM to 32.5 μM in horse serum samples, and little response was observed for caffeine and theobromine. Importantly, this range corresponds to the concentration range from 50 μM to 162.5 μM in the original serum samples, which covers the therapeutic range (60-100 μM).

Due to the high selectivity for theophylline, the present method could be successfully applicable to detect serum theophylline in a therapeutic concentration range. Since neither the covalent labeling with signal transduction units nor the modification with the fluorescent nucleotide analogues is required, the proposed assay is simpler, easier, and more cost-effective than typical assays based on theophylline-binding RNA-aptamers. These characteristics of the proposed method are clearly advantageous for practical use.

In chapter 3, we developed a small ligand CF_3-AMND for the detection of SNPs. It showed increasingly high C/T selectivity as over 50-fold, compared with the parent AMND as 4.2-fold.

The high selectivity of CF_3-AMND might be caused from more favorable protonation at the N1 position than the N8 position due to the electron-withdrawing effect of the CF_3 group, which then enables the effective pseudo-base pairing with C through hydrogen bonding. Furthermore, CF_3-AMND is applicable to the analysis of single-base mutation in 107-mer DNAs (K-ras gene; codon 12, sense strand) amplified by asymmetric PCR, with highly selectivity for C. This will facilitate the accurate analysis of C-related single-base mutation in practical use.

In chapter 4, we developed a series of PNA-TO ligands for the detection of a single terminal mismatches in DNA/RNA sequences. PNA unit recognizes the terminal nucleobases and TO unit intercalate into the DNA or RNA duplex and emit a fluorescent signaling. effective at both 5' and 3' terminals, and introducing pyrene to the ligand as a molecular caphas improved the specificity for the 1st terminal position mismatch at 5'. In addition, Pyrene-PNA-TO is applicable to microRNA detection to recognize let-7d out of let-7 family with LOD as low as 0.9 nmol in 50 μL sample. It's thus expected that our method is promising for terminal mismatch detection and the ligand design would have flexibility for any kind of terminal sequences.

Acknowledgment

Copyright license

Concerning to ref. No. 9:

Other information including author's address, and the terms and conditions of this license are clipped here (not shown).

Concerning to ref. No. 74: